AFOSR-TR-96

0585

REPORT DOCUMENTATION PAGE

1. AGENCY USE ONLY (Leave blank)	2. REPORT DATE	3. REPORT TYPE AND DATES COVERED
	26 Aug 96	Final Technical 01Aug93 - 31Jul196

4. TITLE AND SUBTITLE (AASERT-93)
Tailored Group Velocity Dispersion Using Periodic Structures

5. FUNDING NUMBERS
61103/D
3484/TS

6. AUTHOR(S)
Kamil Agi
Kevin J. Malloy

7. PERFORMING ORGANIZATION NAME(S) AND ADDRESS(ES)
The University of New Mexico
Center for High Technology Materials
125 EECE Building
Albuquerque, NM 87131-6081

8. PERFORMING ORGANIZATION REPORT NUMBER

9. SPONSORING/MONITORING AGENCY NAME(S) AND ADDRESS(ES)
Air Force Office of Scientific Research
(AFOSR/NE)
110 Duncan Avenue, Suite B115
Bolling AFB, DC 20332-0001

10. SPONSORING/MONITORING AGENCY REPORT NUMBER
F49620-93-1-0447

11. SUPPLEMENTARY NOTES

12a. DISTRIBUTION/AVAILABILITY STATEMENT
APPROVED FOR PUBLIC RELEASE: DISTRIBUTION UNLIMITED

12b. DISTRIBUTION CODE

13. ABSTRACT *(Maximum 200 words)*

Photonic crystals are three- or lower-dimensional dielectric structure that exhibits overlapping stop bands in all directions. The focus of this work has been the design and characterization of a novel face-centered-cubic photonic crystal. The characterization was done in four parts. The first was a simple microwave network analyzer measurement where horn antennas were used transmit and receive CW microwave radiation. The second characterization was a direct time-domain characterization using photoconductively switched planar antennas to generate and detect short bursts of electromagnetic radiation. The third method of characterization was the high-power microwave characterization where the Sinus-6 was used as the source to generate high peak power pulses. The final characterization done was the use of infra-red thermal imaging to study the distribution of the scattered signal from a photonic crystal. Furthermore, the infra-red thermal imaging was used to study the localized heating of the crystal due to high average power continuous wave excitation. Finally various applications of the three-dimensional photonic crystal emerged such as a UWB photonic crystal and photonic crystals as quasi-optical component for high-power microwave systems. This work lead to a number of ongoing collaborations including collaborations with Air Force Phillips Laboratory and MIT Lincoln Laboratory.

14. SUBJECT TERMS
photonic crystals, dielectric structures

15. NUMBER OF PAGES

16. PRICE CODE
NSP

17. SECURITY CLASSIFICATION OF REPORT	18. SECURITY CLASSIFICATION OF THIS PAGE	19. SECURITY CLASSIFICATION OF ABSTRACT	20. LIMITATION OF ABSTRACT
UNCLASSIFIED	UNCLASSIFIED	UNCLASSIFIED	UL

DISCLAIMER NOTICE

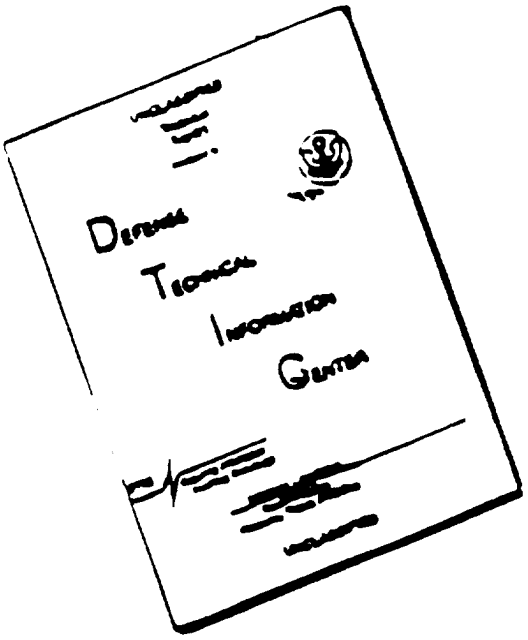

THIS DOCUMENT IS BEST QUALITY AVAILABLE. THE COPY FURNISHED TO DTIC CONTAINED A SIGNIFICANT NUMBER OF PAGES WHICH DO NOT REPRODUCE LEGIBLY.

Final Technical Report
Contract F49620-93-1-0447

for the period

August 1, 1993 to July 31, 1996

Submitted to:

Dr. Howard Schlossberg
Department of the Air Force
Air Force Office of Scientific Research
Bolling AFB, DC 20332-6448

Submitted by:

Professor Kevin J. Malloy
Center for High Technology Materials
University of New Mexico
Albuquerque, NM 87131

Air Force Office of Scientific Research (AASERT) Final Report

Kevin J. Malloy
26 August 1996

Photonic Crystals: Executive Summary

The following are the key technical results that were obtained during the extent of the AASERT grant:

- Designed and fabricated a novel three-dimensional photonic crystal
- First time-domain characterization of the three-dimensional photonic crystal using photoconductively switched planar antennas
- First demonstration of an ultra-wideband photonic crystal
- First to demonstrate high power microwave behavior of three-dimensional photonic crystals
- First to demonstrate beam shaping of high power microwaves using three-dimensional photonic crystals
- First to demonstrate spatial filtering of high power microwave beam using photonic crystals
- First to characterize photonic crystals using infra-red thermal pattern imaging
- Group velocity, as opposed to phase velocity, dictates the evolution of the pass bands in transmission for three-dimensional photonic crystals

The following are key, *ongoing*, collaborations that were established as a result of this work:

- Dr. Elliott Brown, Lincoln Laboratory, Lexington, MA.
  -Initial work on the design, fabrication and characterization of the photonic crystals
- Dr. Edl Schamiloglu, Pulsed Power Laboratory, University of New Mexico, Albuquerque, NM.
  -High power microwave characterization
- Dr. Hugh Pohle and Mr. Joe Sadler, Air Force Phillips Laboratory, Kirtland Air Force Base, NM.
  -Infra-red thermal imaging

PHOTONIC CRYSTALS

A three- or lower-dimensional periodic structure that exhibits a pass- and stop-bands is called a photonic crystal (PC). For the three-dimensional structure, if the stop band overlaps in all 4π steradians, this structure is known as a photonic bandgap structure. FY'94 was spent fabricating and characterizing a new, more robust face-centered-cubic (fcc) PC in collaboration with Dr. Elliott Brown at Lincoln Laboratory. A detailed description of the fabrication process can be found in [1]. Briefly, vertical holes were drilled in plates of a dielectric host in a triangular lattice. These plates are then ordered in an A-B-C configuration to obtain an fcc lattice comprised of cylindrical air atoms. The robust nature of the new crystal is manifested in the ease of fabrication and mechanical stability associated with drilling vertical holes. Furthermore, various applications of PCs were studied [2].

The characterization of the crystals was done in two parts. First, microwave horn antennas were used to transmit and receive electromagnetic radiation through the sample. A network analyzer was used to measure the microwave transmission coefficient, S_{21}, from 15 to 25 GHz [1]. Transmission measurements were obtained for key symmetry directions in the crystal. A limitation of this type of measurement is the narrowband nature of the network analyzer.

In order to study broadband characteristics, the second part of the characterization was done in the time-domain. A mode-locked titanium-sapphire laser was used to generate a 250 fsec optical pulse train at a repetition rate of 76 MHz. These optical pulses were used to photoconductively switch planar antennas to generate freely propagating electromagnetic radiation. The exponentially-tapered-coplanar horn antennas are printed on low-temperature-grown GaAs (LTG-GaAs) using standard deposition techniques. The LTG-GaAs provided a short carrier lifetime (~100 fsec) such that the photoconductively generated current pulse was similar in duration to the optical pulse. The bandwidth of this system is 5-70 GHz which is limited by the antenna design. The characterization was done in transmission for the three-dimensional crystal in different key symmetry directions.

The first demonstration of an ultra-wideband (UWB) PC was done by stacking multiple fcc crystals with different lattice constants in tandem. The response of this crystal was the superposition of the individual responses [3]. Furthermore, the crystals with overlapping stop-bands had to be placed in intimate contact to avoid cavity modes [4]. The response of the UWB-PC was done using both techniques and the UWB-PC had a much wider stop-band than the network analyzer data predicted [5].

FY'95 was focused on the characterization of the spatial evolution of the stop bands by stacking multiple periods of the same lattice constant. To continue the study of the broadband characteristics, the characterization of the three-dimensional PC was done in reflection using a modified version of the time-domain set-up as described above. The antennas were oriented to measure specular reflection at an angle of approximately 30°. Preliminary results indicate that as the number of periods was increased from one to two, the pulse shape changes. However, from two- to three-periods, the pulse shape remains the same for approximately 250 psec. This indicated that the effective index is such that the time it takes for the wave to travel into two periods is the same as the three-period structure in our measurement window. With these measurements, the possibility of pulse shaping techniques using the photonic crystal was also investigated as well as the determination of an effective index that describes the structure.

Furthermore, in collaboration with the Dr. Hugh Pohle and Mr. Joe Sadler at the Air Force Phillips Laboratory, the three-dimensional PC was further characterized by studying the diffraction pattern of these crystals when excited by an amplified continuous-wave (CW) microwave source (50 W) and detected by an infra-red thermal pattern imaging system. Preliminary results indicated that the microwave diffraction from the PC is similar to x-ray diffraction from a face-centered-cubic atomic crystal (e.g. Cu <111>). Similarities and differences of the microwave diffraction patttern are currently being investigated. The infra-red imaging also indicated minimal heating of the PC during excitation due to the incident CW radiation, allowing the possibility of using PCs in high power microwave (HPM) applications.

The PC was then investigated as a new quasi-optical component for HPM. A Sinus-6 high-power relativistic repetitively pulsed electron beam accelerator was used to drive a slow wave structure in vacuum to generate 450 MW at 9.65 GHz. We have shown that the photonic crystal was capable of performing as a quasi-optical reflector similar to metals. The crystals can be designed to operate as efficient frequency-selective reflectors over narrow frequency ranges, beam shaping components and spatial filters. It is proposed that photonic crystals can have many applications in HPM research [6].

FY'96 was focused on the study of the temporal evolution of the pass- and stop-bands in PCs. In order to understand the evolution in three-dimensional PCs, short-pulse propagation through a one-dimensional periodic structure was studied. Initially, a method was derived for a finite crystal to determine the group velocity using a scaled group delay [7]. For the temporal evolution, the time-to-formation of the pass bands, which is defined as the first wave to appear at the observer, is dictated by the peak group velocity in the bands [7]. For the one-dimensional PC, joint time-frequency analysis was performed to

verify the evolution process in the pass bands. The group velocity was obtained using three-methods. First, the group delay was obtained by taking the derivative of the phase of the transmission response with respect to frequency and then scaled to obtain the group velocity. Second, a joint time-frequency algorithm is applied and the time-to-formation is obtained by measuring the time delay. Once again the time delay is scaled to obtain the group velocity. Finally, the results obtained from the finite structure are compared to an infinitely periodic structure using the standard definition for the group velocity. All three methods were in good agreement.

The results obtained for the one-dimensional PC were then extended into three-dimensions. For the three-dimensional PC, the group delays are compared directly since the theoretical calculation for the infinitely periodic structure was not available. Good agreement was shown for the calcualtion of the group delay using the derivative of the phase and the joint time-frequency analysis.

Finally, this work will be utilized in designing and developing an efficient UWB radiator. It is proposed that by knowing the temporal transmission and reflection evolution, a UWB antenna can be placed on top of the UWB PC, to enhance the gain of the antenna. The UWB antenna work will be sponsored by Dr. H. Everitt and will be done in collaboration with Dr. M. Litz at ARL.

PUBLICATIONS

1. E.R. Brown, K. Agi, C.D. III, C.D. Parker and K.J. Malloy, "A New Face-Centered-Cubic Photonic Crystal for Microwave and Millimeter-Wave Applications," Microwave and Opt. Tech. Lett., 1994, **7**(17): p. 777-779.

2. E.R. Brown, O.B. McMahon, C.D. Parker, C.D. III, K. Agi and K.J. Malloy, *Microwave Applications of Photonic Crystals*. NATO ASI Series vol. on Photonic Band-Gap Materials, ed. C. Soukoulis. 1995, Dordrecht: Kluwar.

3. K. Agi, E.R. Brown, C.D. III, O.B. McMahon and K.J. Malloy, *An Ultra-Wideband Photonic Crystal*. Ultra-Wideband, Short-Pulse Electromagnetics 2, eds. L. Carin and L.B. Felsen. 1995, New York: Plenum Press.

4. K. Agi, E.R. Brown, O.B. McMahon, C.D. III and K.J. Malloy, "Design of Ultrawideband Photonic Crystals for Broadband Antenna Applications," Elec. Lett., 1994, **30**(25): p. 2116-2167.

5. K. Agi, E.R. Brown, C.D. III, K.A. McIntosh, O.B. McMahon, K.M. Molvar and K.J. Malloy, *Applications and Characterization of a New Face-Centered-Cubic Photonic Crystal*. Guided-wave Optoelectronics: Device Characterization, Analysis and Design, eds. T. Tamir, G. Griffel, andH.L. Bertoni. 1995, New York: Plenum Press.

6. K. Agi, L.D. Moreland, E. Schamiloglu, M. Mojahedie, K.J. Malloy and E.R. Brown, "Photonic Crystals: A New Quasi-Optical Component for High-Power Microwaves," IEEE Trans. Plasma Science, 1996, **24**(3).

7. K. Agi, M. Mojahedi and K.J. Malloy. "The Time Evolution of Photonic Crystal Bandgaps", *to appear in Ultrawideband, Short-Pulse III*. New York: Plenum Press.

A NEW FACE-CENTERED-CUBIC PHOTONIC CRYSTAL FOR MICROWAVE AND MILLIMETER-WAVE APPLICATIONS

E. R. Brown
Lincoln Laboratory
Massachusetts Institute of Technology
Lexington, Massachusetts 02173

K. Agi
Center for High Technology Materials
University of New Mexico
Albuquerque, New Mexico

C. Dill III and C. D. Parker
Lincoln Laboratory
Massachusetts Institute of Technology
Lexington, Massachusetts 02173

K. J. Malloy
Center for High Technology Materials
University of New Mexico
Albuquerque, New Mexico 87131

KEY TERMS

Photonic crystals, synthetic dielectrics, photonic band gaps

ABSTRACT

Three-dimensional photonic crystals are fabricated that consist of a face-centered-cubic lattice of air atoms embedded in a synthetic dielectric matrix. The crystals are formed by stacking triangular arrays of cylindrical atoms in a close-packed arrangement. The fabrication technique is much simpler than previous methods and is well suited to producing photonic band gaps in the microwave and millimeter-wave regions. Microwave measurements provide strong evidence for a photonic band gap between approximately 17 and 18 GHz in a crystal having a volumetric air fraction of 60%.

The photonic crystal is a periodic dielectric structure in three or lower dimensions whose electromagnetic dispersion relation has a band structure similar to that for electrons in crystalline solids and, when properly designed, can exhibit a band gap in frequency. The demonstration of a large gap in a three-dimensional photonic crystal [1, 2] initiated widespread investigation aimed at finding both optical and microwave applications. The three-dimensional photonic crystal having a band gap is in many ways the electromagnetic analog of a semiconductor; therefore it is not surprising that one application would be the integration of photonic crystal structures with printed circuits (e.g., photonic-crystal planar antennas) for the control and propagation of radiation [3]. Unfortunately, the only three-dimensional photonic crystals demonstrated to date [1, 4] are difficult to use with printed circuits either because they are difficult to fabricate or because they offer no planar surfaces on which to readily deposit circuit metal.

To make the photonic crystal more useful in these applications, we have devised a new method to fabricate a three-dimensional structure that is amenable to both synthetic dielectrics and semiconductors. It consists of a vertical stack of two-dimensional triangular-lattice slabs containing cylindrical air atoms. The vertical repeat unit consists of three layers (A, B, and C) in which the middle layer (B) is stacked below the top layer (A) in such a way that each atom lies directly below the center of a triangular unit cell in (A). The bottom layer (C) is aligned so that its atoms lie directly below the remaining unit cells in (A). A top view of this stacking arrangement (ABC) is shown in Figure 1. If the atoms were spherical and there was no dielectric matrix, this stacking arrangement would result in the (111)-oriented face-centered-cubic (fcc) close-packed lattice [5]. The (111) fcc lattice results from the arrangement of Figure 1, provided that the triangular lattice constant t is related to the slab thickness s by $t = (\frac{3}{2})^{1/2}s$. The fcc conventional cubic lattice constant a is then given by $a = 2^{1/2}t$. Our crystals were fabricated from the synthetic dielectric material Stycast having a permittivity ϵ of 13. Six Stycast sheets of dimension $0.64 \times 15.2 \times 15.2$ cm were piled on a milling machine and a triangular lattice of cylindrical holes having $t = 0.78$ cm was drilled vertically. This particular Stycast was chosen because it has similar dielectric characteristics to semiinsulating GaAs ($\epsilon = 12.8$), which is the semiconductor of choice for most microwave and millimeter-wave integrated circuits.

The photonic crystals were characterized by measuring the microwave transmission between the broad facets. Radiation from a sweep oscillator was fed into a Ku-band waveguide and coupled to free space through a pyramidal feed horn. The feed horn was first oriented to illuminate the sample along one of the following two directions: (1) normal to the broad facet along the [111] direction in the cubic unit cell (wave vector at the L point in the Brillouin zone), and (2) 39° away from normal along the [210] direction in the unit cell (W point in the Brillouin zone). At each orientation, both TE and TM polarizations of the incident radiation were applied (TE is where the electric field is polarized perpendicular to both the incident propagation vector and the axis normal to the crystal). On the opposite side of the crystal, the transmitted radiation was measured with an identical feed horn oriented in the same manner with respect to the photonic-crystal lattice and with the same polarization as the incident feedhorn. The power collected by the second feedhorn was coupled into a coaxial transmission line and measured with a network analyzer. For each orientation, the power transmitted through the photonic crystal was normalized to the background power (i.e., the power transmitted between the two horns without the photonic crystal in place).

The experimental result for transmission at normal incidence on the $\eta = 0.60$ crystal is shown in Figure 2. In this case the TM and TE designations are ambiguous, so we characterize the polarization state by the orientation of the electric field relative to the photonic crystal unit cell. In Figure 2 the electric field was polarized along the [01−1] axis. On the fine scale of Figure 2(a), we observe an abrupt drop in the photonic-crystal normalized transmission (henceforth called the maximum rejection) starting at approximately 16.8 GHz, a region of reduced transmission extending over about 1 GHz, and a more gradual return to high transmission above 18 GHz. On the coarser scale of Figure 2(b), we observe two sharp transmission notches at approximately 16.6 and 16.9 GHz. The nature of these notches is not entirely clear, but they may be related to multiple-pass interference between the front and back facets of the sample. Aside from the notches, the maximum rejection is about 20 dB at 17.7 GHz. This corresponds to about 6 dB of rejection per lattice constant. For the orthogonal polarization, the transmission spectrum was similar in character to that shown in Figure 2, although the notches occurred at slightly different frequencies.

The radiation propagating along the [210] (W-point) direction was the most interesting from a scientific standpoint, because this is the only known orientation for which an fcc

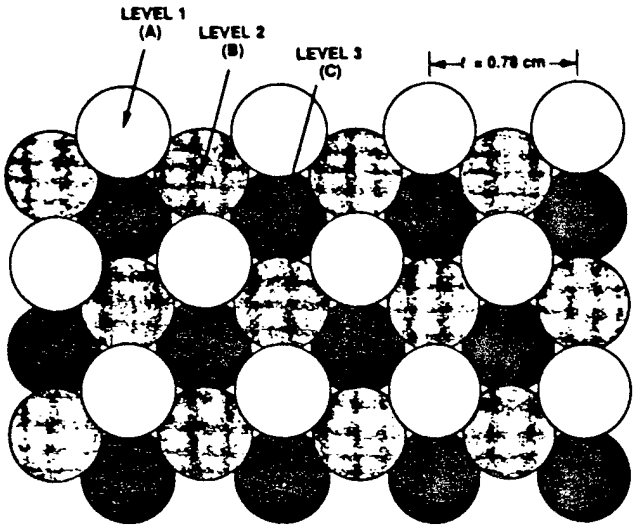

Figure 1 A top view of ABC stacking arrangement

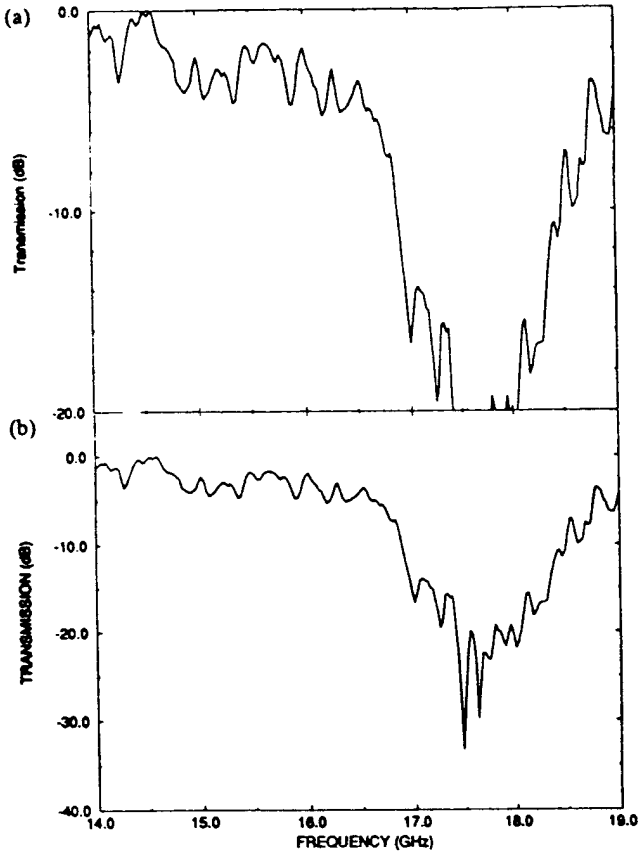

Figure 2 Experimental results for transmission at normal incidence (a) on the fine scale (b) on the coarser scale

lattice with round atoms fails to exhibit a stop band [6]. Figures 3(a) and 3(b) show the experimental transmission spectra for radiation incident along the [210] direction and having TE and TM polarizations, respectively. The photonic stop band for TE polarization extends from about 16.8 to 18.0 GHz, and for TM polarization it extends from about 16.5 to 18.0 GHz. This is the widest stop band that we observed for any orientation. The dominant feature of the TE spectrum is

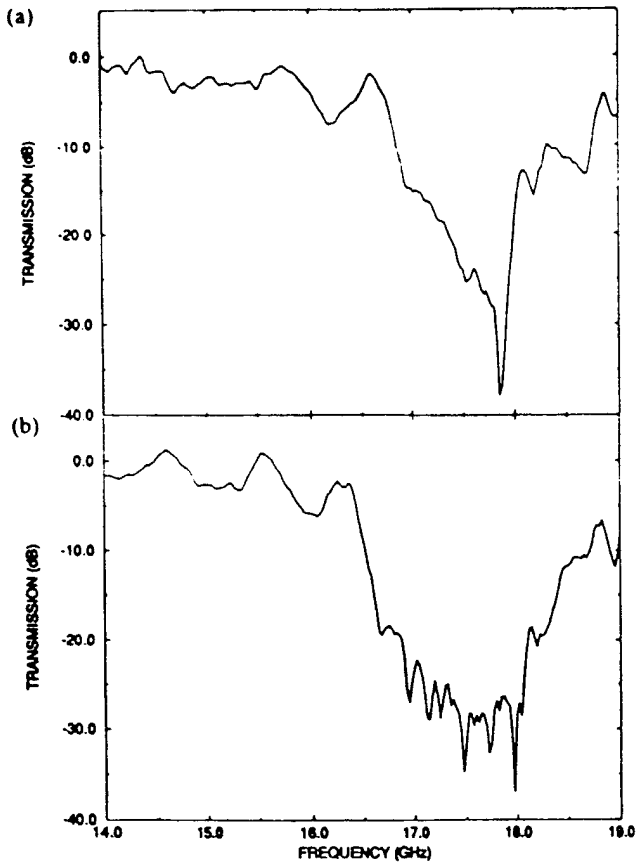

Figure 3 Experimental transmission for radiation incident along the [210] direction. (a) TE polarization (b) TM polarization

the deep notch centered around 17.8 GHz. The rejection associated with this notch was approximately 35 dB. Aside from this notch, the maximum rejection for TE polarization was about 25 dB near 17.8 GHz, corresponding to a rejection of 7.5 dB per cubic lattice constant. For the TM polarization in Figure 3(b), the maximum rejection away from the small notches was approximately 25 dB at 17.6 GHz.

To help determine whether the present crystal is exhibiting a photonic band gap, we examined the transmission at several other angles of incidence, such as 35° away from the normal along the [110] direction of the unit cell (K point in the Brillouin zone), and 45° and 60° away from the normal with arbitrary azimuth. In each case, we observed a stop band between approximately 17.5 and 18.0 GHz for TE polarization and between roughly 16.5 and 18.0 for TM polarization. This suggests that the 17–18-GHz region is a photonic band gap. Although it is difficult to prove the existence of a band gap without theoretical simulations, the measured rejection is already sufficient for many microwave and millimeter-wave printed circuit applications. Certainly this is true for the application of planar antennas on high-permittivity substrates, because in the absence of the photonic crystal the radiation efficiency from such an antenna into free space is just a few percent [7].

ACKNOWLEDGMENTS

The authors acknowledge J. Zayhowski and J. P. Mattia for helpful discussions, and R. A. Murphy and T. Y. Fan for useful comments on the manuscript. This work was sponsored by the Department of the Air Force, in part through an

AASERT grant from the Air Force Office of Scientific Research.

REFERENCES

1. E. Yablonovitcth, T. J. Gmitter, and K. M. Leung, *Phys. Rev. Lett.*, Vol. 67, 1991, p. 2295.
2. K. M. Ho, C. T. Can, and C. M. Soukoulis, *Phys. Rev. Lett.*, Vol. 65, 1990, p. 3152.
3. E. R. Brown, C. D. Parker, and E. Yablonovitch, *J. Opt. Soc. Am. Ser. B*, Vol. 10, 1993, p. 404.
4. E. Özbay, E. Michel, G. Tuttle, R. Biswas, M. Sigalas, and K.-M. Ho, *Appl. Phys. Lett.*, Vol. 64, 1994, p. 2059.
5. N. W. Ashcroft and N. D. Mermin, *Solid State Physics*, Saunders College, Philadelphia, 1976.
6. E. Yablonovitch and T. J. Gmitter, *J. Opt. Soc. Am. Ser. A*, 7, Vol. 7, 1990, p. 1792.
7. D. B. Rutledge, D. P. Neikirk, and D. P. Kasilingam, in *Infrared and Millimeter Waves*, Academic, Orlando, FL, 1983, Vol. 10, p. 1.

Received 6-17-94

Microwave and Optical Technology Letters, 7/17, 777–779

CCC 0895-2477/94

DESIGN OF TWO-LAYER WAVE ABSORBERS FOR METALLIC CYLINDERS WITH MIRROR-SYMMETRIC CROSS SECTION

Osamu Hashimoto*
Electromagnetic Communicaton Laboratory
University of Illinois
Urbana, Illinois 61801

Takanori Setsu
The Department of Electrical and Electronics Engineering
Aoyama Gakuin University
Tokyo, 157 Japan

KEY TERMS

Wave absorbers, wave propagation

ABSTRACT

This article discusses the method for analyzing the reflection characteristics of a metallic cylinder coated with a two-layer wave absorber. Various design curve and numerical results of the reflection characteristics are shown for wave absorbers that are optimum for masts with elliptical cross sections. © 1994 John Wiley & Sons, Inc.

1. INTRODUCTION

In recent years, a number of planar, film-type layered absorbers for electromagnetic waves have been developed that suppress radar ghost images and interference from extraneous radiation. Many situations exist, however, where it is desired to coat a curved object, for example, the mast of a ship. Although there are a number of available methods for designing general-purpose planar wave absorbers, they are not well suited for designing absorbers mounted on curved objects [1–3].

In an earlier work, the authors studied wave absorbers useful for circular cylinders, henceforth referred to as cylindrical absorbers, which are structurally simple and widely used [4]. However, there are other situations often encountered in which the curvature and shape of the structure are not circular. In this article we carry out a waveguide analysis for the problem of scattering from a dielectric body and develop a methodology for designing an effective absorber for metallic cylinders with symmetrical cross sections. To illustrate the application of this method, the design curves and absorbing characteristics are presented for masts with elliptical cross sections.

2. ANALYSIS

We consider a model consisting of an infinitely long metallic cylinder with an elliptical cross section coated with a two-layer absorbed, as shown in Figure 1. In this case, where a plane wave traveling in the x direction with a z-directed electric field is incident upon the metal cylinder, the incident electric field E_z^I, the scattered electric field E_z^s, and the electric field E_z^1, E_z^2 in the absorbers are assumed as follows:

$$E_z^I = E_0^I \exp(jk_0 x) \qquad \text{(free space)},$$

$$E_z^s = E_0^I \sum_{m=0}^{\infty} b_m H_m^{(2)}(k_0 \rho) \cos m\phi \qquad \text{(free space)},$$

$$E_z^1 = E_0^I \sum_{m=0}^{\infty} \{a_{1m} J_m(k_1 \rho) + a'_{1m} N(k_1 \rho)\} \cos m\phi$$

(in the absorber),

$$E_z^2 = E_0^I \sum_{m=0}^{\infty} \{a_{2m} J_m(k_2 \rho) + a'_{2m} N(k_2 \rho)\} \cos m\phi$$

(in the absorber).

Here, $a_{1m}, a'_{1m}, \ldots, b_m$ are arbitrary amplitude coefficients. In what follows, the amplitude coefficients of the electric field component assumed as above are determined by the point-matching method [5].

The magnitude of the scattered field for the coated cylinder may be calcualted by using the equation

$$E(\rho, \phi = 0°) = \left| \sum_{m=0}^{n} b_m H_m^{(2)}(k_0 \rho) \right|.$$

The effectiveness of the absorber can be evaluated by comparing the scattered field from the aboe equation with the

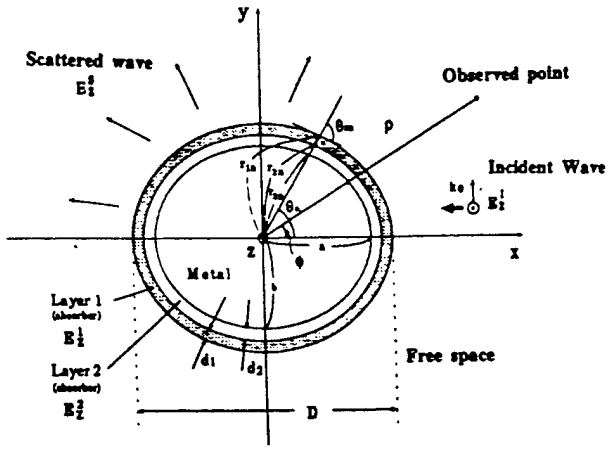

Figure 1 Geometry of the two-layer absorber coating a cylinder with a mirror symmetrical cross section

*On leave from the Department of Electrical and Electronics Engineering, Aoyama Gakuin University, Tokyo, 157 Japan.

To appear in Nato ASI Series Vol.
on Photonic Band-Gap Materials,
ed. C. Soukoulis (Kluwer,
Dordrecht, 1995)

MICROWAVE APPLICATIONS OF PHOTONIC CRYSTALS

E. R. BROWN, O. B. MCMAHON, C. D. PARKER, C. DILL III
Lincoln Laboratory, Massachusetts Institute Of Technology,
Lexington, Ma 02173-9108 USA

K. AGI and K. J. MALLOY
Center for High Technology Materials
University of New Mexico,
Albuquerque, NM 87131 USA

Abstract

This paper reviews three applications we have investigated using conventional (i.e., all dielectric) photonic crystals at frequencies up to about 30 GHz: (1) microwave mirrors, (2) substrates for planar antennas, and (3) photonic-crystal heterostructures. In each case, an important characteristic of the photonic crystal is that the reflection at frequencies in the stop band is distributed over at least one lattice constant in depth. Thus, the heat generated by residual dielectric absorption is distributed over a much larger volume than the heat generated by surface losses in a metal mirror, enabling a lower operating temperature. An additional characteristic of the photonic crystal, essential to the antenna application, is that its stop band is three-dimensional and thus rejects the majority of power radiated by an antenna mounted on its surface. This makes the planar antenna much more efficient than the same antenna placed on a homogeneous substrate made from the same dielectric material as the photonic crystal. A key factor in the ultimate practicality of these applications is the development of new types of photonic crystals that are superior structurally to conventional crystals or that display enhanced stop-band characteristics. To widen the stop band, we have studied a photonic-crystal heterostructure consisting of a stack of monoperiodic sections having different lattice constants. The resulting structure is shown to have a stop band of nearly one octave.

1. Introduction

Photonic crystals are two- or three-dimensional periodic dielectric or metallic structures that display a stop band in their electromagnetic transmission characteristics. If this stop band is omnidirectional, then the photonic crystals have a forbidden region or band gap in their ω-k dispersion relation. As such, photonic crystals are well suited to a number of microwave and millimeter-wave applications for which conventional materials and components are unsatisfactory. Paramount among these are applications that require high reflectivity without the presence of metal.

The first photonic crystal to exhibit a three-dimensional stop band was a (111)-oriented face-centered-cubic (fcc) structure with nonspherical air atoms. The crystal was fabricated at Bellcore from the synthetic dielectric material Stycast [1], and displayed a band stop in the microwave range between 13 and 16 GHz. More recently, it has been shown that superior band-stop characteristics can be obtained from the diamond crystal structure, and such a crystal can be fabricated by stacking dielectric rods in a "woodpile" structure [2,3]. The technique of silicon micromachining has enabled the fabrication of diamond photonic crystals having stop bands up to 450 GHz [4].

At Lincoln Laboratory we have devised a (111)-oriented fcc structure whose repeat unit is a stack of three slabs, each slab containing a two-dimensional triangular lattice of cylindrical air atoms [5]. Because the atomic shape in this fcc structure is cylindrical, one does not expect the band-stop properties (or the band structure) to be the same at common-symmetry points (i.e., the 6 X points) in the fcc Brillouin zone. Nevertheless, the structure displays a sizable stop band along the axis normal to the top facet (corresponding to one of the L points in the Brillouin zone) and over a large angle about the normal. Furthermore, the triangular lattice constituting each slab is known to have good two-dimensional band-stop properties in the plane [6]. Hence, this fcc structure is very useful as a substrate for planar antennas or transmission lines operating at frequencies near the center of the first stop band.

Our choice of photonic crystal exemplifies the strategy we have generally applied in the investigation of microwave applications. That is, the presence of an omnidirectional stop band or, equivalently, a band gap, is usually not as important an issue as it is in most theoretical studies of photonic crystals. The more important issues are: (1) the stop-band properties along the directions involved in the application at hand, and (2) the mechanical compatibility of the photonic crystal with the metallic antennas or transmission lines that must be fabricated on its surface. Mechanical compatibility bears on ruggedness and cost — both of which often determine whether or not an application becomes popular.

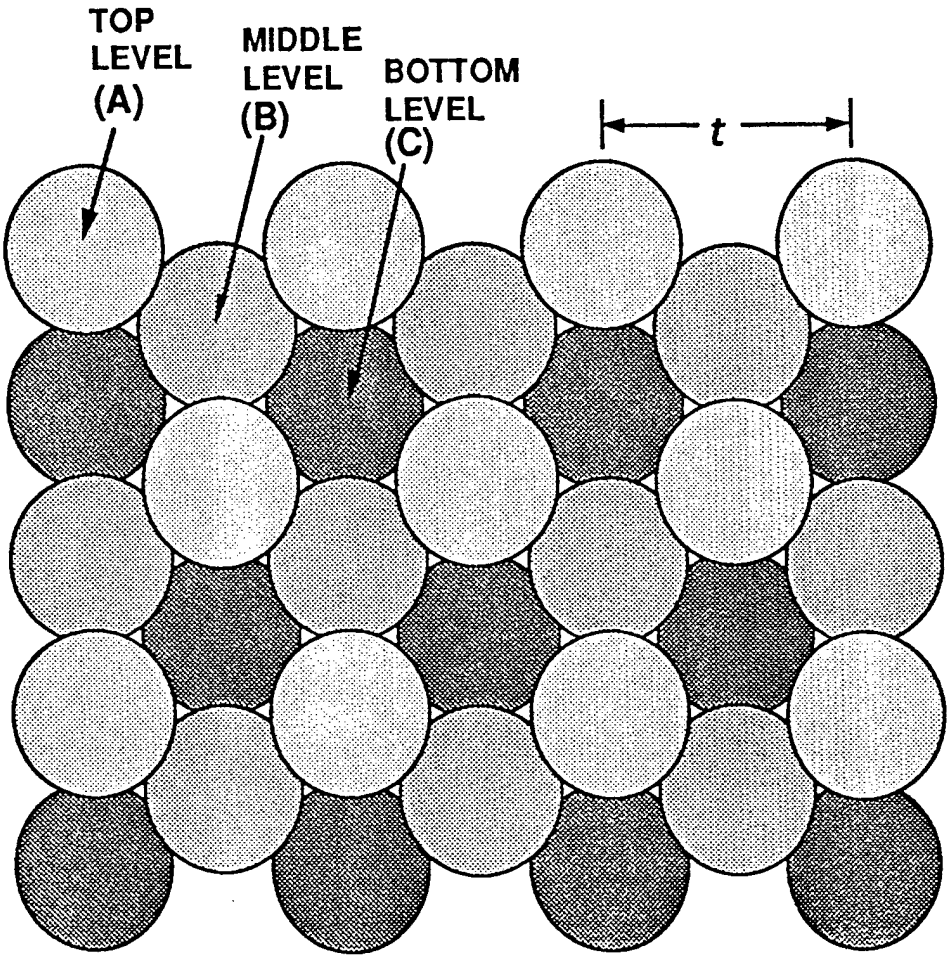

Fig. 1. Top view of Lincoln Laboratory (111)-oriented photonic crystal. The shaded circles represent the cylindrical atoms in three successive layers of the fcc repeat unit.

2. Crystal Fabrication

The vertical repeat unit of our fcc photonic crystal consists of three slabs (A,B,C) in which the middle layer (B) is stacked below the top layer A in such a way that each atom lies directly below the center of a triangular unit cell in A. The bottom layer (C) is aligned so its atoms lie directly below the remaining unit cells in (A). The top view of this stacking arrangement (ABC) is shown in Fig. 1. If the atoms were spherical and there was no intervening dielectric material, this stacking arrangement would result in the (111)-oriented fcc close-packed lattice

[7]. The (111) fcc lattice requires the triangular lattice constant t be related to the slab thickness s by $t = (3/2)^{1/2}s$. The fcc conventional cubic lattice constant a is then given by $a = 2^{1/2}\,t$.

All of our conventional photonic crystals were fabricated from Stycast, a synthetic dielectric material consisting of titanium dioxide grit immersed in a polymeric binder. The dielectric constant of the Stycast has nominally been either 10, 12, or 13, depending on the concentration of titanium dioxide. The Stycast was obtained commercially in 1x1 ft by 1/4-inch-thick plates, and fabricated into 6x6x1/4-inch triangular-lattice slabs by sawing and numerical routing. The router is a custom-built computer-controlled machine with a three-axis control system. The x, y, and z position stages are driven by stepper motors having 2000 steps/revolution, corresponding to a linear displacement of 0.0005 inch/step and a bidirectional repeatability of 0.0008 inch/inch. The x and y stepper motors are controlled in velocity and acceleration over a total travel of 12 inches. The z stage offers 2 inches of travel. The router speed is adjustable from 0 to 22,000 RPM. The control programs are written and executed on an IBM 386 in a Microsoft Windows environment.

3. Transmission and Reflection Characteristics

3.1. MEASUREMENT TECHNIQUES

After fabrication, the microwave transmission or reflection through a photonic crystal is routinely measured from 5 to 26 GHz with an HP 8510 network analyzer in the setup shown in Fig. 2. A set of three pyramidal feedhorns is used in sequence at the generator and transmission ports to transform the radiation from coaxial cable to free space. Each horn is used only within its designated bandwidth (less than 1 octave) to ensure good beam characteristics incident on the sample. As in all microwave antennas, the beam from a feedhorn is characterized by its emitted or collected intensity vs polar angle q in at the electric E plane (coincident with the polarization) and in the orthogonal H plane. The full width of the beams is defined by the difference in q between the points where the collected radiation is down 10 dB (10%) relative to that at broad side. For the feedhorns used in our experiments the 10-dB full widths were 30° in the E plane and 22° in the H plane. As displayed by other feedhorns of this type, the E-plane pattern is broader than the H-plane pattern because of small sidelobes.

An important factor in the transmission or reflection measurements is the spot size of the incident microwave beam at the surface of the photonic crystal. Our experience is this spot size must be substantially greater than the separation of nearest-neighbor lattice sites to see well-defined stop bands with precipitous band edges. With

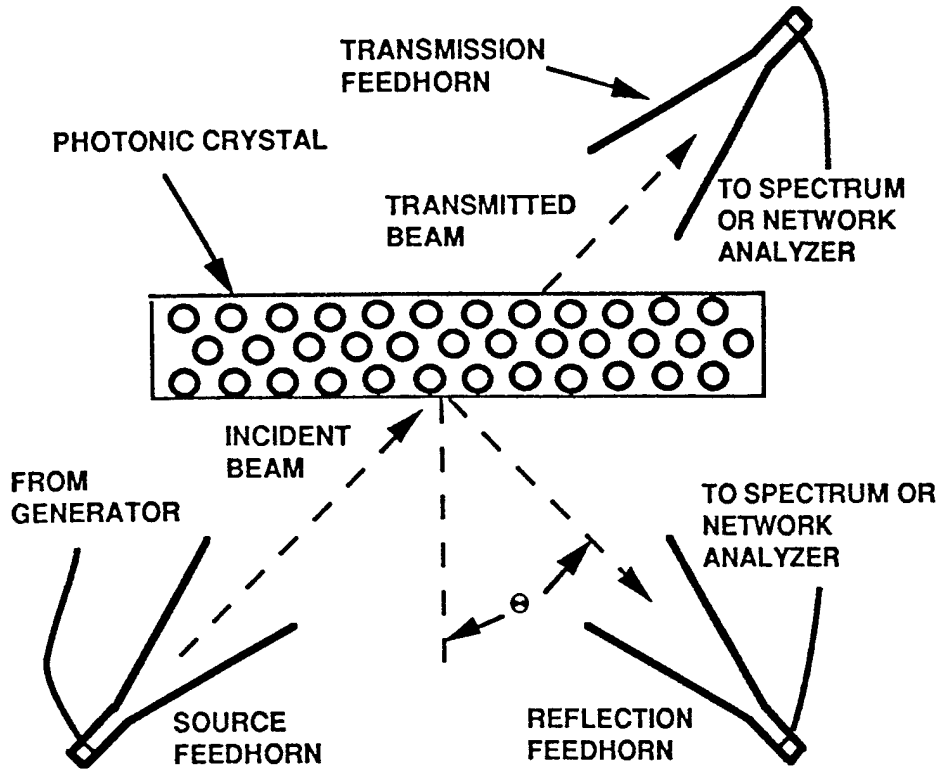

Fig. 2. Schematic diagram of experimental setup used to measure the transmission and reflection properties of photonic crystals.

the 22 to 30° Gaussian-like beam patterns of our feedhorns, this is accomplished by separating the sample from the feedhorn by roughly 20-cm or more. For the 20-cm separation, the spot diameter on the crystal is about 8 cm, which is roughly 10 times the nearest-neighbor separation in a photonic crystal having its first band stop in the 10-to-20-GHz range.

In the transmission measurements, the sample is placed between the feedhorns with its front and back facet at a specific angle Θ relative to the beam propagation direction. The most interesting angles in our measurements have been the following four high-symmetry propagation directions in the conventional cubic unit cell: [111], [100], [1, 1/2, 0], and [110]. These directions correspond to vectors in the first fcc Brillouin zone that pass through the following points: (1) Γ to L, (2) Γ to X, (3) Γ to W, and (4) Γ to K. The Γ to W direction is particularly interesting from a scientific standpoint since this the direction in which the fcc crystal with spherical atoms fails to demonstrate a strong stop band [8].

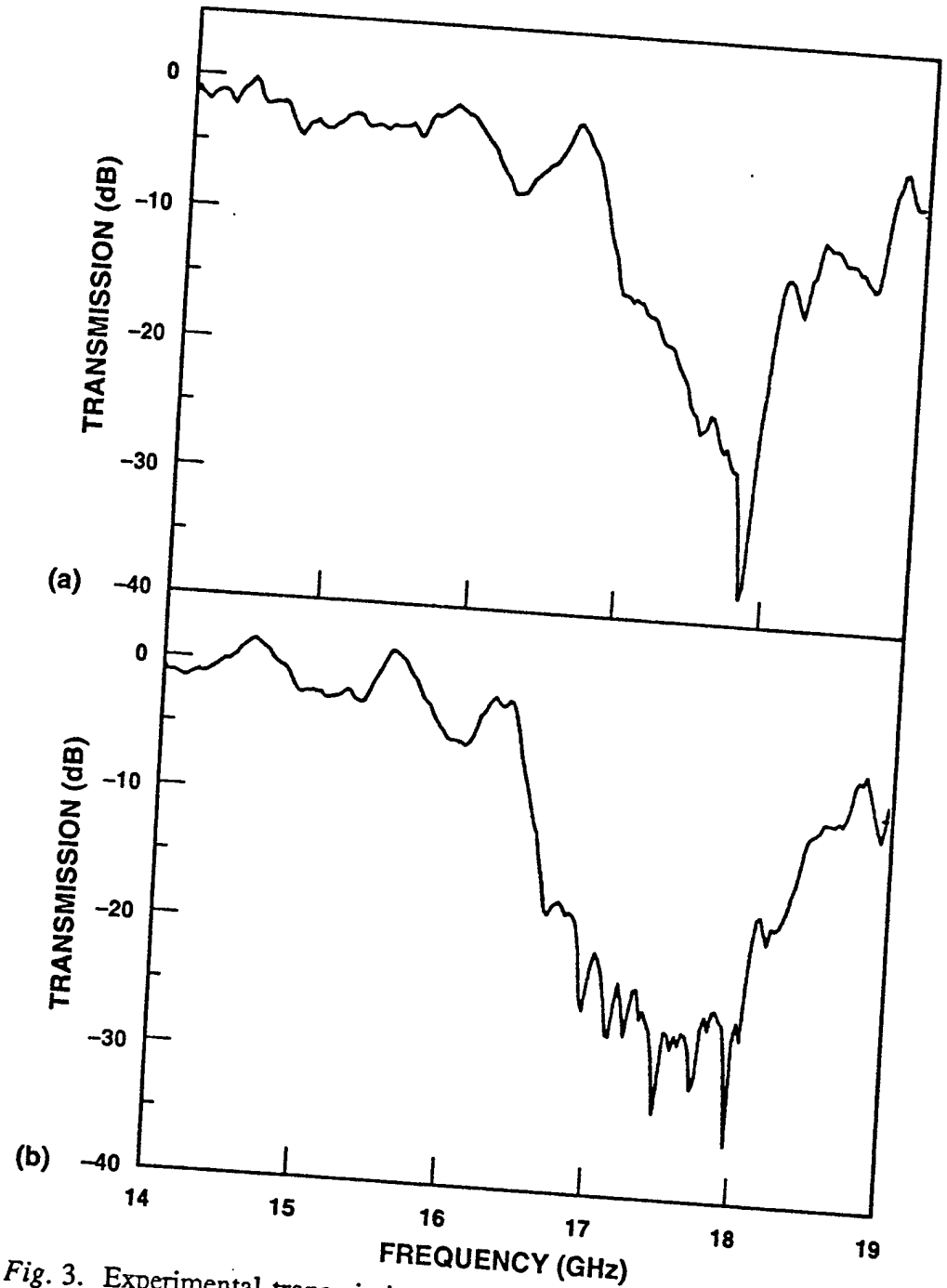

Fig. 3. Experimental transmission through (111)-oriented fcc photonic crystal for radiation incident along the [210] direction. (a) TE polarization. (b) TM polarization.

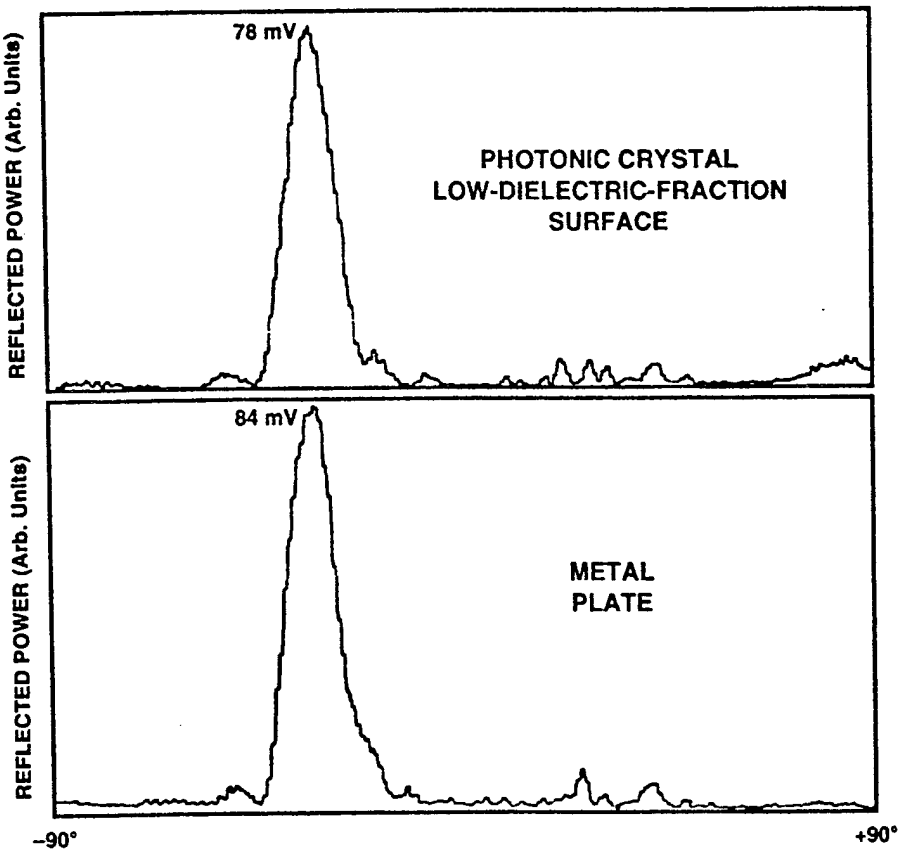

Fig. 4. Reflection from fcc photonic crystal for incident radiation at 39° and the reflected radiation measured over the front hemisphere. The incident frequency was fixed at the center of the stop band.

3.2. TRANSMISSION AND REFLECTION RESULTS

Shown in Figs. 3(a) and (b) are the transmission spectrum through 3 repeat units (9 slabs) of our fcc crystal for radiation incident along the [210] direction and polarized either transverse to the plane of incidence (TE polarization) or parallel to the plane of incidence (TM) polarization. For TE polarization, the stop band occurs between roughly 16.8 and 18.0 GHz. For TM polarization, the stop band occurs between about 16.5 and 18.0 GHz. The dominant feature of the TE spectrum is the deep notch centered around 17.8 GHz. The rejection associated with this notch is approximately 35 dB. Aside from this feature, the maximum rejection is about 25 dB, corresponding to a rejection of 7.5 dB per cubic lattice constant. For the TM polarization in Fig. 3(b), the maximum rejection outside of the small notches is approximately 25 dB at 17.6 GHz.

The set-up in Fig. 2 allows measurement of the reflection coefficient by moving the feedhorn from the back side of the crystal to the front side.

Our experience has been that the reflection is a better indicator of subtleties in the electromagnetic propagation through the photonic crystal than the transmission. A good example is shown in Fig. 4 which was obtained with the generator feedhorn oriented for propagation along the [210] direction 39° away from the normal and the reflection feedhorn varied in angle Θ over the entire front hemisphere. Both feedhorns were set for TE polarization. The frequency of the generator is set at the center of the photonic band stop along this direction. Clearly, the reflection from the photonic crystal is not quite specular, because the reflected signal amplitude is lower than the generator amplitude by about 7%. Although part of this difference is certainly caused by imperfect specular alignment of the feedhorns and losses in the coaxial cables, there is a significantly increased strength of the reflection from the photonic crystal at $\Theta = +90°$ (in the plane of the crystal, 129° away from the generator feedhorn). This is probably caused by the excitation of surface modes, which are thought to exist at the surfaces of all photonic crystals, particularly those having high dielectric surface density (i.e., the fraction of the surface area that is dielectric).

4. Planar Antennas on Photonic-Crystal Substrates

The application of the photonic crystal as an antenna substrate is important from a historical perspective because it was the first known microwave application in which the omnidirectional stop band of the three-dimensional photonic crystal was essential to the performance. Therefore, in this section we start with a thorough conceptual review.

4.1. PHYSICAL PRINCIPLES

Planar antennas play the important role in microwave and millimeter-wave integrated circuits of radiating signals off chip into free space. When fabricated monolithically on a semiconductor substrate such as silicon, such circuits greatly enhance the performance and functional density compared to the alternative hybrid circuits. High-resistivity ($\approx 10^4\ \Omega$ cm) silicon has weak enough electromagnetic absorption ($\alpha < 0.2$ cm^{-1}) to be useful up to millimeter-wave frequencies (> 30 GHz) [9]. However, silicon has a high dielectric constant, which generally makes the performance of planar antennas inferior to that of metallic feedhorns. At the present time, feedhorns are used in the majority of applications at frequencies above 20 GHz.

The problems associated with planar antennas on semiconductor substrates originate in the fundamental electromagnetics of a conductor on a dielectric surface. Shown in Fig. 5 is the conductor-substrate interface for a generic metallic planar antenna on a uniform substrate

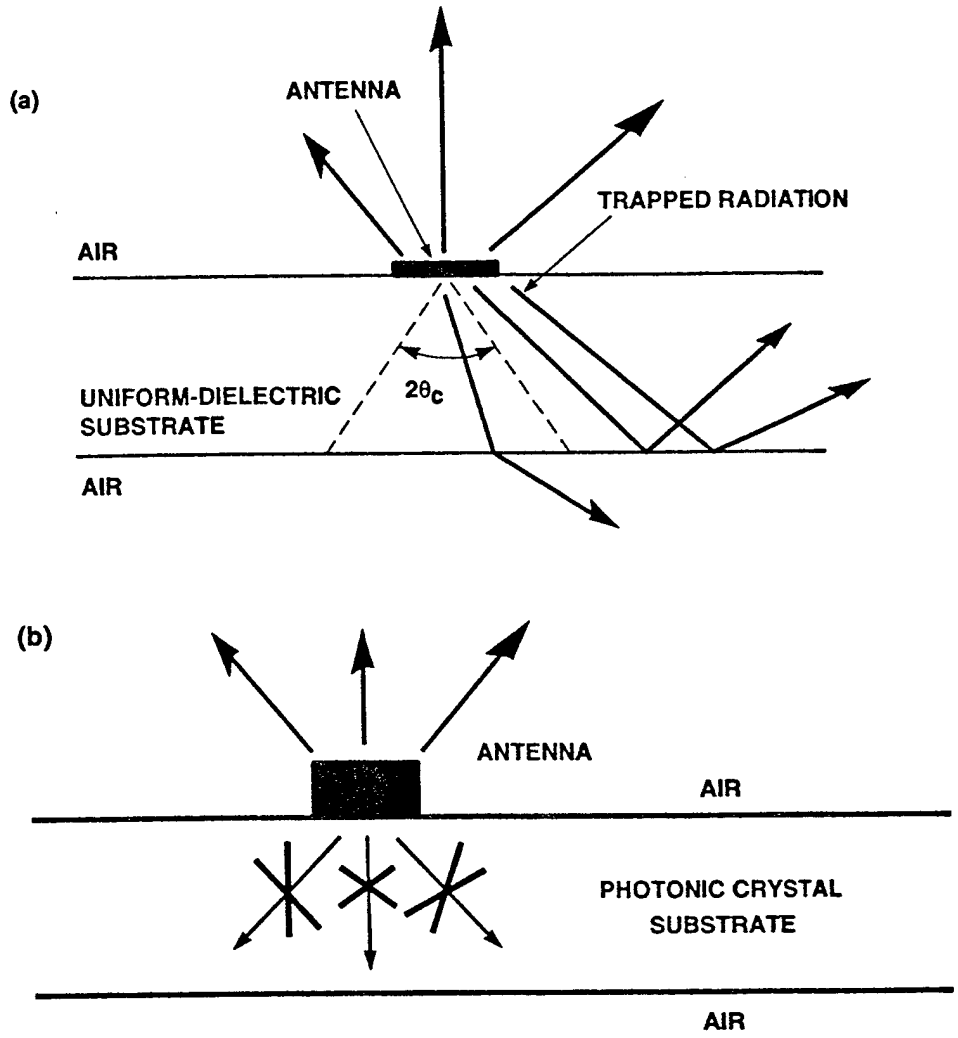

Fig. 5. (a) Cross-sectional view of propagation of radiation from a planar antenna on a uniform-dielectric substrate. (b) Same view for planar antenna on photonic-crystal substrate.

having a purely real dielectric function (i.e., no electromagnetic attenuation) represented by the dielectric constant ε. Independent of its shape, the antenna has a tendency to radiate more power into the substrate than into the free space above the substrate. The ratio of the power into the substrate to the power into free space increases with e. For example, an infinitesimal planar dipole radiates approximately $\varepsilon^{3/2}$ more power into the substrate than into free space [10]. Thus, a dipole on a silicon substrate ($\varepsilon = 11.8$) radiates 40 times more power into the substrate. A second problem is that the power radiated into the substrate

at angles greater than $\theta_c = \sin^{-1}\varepsilon^{-1/2}$ is totally internally reflected at the top and bottom substrate-air interfaces. For silicon, this occurs at $\theta_c = 17^\circ$, so that in many antenna structures the vast majority of the radiated power is trapped in the substrate, as shown in Fig. 5(a).

An elegant way to alleviate these problems is to use a three-dimensional photonic crystal as the antenna substrate, as depicted in Fig. 5(b). If the driving frequency of the antenna lies within the photonic band gap, one expects that no power will be radiated into the substrate at any angle, since at every point along the conductor-substrate interface there is no propagation over the full hemisphere on the substrate side. However, it is not clear what fraction of the driving power will be radiated into the air side, since evanescent modes still exist at the air-substrate interface [11], and impedance mismatch can reflect power back to the generator.

4.2. FABRICATION AND MEASUREMENT OF ANTENNAS

Two types of planar antennas have been studied to date: bow-ties (i.e., long, tapered dipoles) and resonant dipoles. The bow-tie was studied first because of its nonresonant nature and well-known impedance properties on uniform dielectric substrates. It was the first antenna type to demonstrate the nearly complete rejection of radiation by the Bellcore fcc photonic crystal [12]. However, its radiation pattern was always highly scalloped, partly because of the complicated nature of the antenna pattern of the bow-tie even in free space, and partly because it was fabricated with thin copper tape that was easily twisted and lifted off the substrate by the coaxial feed lines. To start with a simpler antenna pattern, we then investigated planar dipole antennas [13], which will be the only results displayed here. In this case, the antennas were fabricated with either thin copper tape stuck directly on the surface or free-standing metal shimstock abutted to the crystal. As will be shown later, the stiffness and maneuverability of the shimstock dipole yielded the most desirable antenna patterns that we have observed to date.

After fabrication, the radiation patterns from planar antennas are measured with the compact, scalar antenna test range shown schematically in Fig. 6. The photonic crystal is mounted on one end of the range in a plastic yoke designed to rotate in azimuth and elevation by mechanical coupling to metallic gear assemblies. The gear assemblies are shielded from the photonic crystal by microwave absorbing foam. The electric E-plane pattern of a dipole antenna, for example, is measured by rotating the mounting yoke through 180° in elevation with the crystal and feedhorn configured as in Fig. 6. The mounting yoke is then rotated 180° in azimuth to obtain the magnetic H-plane pattern. The separation between the crystal and the mouth of the feedhorn is approximately 1.4 m.

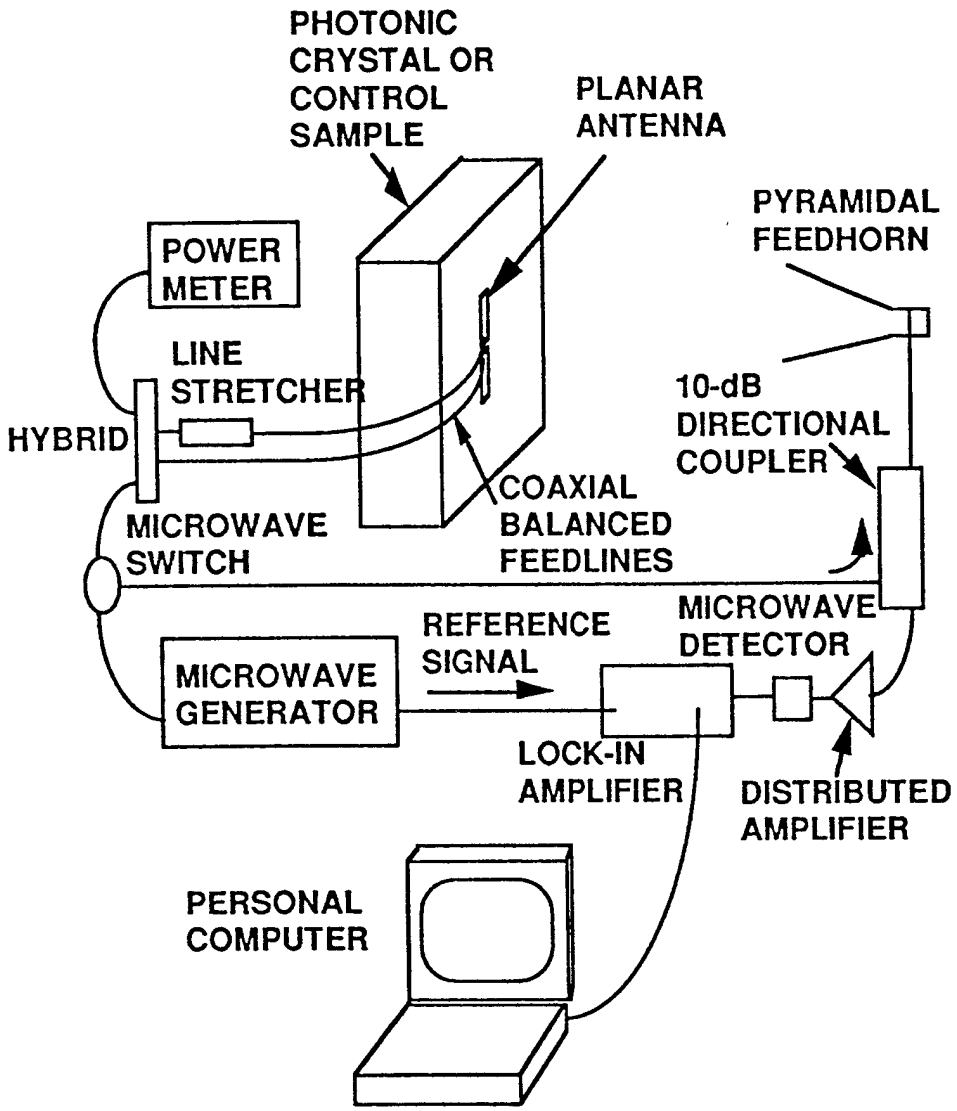

Fig. 6. Diagram of compact antenna test range used to measure the radiation pattern from planar antennas on photonic crystals.

The source of microwave drive radiation is an amplitude-modulated generator with a coaxial output port. To drive the planar antenna in a balanced manner, the oscillator power is divided equally by a 3-dB, 180° hybrid coupler into two thin (2.2-mm diameter) coaxial feed lines. The feed lines are routed to the planar antenna with a line-stretcher-type phase shifter added in one line to achieve a balanced drive at the end of the lines. To determine how balanced the drive is, the power is monitored in

the unused port of the hybrid and the line stretcher is adjusted to minimize this power. The radiated power is measured with the scalar receiver of Fig. 6. The receiver consists of a pyramidal feedhorn connected to a standard-height waveguide, waveguide-to-coaxial transition, distributed amplifier, and microwave power detector. To enhance the sensitivity, the output of the microwave detector is synchronously detected with a lock-in amplifier tuned to the modulation frequency of the generator.

4.3. PLANAR-DIPOLE RESULTS

For the sake of brevity, the experimental results presented here will be limited to the E-plane patterns of a copper-tape dipole on the Bellcore fcc crystal and the shimstock dipole on the Lincoln Laboratory fcc crystal, since these are the most educational results obtained to date. The Bellcore crystal is particularly interesting because it afforded two different surface dielectric densities by virtue of its nonspherical and noncylindrical atoms. Figure 7(a) shows the E-plane pattern for a dipole mounted on the high-dielectric surface and the driving point positioned at the center of the dielectric rib between two nearest-neighbor air holes. The zero of the polar angle defines the zenith. The pattern is characterized by multiple narrow peaks and a lack of symmetry about the zenith. In addition, it shows a significant amount of power at one of the horizons and some radiation into the back hemisphere. Since the photonic crystal cannot propagate bulk electromagnetic modes into the back side at the given drive frequency, this is a clue that surface waves are playing a role. Surface waves propagate from the dipole to the edge of the crystal, and can then radiate into the back-side hemisphere because of the abrupt discontinuity in the dielectric properties at the edge.

Figure 7(b) shows the E plane pattern of the same dipole mounted on the surface with low dielectric density, shown in Fig. 7(b). In this case, the driving point of the dipole was placed over an air atom between dielectric mesas. The antenna pattern is the most desirable that we observed from the Bellcore crystal. It peaked near the zenith and contained practically no power in the back-side hemisphere. However, it was somewhat asymmetric about the zenith, displaying a predominant side lobe near $\Theta = -70°$. The cause of this asymmetry was not understood, although distortion of the dipoles by the coaxial drive lines was suspected.

The experimental results for the shimstock dipole on the Lincoln Laboratory fcc crystal are shown in Fig. 8. The overall length of the dipole was equal to one-half of a free-space wavelength at the drive frequency of 17.4 GHz. Several orientations of the dipole antenna were attempted relative to the unit cell of the fcc lattice. The best pattern, by

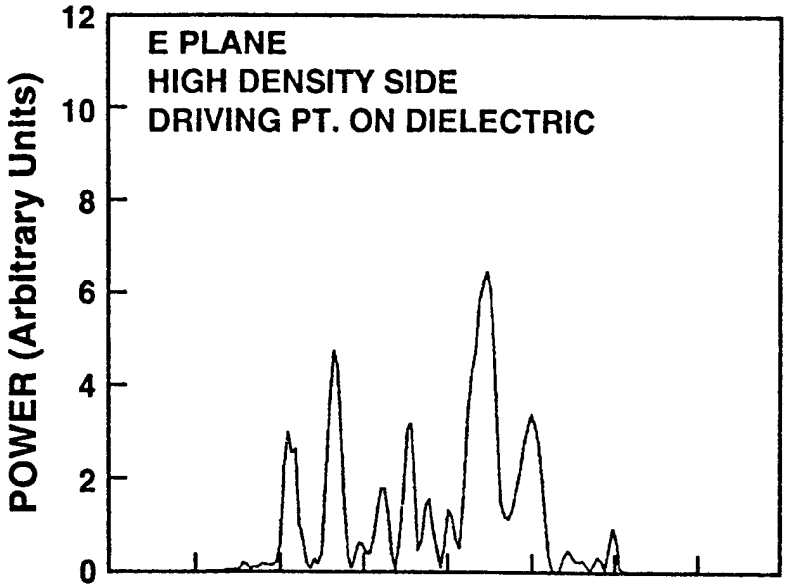

(a)

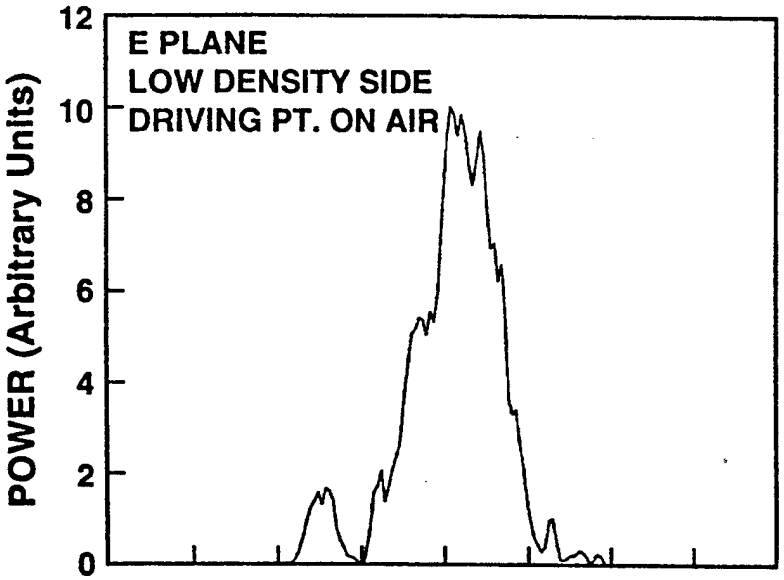

(b)

Fig. 7. E-plane radiation patterns from copper-tape dipole antenna mounted on two difference surfaces of the Bellcore fcc photonic crystal. (a) High dielectric density. (b) Low dielectric density.

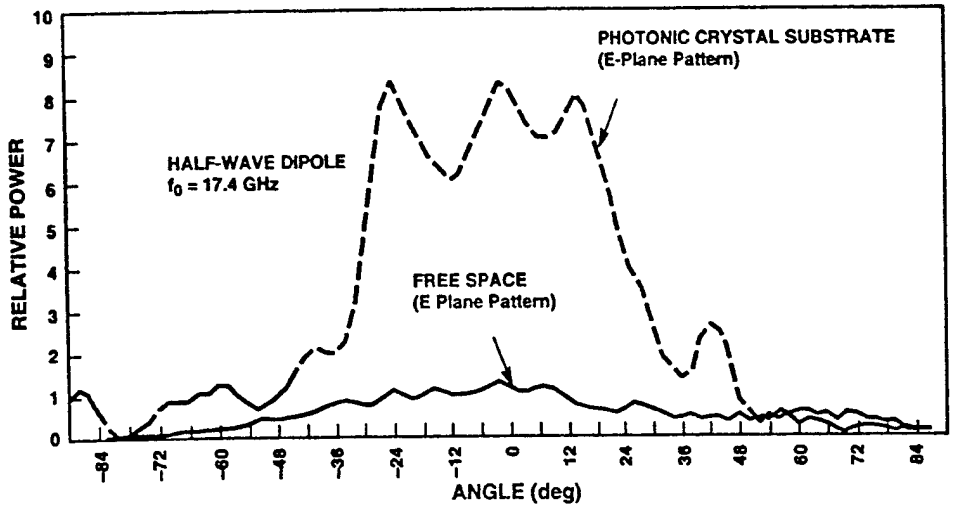

Fig. 8. E-plane radiation pattern from a shimstock-dipole antenna on Lincoln Laboratory fcc photonic crystal and the same dipole in free space.

far, was obtained for the dipole antenna mounted with its driving point located directly over a cylindrical air atom along a line through nearest neighbors of the surface triangular lattice. The resulting E-plane pattern displays a strong central lobe consisting of three local peaks and sharp skirts that occur at roughly ±30° in polar angle. Secondary lobes occur at roughly ±42°, outside of which the power drops to 10 dB below the main lobe at roughly ±48°.

A big advantage of the free-standing shimstock dipole is that it affords calibration of the antenna pattern by removal of the photonic crystal from the scene. Figure 8 also plots the E-plane radiation pattern of the same shimstock dipole in free space. As expected, the pattern of the free-space dipole is rather featureless with a broad peak at the zenith and decrease with polar angle that goes roughly as $\cos^2\theta$. Clearly, over the entire central lobe, the dipole on the fcc sample radiates with much more intensity than it does in free space. At the zenith, the ratio of the intensities is a factor of 6.8.

5. High-Reflectivity Mirrors

A straightforward application of photonic crystals in both the optical and microwave regions is high reflectivity mirrors. In the optical regime, such a mirror has the attribute of suppressing the three-dimensional density of photon states, which was the reason for the expression "photonic crystal" and is the basis for the optical applications low-threshold lasers and very efficient LEDs [14]. In the microwave region

we have confirmed that aside from small surface-mode generation, the reflection is specular provided the impinging free-space beam is extended laterally over many (at least ten) interatomic lengths.

5.1. PHYSICAL CONCEPT

In the microwave region, omnidirectional reflection is readily provided by a standard metal mirror with the following limitation. Because of the skin effect, the small fraction of power absorbed during the reflection of a high-power beam is dissipated in a small depth of metal. Because of the finite thermal conductivity of metals at room temperature, this small fraction of absorbed power can still result in high surface temperatures and ultimately mirror damage or destruction. The solution offered by the photonic-crystal reflector is to distribute this absorbed heat over a much greater volume and, hence, render much lower operating temperatures at the surface. In addition, many of the high-permittivity dielectric materials that are well suited to conventional photonic crystals (e.g., sapphire) are highly refractory and have comparable thermal conductivity to mirror metals at room temperature, so they tend to withstand absorbed power better in any case.

To demonstrate this concept quantitatively, we start with the conventional flat metal mirror having electrical resistivity ρ and subject to a powerful incident microwave beam of intensity I_i and frequency 10 GHz. In this case, the penetration or skin depth of the radiation at the surface of the metal is $\delta = (2\rho/\mu\omega)^{1/2}$ [MKSA Units], the surface impedance is $Z_S \approx \rho/\delta$, and the power reflectivity $R = [(Z_S - Z_0)/(Z_S + Z_0)]^2$, where Z_0 is the characteristic impedance of free space (377 Ω). The power absorbed per unit area by the mirror is $(1 - R)I_{inc}$ and the power absorbed per unit volume and averaged over the skin depth, $\overline{P_{abs}}$, is roughly $(1.0 - R)I_{inc}/\delta$. For example, when the metal is high-purity copper, we have $\rho \approx 2\times10^{-6}$ Ω–cm, $\delta \approx 0.7$ μm at 10 GHz, $Z_S \approx 0.028$ Ω, and $R \approx 0.9997$. This leads to the rough approximation $\overline{P_{abs}} \approx 4.2\ I_i$ [W cm^{-3}]. Given this absorbed power, the surface temperature can rise to a very high level, potentially leading to mirror damage. The surface temperature is determined largely by the thermal conductivity of copper, which, in pure form, is approximately 4.0 W-cm^{-1} K^{-1} at 300 K.

Unlike the metal, the absorbed power in the photonic crystal is a parasitic mechanism, unrelated to the distributed reflection. Intuitively, we expect the intensity of a broad beam (compared to a lattice constant) will decay in the photonic crystal as $I(z) = I_0\exp[-(\alpha_r + \alpha_a)z]$, where α_r is the decay constant associated with the (lossless) reflection, α_a is the

decay constant associated with the real absorption in the dielectric material, and z = 0 is at the air photonic-crystal interface. The decay of power per unit volume (caused by reflection and absorption) is given by $-dI/dz = (\alpha_r + \alpha_a)I_0\exp[-(\alpha_r + \alpha_a)z] = (\alpha_r + \alpha_a)I_0$. The portion of this decay associated with absorption is given by $\alpha_a I_0 \equiv P_{abs}$, so the net power absorbed per unit area down to a depth z is

$$I_{abs} \equiv \int_0^z P_{abs}dz' = \frac{\alpha_a I_0}{\alpha_a + \alpha_r}\left[1 - \exp(-[\alpha_a + \alpha_r]z)\right], \qquad (1)$$

and the average absorbed power per unit volume is

$$\overline{P_{abs}} = z^{-1}\int_0^z P_{abs}dz' = \frac{\alpha_a z^{-1} I_0}{\alpha_a + \alpha_r}\left[1 - \exp(-[\alpha_a + \alpha_r]z)\right]. \qquad (2)$$

Note, in the usual case where $\alpha_r >> \alpha_a$, $\overline{P_{abs}}$ saturates much more rapidly with z than it does in bulk dielectric material having loss α_a. This illustrates the fact that little power can be absorbed after most of it is already reflected from the crystal.

For example, we consider a photonic crystal made from high-resistivity ($\rho \approx 1\times10^4$ Ω-cm) silicon. In bulk form, this material has an absorption coefficient α_0 of approximately 0.1 cm^{-1} [9]. The value of α_a in the photonic crystal should be less than this, since the volumetric fraction of the silicon will be much less than unity. In the present analysis, we make a worst case estimate of $\alpha_a = \alpha_0$. For consistency, we also assume that the photonic crystal has an overall thickness that yields approximately the same reflection (0.9997) as the copper mirror. In a typical photonic crystal at 10 GHz, $\alpha_r \approx 2.0$ cm^{-1} and a ≈ 1 cm, so the same reflectivity as the copper is achieved with roughly four lattice constants, 4a. Substituting these parameters into Eq. (2), we find $\overline{P_{abs}}(z=4\text{ cm}) \approx 0.012\cdot I_0$ W-cm^{-3}. This is 0.3% of the same quantity estimated above for the copper mirror. This result coupled with the fact that the thermal conductivity of silicon (1.5 W-cm^{-1}-K^{-1} [15]) is within a factor of three of copper at room temperature means the surface temperature of the silicon photonic-crystal mirror is probably much lower for a given incident intensity. Similar reasoning would suggest other high-permittivity dielectric materials with good thermal conductivity may be even better because of their higher electrical resistivity and, hence, lower absorption coefficient. One notable material would be sapphire ($\varepsilon \approx 9.4$), whose resistivity is so high that the residual alternative is probably caused by a mechanism other than free-carrier absorption at microwave frequencies.

6. Photonic-Crystal Heterostructures

Most conventional photonic crystals studied to date provide a limited stop-bandwidth of about 15% of the center frequency. To overcome this limit, we have investigated a composite structure fabricated by stacking monolithic sections of our (111)-oriented fcc crystal as shown in Fig. 9 [16]. By making a discrete change in the lattice constant between adjacent monolithic sections, the net stop-bandwidth can be extended well beyond that of a given section.

One of the features that makes the composite crystal attractive is the high transmission through the individual monolithic sections *outside* the stop band. This was exemplified in Fig. 3, where we saw the experimental transmission just below the stop band approached 90%. This means the net reflection can be very high at frequencies within the stop band of sections lying well below the top of the heterostructure. Without this property, large standing waves would likely be established between the photonic band gap buried section and the partially reflecting upper layer or layers above it. This would lead to a resonantly high net reflection at some frequencies, but very low reflection at others. Of course, such behavior would be undesirable for most applications.

6.1. CRYSTAL DESIGN

In the absence of standing waves between the individual sections, the net reflection from the photonic-crystal heterostructure can be determined by an incoherent addition of the power reflected from each section. This leads to the following expression for the total reflection,

$$R_T \approx R_1 + T_1R_2T_1 + T_1R_2^2R_1T_1 + T_1R_2^3R_1^2T_1 + \ldots = R_1 + \frac{T_1^2R_2}{1-R_1R_2}, \qquad (3)$$

where R_1 (T_1) and R_2 are the reflections (transmissions) from the upper- and lower-frequency, respectively, associated with each heterojunction.

In a rough sense, the maximum overall bandwidth will result from a contiguous arrangement of the band gaps of the adjacent sections in the composite structure. Assuming the band gap of each section has a constant fractional width d about the center frequency, one can derive (by mathematical induction) the following expressions for the overall fractional width Δ,

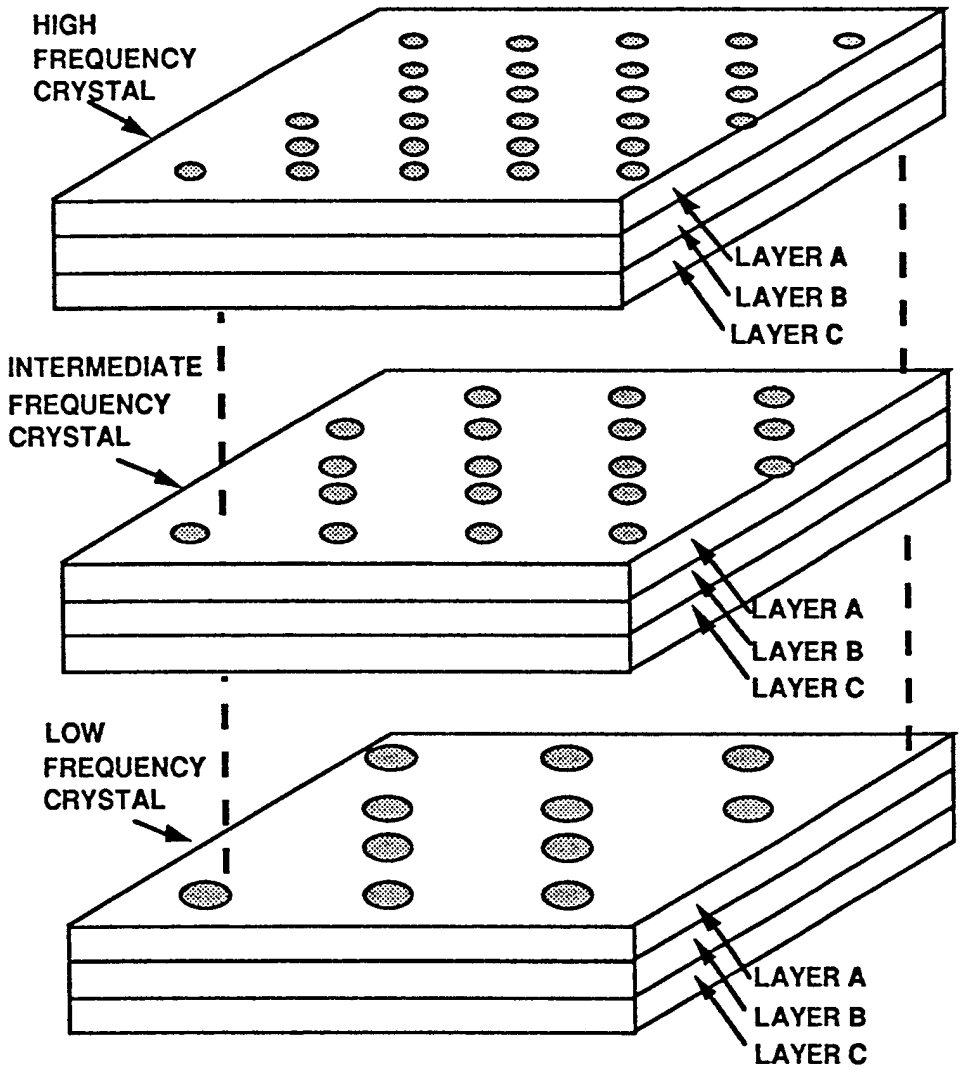

Fig. 9. Photonic crystal heterostructure consisting of a vertical stack of fcc crystals having different lattice constants.

$$\Delta = \frac{(1+\delta/2)^N - (1-\delta/2)^N}{(1+\delta/2)^N + (1-\delta/2)^N}, \qquad (4)$$

and the ratio r of the maximum and minimum frequencies of the overall band gap, $r = (1 + \delta/2)^N/(1 - \delta/2)^N$. The values of r for various values

Table I. Ratio of maximum to minimum frequency of the stop band of a heterostructure consisting of N sections of monolithic photonic crystal, each having $\delta = 15\%$

N	1	2	3	4	5	6	7	8	9	10
r	1.16	1.35	1.57	1.82	2.12	2.46	2.86	3.33	3.87	4.49

of N are listed in Table I, assuming a δ of 15%. Notice a gap width of over one octave ($r = 2$) can be obtained with just 5 sections and over two octaves with 10 sections.

6.2. EXPERIMENTAL RESULTS

A photonic crystal heterostructure consisting of three different sections of the Lincoln Laboratory fcc crystal has been constructed and tested in the range of 15 to 25 GHz. Figures 10(a) through 10(d) show the experimental transmission at normal incidence through the heterostructure, the high-frequency component crystal, the middle-frequency component crystal, and the low-frequency component crystal. The heterostructure has a maximum rejection of approximately 48 dB at 22.5 GHz, a minimum rejection of approximately 7 dB at 17.9 GHz, and a stop band that extends from 16 to at least 25 GHz. The low rejection at 17.9 GHz occurs from too little overlap between the component band stops as seen in Figs. 10(c) and 10(d). Clearly, the rejection of the heterostructure around 22.5 GHz is being assisted by the 2nd stop band of the low-frequency crystal, as seen in Fig. 10(d). The fact that it is much deeper than the 1st stop band is typical for the Lincoln Laboratory fcc crystal.

7. Summary

The existence of a three-dimensional stop band in photonic crystals enables several interesting applications, such as high-power mirrors and planar-antenna substrates. The mirror application utilizes the fact that the reflection process is distributed in space over at least one lattice constant, so the heat generated by residual absorption density (power absorbed per unit volume) in the dielectric component of the crystal is much smaller than it is in conventional, all-metal mirrors. The heat problem is also alleviated by the fact that the high-permittivity materials required for conventional photonic crystals tend to have high thermal conductivity. The application of photonic crystals as substrates for planar antennas is unique in the sense that it requires the presence of the three-dimensional

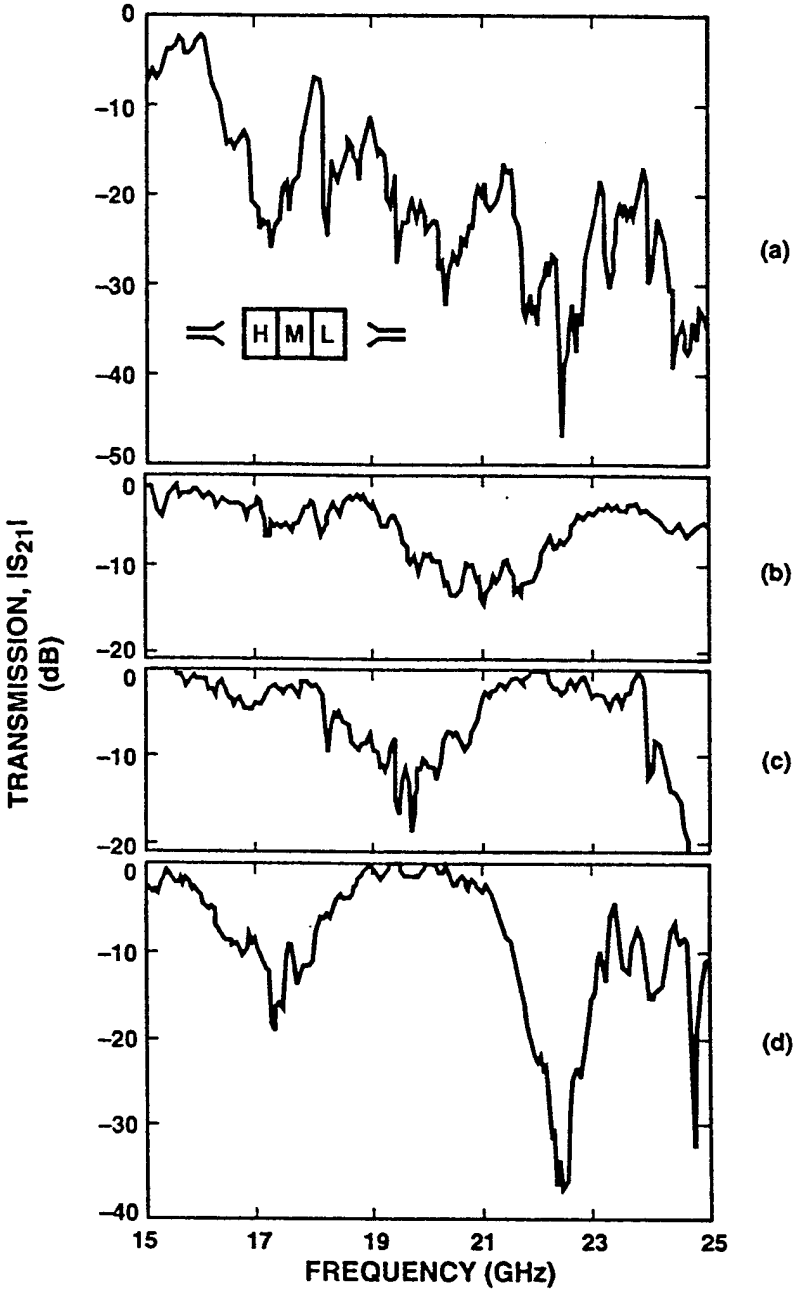

Fig. 10. (a) Magnitude of transmission for three-section photonic-crystal heterostructure over the range of 15 to 25 GHz. (b) Also shown is the isolated transmission through the (b) high-frequency section, (c) mid-frequency section, and (d) low-frequency section.

stop band, antennas naturally being three-dimensional radiators. In addition, the fact that the reflection is distributed means that the antenna is not shorted out at the driving point, as are planar antennas mounted directly on metal. Finally, we have explored a way of increasing the spectral bandwidth of photonic crystals in these applications. The technique is to stack sections of photonic crystal having different lattice constants. This technique, which is analogous to constructing heterostructures in electronic semiconductors, is well suited to the high-power mirror application.

References

[1] E. Yablonovitch, T. J. Gmitter, and K. M. Leung, Phys. Rev. Lett. **67**, 2295 (1991).

[2] K. M. Ho, C. T. Chan, C. M. Soukoulis, R. Biswas, and M. Sigalas, Solid. State Commun. **89**, 413 (1994).

[3] H. S. Sözüer and J. P. Dowling, J. Mod. Opt. **41**, 231 (1994).

[4] E. Özbay, E. Michel, G. Tuttle, R. Biswas, M. Sigalas, and K.-M. Ho, Appl. Phys. Lett. **64**, 2059 (1994).

[5] E. R. Brown, K. Agi, C. D. Dill III, C. D. Parker, and K. J. Malloy, Microw. Opt. Tech. Lett. **7**, 777 (1994).

[6] R. D. Meade, K. D. Brommer, A. M. Rappe, and J. D. Joannopoulos, Appl. Phys. Lett. **61**, 495 (1992).

[7] N.W. Ashcroft and N.D. Mermin, *Solid State Physics* (Saunders College, Philadelphia, 1976).

[8]. K. H. Ho, C. T. Chan, and C. M. Soukoulis, Phys. Rev. Lett. **65**, 3152 (1990).

[9] M. N. Afsar and K. J. Button, Proc. IEEE **73**, 131 (1985).

[10] D. B. Rutledge, D. P. Neikirk, and D. P. Kasilingam, "Integrated-Circuit Antennas," in *Infrared and Millimeter Waves,* Vol. 10 (Academic, Orlando, 1983), p. 1.

[11] R. D. Meade, K. D. Brommer, A. M. Rappe, and J. D. Joannopoulos, Phys. Rev. B **44**, 10961 (1991).

[12] E. R. Brown, C. D. Parker, and E. Yablonovitch, J. Opt. Soc. Am. B **10**, 404 (1993).

[13] E. R. Brown, C. D. Parker, and O. B. McMahon, Appl. Phys. Lett. **64**, 3345 (1994).

[14] E. Yablonovitch, Phys. Rev. Lett. **58**, 2059 (1987).

[15] S. Sze, *Physics of Semiconductor Devices* , 2nd Ed. (Wiley, New York, 1981), p. 850.

[16] K. Agi, E. R. Brown, O. B. McMahon, C. Dill III, and K. J. Malloy, Electron. Lett. **30**, 2166 (1994).

To appear in: Ultra-Wideband, Short-Pulse Electromagnetics 2
H.L. Bertoni, L. Carin, L.B. Felsen, and S.U. Pillai, eds.
Plenum Publishing

AN ULTRA-WIDEBAND PHOTONIC CRYSTAL

K. Agi,[1] E.R. Brown,[2] C. Dill III,[2] O.B. McMahon,[2] and K.J. Malloy[1]

[1]Center for High Technology Materials
University of New Mexico
Albuquerque, NM 87131

[2]Lincoln Laboratory, Massachusetts Institute of Technology
Lexington, MA 02173-9108

ABSTRACT

We report the fabrication and characterization of a novel photonic crystal in which multiple face-centered-cubic (fcc) crystals of different lattice constants are stacked in tandem. This results in a photonic stop band that is broadened well beyond that achievable with a single lattice periodicity. The sample reported here is comprised of two fcc crystals having photonic stop bands centered around 16.5 and 21.5 GHz, respectively. K-band feedhorns were used to transmit and receive radiation through the sample. A network analyzer was used to measure S_{21} and S_{11} between 14 and 26 GHz. The overall stop band is approximately the superposition of the individual stop bands of the component fcc crystals.

A photonic bandgap (PBG) structure is a periodic arrangement of dielectric material that exhibits a frequency stop band in three-dimensions.[1] The original PBG structure, developed by Yablonovitch, was a face-centered-cubic (fcc) arrangement of quasi-spherical air atoms in a dielectric host. The fabrication of this crystal consisted of precisely drilling holes in a dielectric block of Stycast-12 (three holes drilled 35° off normal and rotated azimuthally by 120°) [2]. The shape, depth and location of the bandgap are determined by the shape of the atoms, their periodicity, and the dielectric constant of the host in a photonic crystal. PBG structures are in many ways analogous to semiconductors with forbidden energy gaps.

Recently, we have devised a new, more robust method of fabricating a photonic crystal.[3] It consists of a vertical stack of dielectric slabs, each slab containing a two-dimensional triangular lattice of cylindrical air atoms. In principle, the cylindrical air atoms could provide a wider stop band due to their larger electromagnetic scattering cross section in comparison with the quasi-spherical atoms used in the past. This pattern is achieved very simply by simultaneously drilling vertical holes through all the plates on a milling machine. To obtain a three-dimensional PBG structure, the plates are stacked one on top of the other in an offset manner. To obtain the fcc arrangement, the repeat unit consists of three slabs (A,B,C) in which the second slab (B) is aligned such that each atom lies directly above the center of the triangular unit cell in the first layer. The third slab (C) is aligned such that the atoms lie directly above the remaining unit cells in the first layer. A top view of the stack is shown in Fig. 1. The fcc lattice results when the triangular lattice constant t is related to the slab thickness, s, by $t = \sqrt{\frac{3}{2}}s$. Hence, the conventional lattice constant, a, for the fcc is given by $a = \sqrt{2}t$. The robust nature of the new crystal is manifested by the ease of fabrication and mechanical stability associated with drilling vertical holes.

To obtain the ultra-wideband (UWB) photonic crystal, multiple fcc crystals with different lattice constants are stacked vertically as shown in Fig. 2(a). This will result in a photonic stop band which is much broader than that achievable with a single lattice constant. The host material for the crystals is a synthetic low-loss dielectric such as Stycast, whose permittivity of 13 remains constant over the frequency range of interest. The patterns are drilled in the respective Stycast slabs in a single milling operation. The sections of a given lattice constant are then clamped together.

The electromagnetic response of the system is characterized in both transmission and reflection. K-band feedhorns were used to transmit and receive electromagnetic radiation through the sample. An HP 8510 network analyzer was used to measure the microwave reflection coefficient, S_{11}, and transmission coefficient, S_{21}, from 14 to 26 GHz. The experimental set up is shown in Fig. 2(b).

As a first demonstration, we have constructed a UWB crystal with two lattice constants. The triangular lattice constant for the first periodicity is t=0.778 cm and the dimensions of the sheets used are 15.2 cm x 15.2 cm x 0.635 cm. The triangular lattice constant for the second periodicity was t=0.622 cm with the dimensions of the plates being 15.2 cm x 15.2 cm x 0.508 cm. The sample reported here consisted of two fcc crystals whose stop bands were centered about 16.5 GHz for the t=0.778 cm crystal and 21.5 GHz for the t=0.622 cm crystal. Transmission measurements for the these crystals are shown in Fig 3(a) and (b) respectively.

In order to maintain the offset, three alignment holes are drilled in the corners of the slabs. The alignment holes are positioned at the apex of an equilateral triangle with side $l = \frac{a}{\sqrt{3}}$. Since there are two separate periodicities in the UWB crystal, the alignment holes of one component crystal do not coincide with the holes of the other. One way to overcome this is to drill a set of global alignment holes. However, here we chose to use a series of small pins passing through each of the individual alignment holes, then clamping the entire structure together. The UWB-PBG structure consists of only one unit cell (3 sheets) for each periodicity. It has been shown elsewhere that as the number of units cells is increased, the depth of the gap is increased.[3]

For the UWB crystal, transmission (S_{21}) results taken along the [111] direction (L-point in the Brillouin zone), shown in Fig. 3c, indicate that the overall stop band is approximately the superposition of the individual stop bands. S_{21} measurements were also taken in the [110] direction (K-point in the Brillouin zone) (Fig. 4) and [210] direction (W-point in the Brillouin zone) (Fig. 5). All measurements indicate that the overall stop band is the superposition of the component stop bands.

Reflection (S_{11}) measurements for the UWB crystal and the component fcc crystals are shown in Fig. 6. The reflection coefficient increases inside the stop band for all cases. S_{11} measurements for the UWB crystal indicate that the overall stop band is again the superposition of the respective stop bands of the component crystals. Due to the complexity of doing S_{11} measurements, only normal incidence (L-point) was considered here. However, for the 16.5 GHz crystal, reflection measurements in other directions can be found elsewhere.[3]

In summary, we have fabricated and characterized a novel UWB photonic crystal. Our first sample, which consisted of two fcc crystals stacked in tandem, displayed an overall stop band that was approximately the superposition of the component crystals. This stop band is broadened well beyond that achievable with a single crystal. Currently, we are investigating methods of integrating photonic crystals with antennas and other microwave

printed circuits such as microstrip and coplanar strip transmission lines.

ACKNOWLEDGMENTS

This work was sponsored by the Department of the Air Force, in part through an AASERT grant from the Air Force Office of Scientific Research.

REFERENCES

1. E. Yablonovitch and T.J. Gmitter, "Photonic Band Structure: The Face-Centered-Cubic Case," Phys. Rev. Lett., vol. 63, no. 18, Oct. 30, 1989.

2. E. Yablonovitch, T.J. Gmitter and K.M. Leung, "Photonic Band Structure: The Face-Centered-Cubic Case Employing Nonspherical Atoms," Phys. Rev. Lett., vol. 67, no. 17, Oct. 21, 1991.

3. E.R. Brown, K. Agi, C.D. Dill, C.D. Parker, K.J. Malloy," A New Face-Centered-Cubic Crystal For Microwave and Millimeter Wave Applications," submitted to Appl. Phys. Lett..

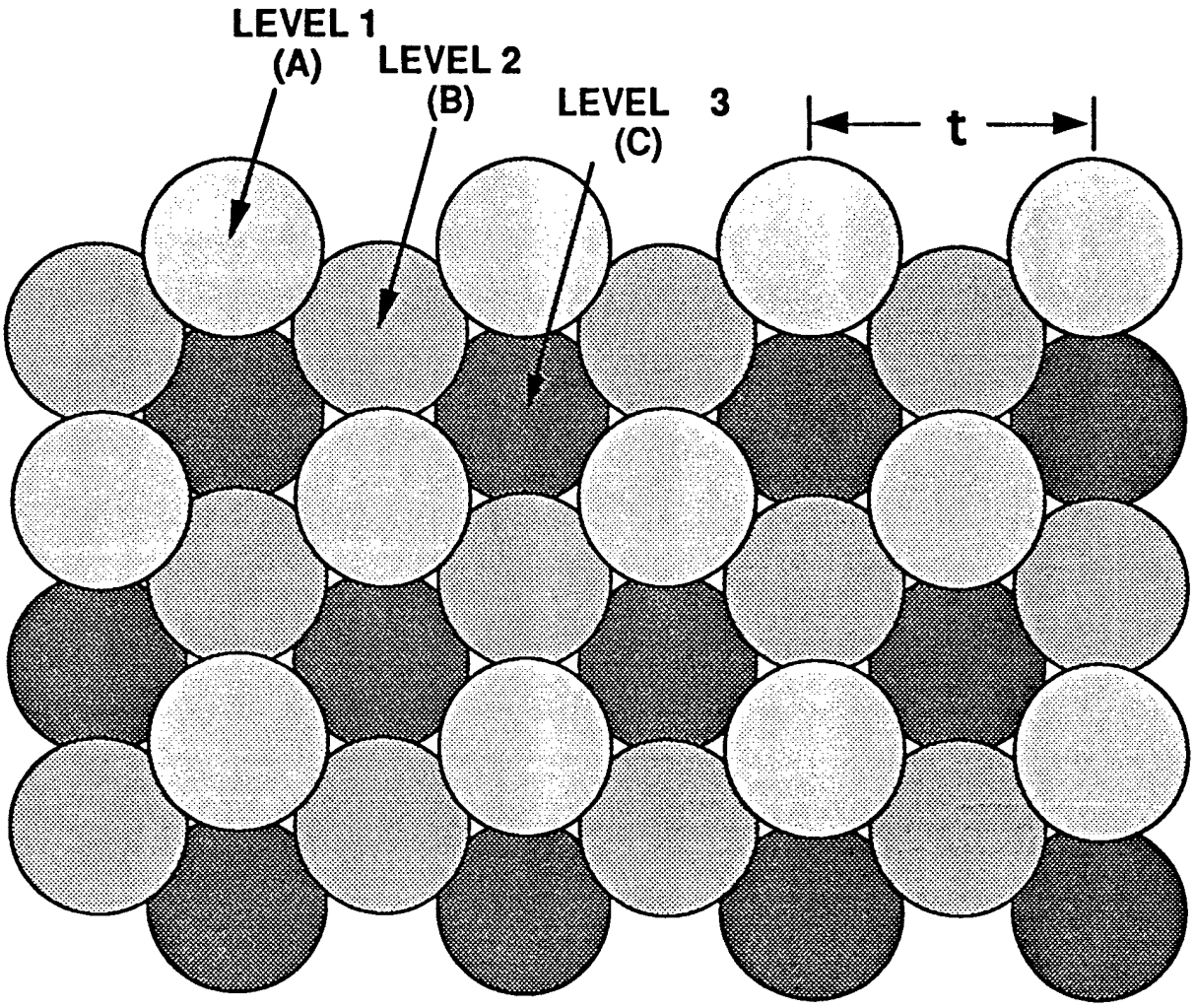

Figure 1. Top view of three successive layers of the component fcc component crystal. The circles represent the cylindrical basis drilled into each layer. The top layer is shown as lightly shaded, the middle layer is intermediately shaded and the bottom layer is the dark shaded.

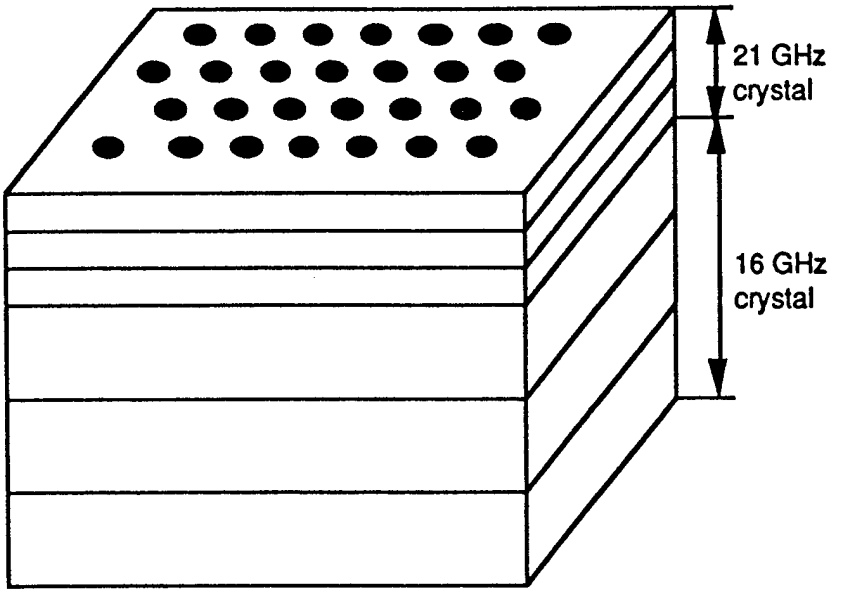

(a)

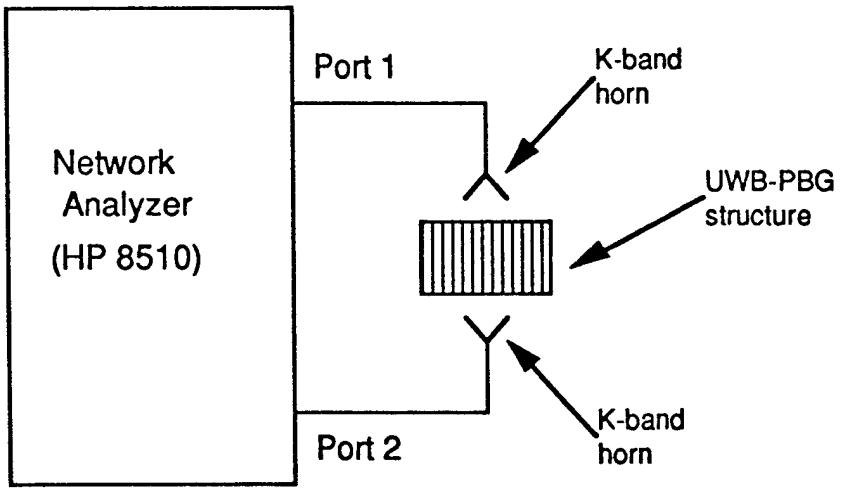

(b)

Figure 2. (a) Diagram of UWB photonic crystal. The holes are drilled perpendicular to the face of the slabs. (b) Experimental set-up for transmission (S_{21}) and reflection (S_{11}) measurements. The photonic crystal is rotated off normal to obtain TE polarization measurements and azimuthally to obtain TM polarization measurements.

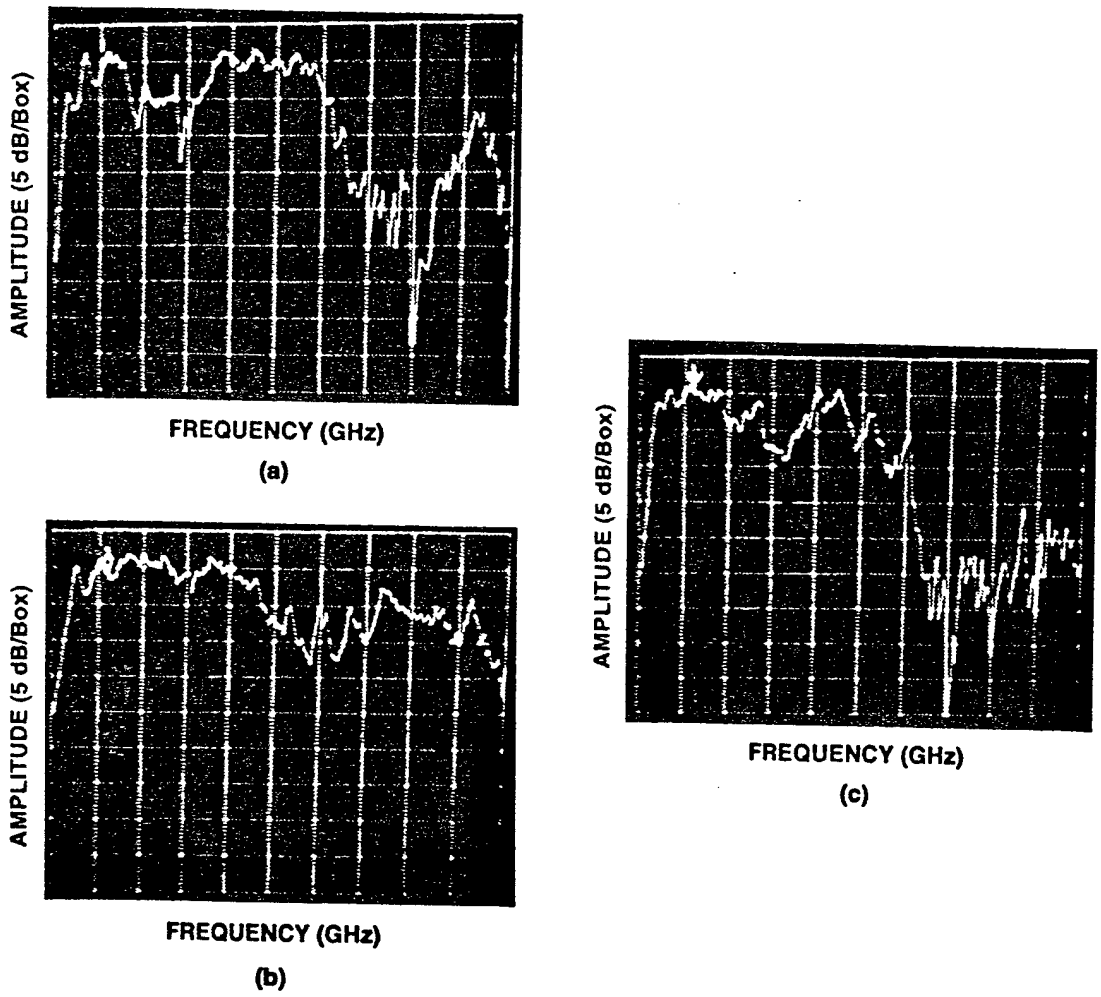

Figure 3. Transmission along [111] direction (L-point in Brillouin Zone). (a). Ku-band crystal from 14-26 GHz. (b). K-band crystal from 14-26 GHz. (c). Ultra-Wideband crystal from 14-26 GHz. Response is approximately the superposition of the component crystals.

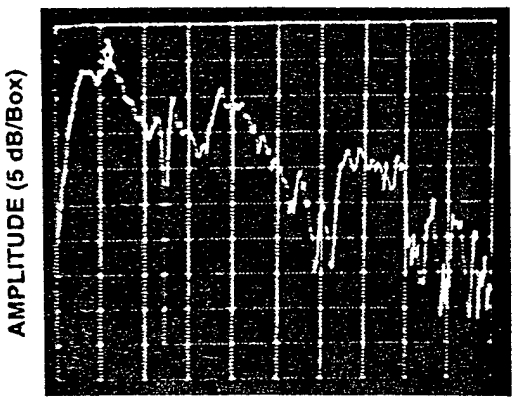

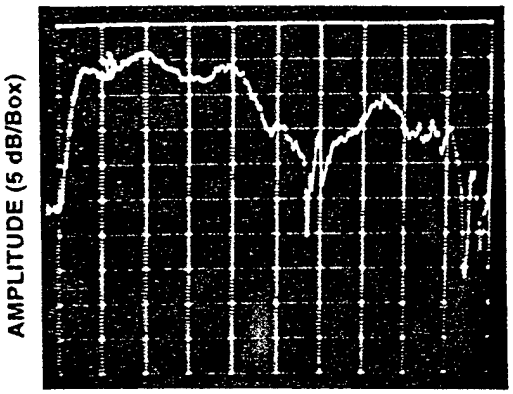

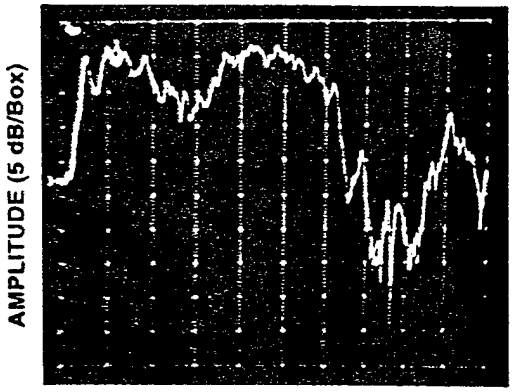

Figure 4. Transmission along [110] direction (K-point in Brillouin Zone). (a). Ku-band crystal from 14-26 GHz. (b). K-band crystal from 14-26 GHz. (c). Ultra-Wideband crystal from 14-26 GHz. Response is approximately the superposition of the component crystals.

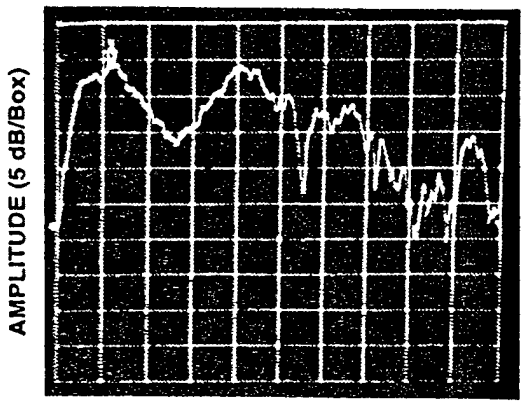

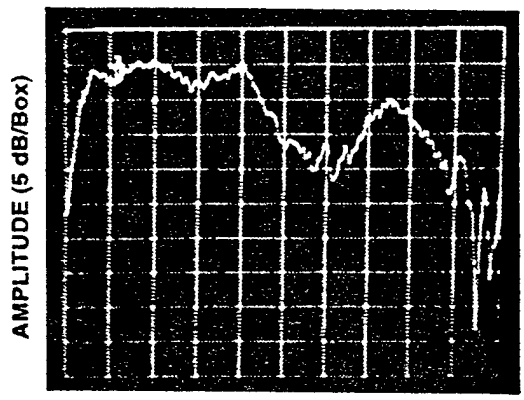

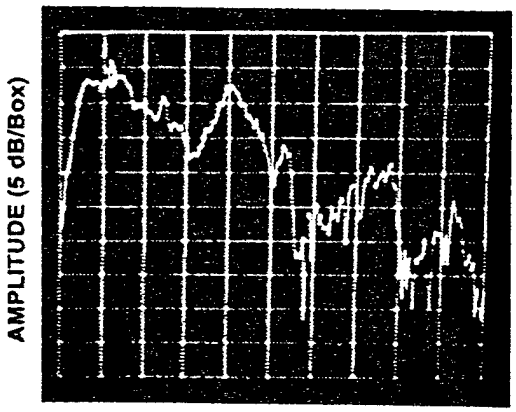

Figure 5. Transmission along [210] direction (W-point in Brillouin Zone). (a). Ku-band crystal from 14-26 GHz. (b). K-band crystal from 14-26 GHz. (c). Ultra-Wideband crystal from 14-26 GHz. Response is approximately the superposition of the component crystals.

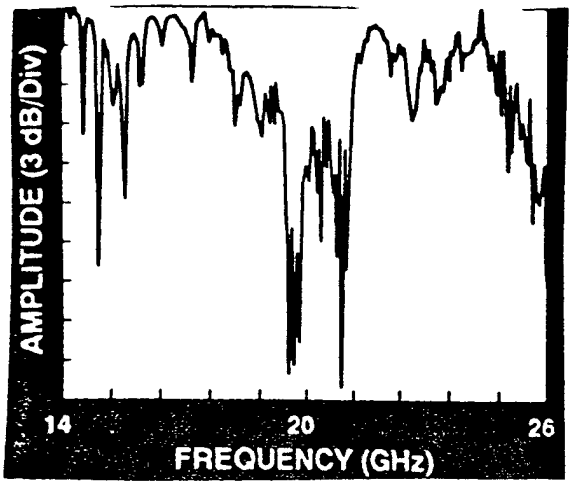

(a)

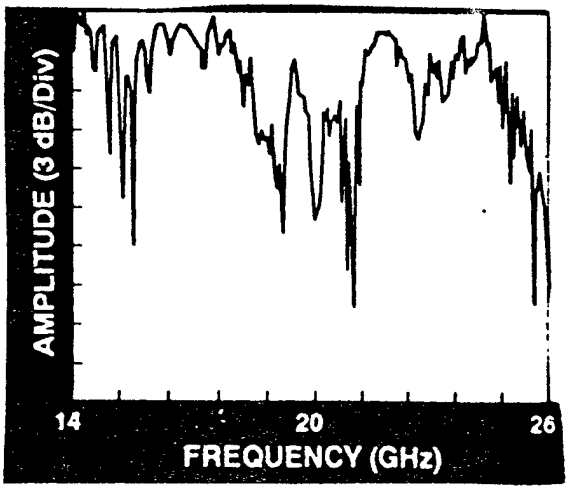

(c)

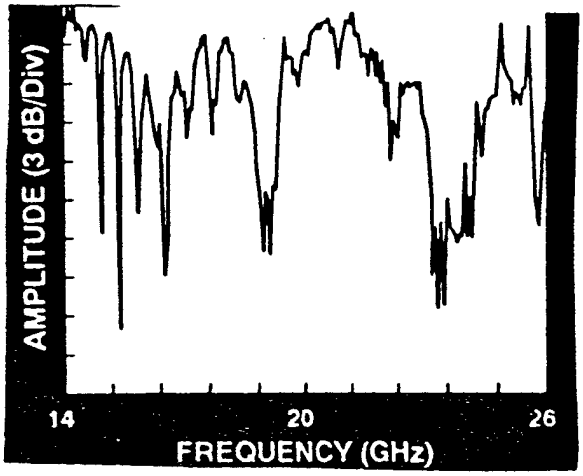

(b)

Figure 6. Reflection from [111] direction (L-point in Brillouin Zone). (a). Ku-band crystal from 14-26 GHz. (b). K-band crystal from 14-26 GHz. (c). Ultra-Wideband crystal from 14-26 GHz. Response is approximately the superposition of the component crystals.

It can be seen from Fig. 1 that the UV exposure has shifted the pass and rejection bands by ~30nm towards longer wavelengths. This is consistent with an overall increase in the refractive indices of both cores, because the increased mode confinement will decrease the coupling coefficient C, and consequently increase the beat length $L_b = \pi F C$ provided that F, the fractional power transferred, is close to unity [1]. No significant change in the passband signal level was observed during exposure.

Conclusions: By preferentially exposing one core to UV radiation, the coupling of twin-core fibres with nominally identical cores has been improved to give isolation in excess of 22dB over a 20nm bandwidth. This performance is superior to that offered by commercially available single-stage tapered coupler demultiplexers, and the ability to improve the isolation relaxes the stringent tolerances on fabricating twin-core fibres for demultiplexing applications.

Acknowledgements: The authors thank M.G. Sceats and S.B. Poole of the Optical Fibre Technology Centre, J.D. Love of the Optical Sciences Centre and P.L. Chu of the Optical Communications Group for valuable discussions, and B. Wu of the Optical Communications Group for assistance with sample preparation. This work was performed as part of the Multicore Optical Fibre Devices project funded by Siemens (Australia) Ltd through the Generic Industrial Research and Development (GIRD) programme. The Optical Fibre Technology Centre, Optical Communications Group and Optical Sciences Centre are members of the Australian Photonics Co-operative Research Centre.

13 October 1994

Electronics Letters Online No: 19941432

G.R. Atkins (*Optical Fibre Technology Centre, University of Sydney, NSW 2006, Australia*)

J.W. Arkwright (*Siemens (Australia) Ltd, 885 Mountain Highway, Bayswater, VIC 3153, Australia*)

(*Currently seconded to the Optical Communications Group, School of Electrical Engineering, University of New South Wales, NSW 2052, Australia*)

S.J. Hewlett (*Optical Sciences Centre, Institute of Advanced Studies, Australian National University, Canberra, ACT 0200, Australia*)

References

1 SNYDER, A.W., and LOVE, J.D.: 'Optical waveguide theory' (Chapman and Hall, London, 1983), pp. 567–585

2 HIMENO, K., SAWADA, M., YAMASAKI, S., KAWAMAKI, N., and YAMAUCHI, R.: 'Novel optical-fiber-coupler fabrication technique using multicore fibers', Optical Fiber Communication Conf. (OFC'93), San Jose, 1993, Paper WG1

3 OKAMOTO, K., and NODA, J.: 'Fibre-optic spectral filter consisting of concatenated dual-core fibres', *Electron. Lett.*, 1986, **22**, (4), pp. 211–212

4 ARKWRIGHT, J.W., GILLHOF, B., ALLEN, P.M., CHU, P.L., WHITBREAD, T.W., WU, B., HEWLETT, S.J., LOVE, J.D., ATKINS, G.R., POOLE, S.B., SCEATS, M.G., and THORNCRAFT, D.A.: 'Demonstration of an optical to electrical demultiplexing detector using critically fabricated twin-core fibre', Submitted to 19th Australian Conf. on Optical Fibre Technology (ACOFT'94), December 1994, (Melbourne)

5 KASHYAP, R., MAXWELL, G.D., and AINSLIE, B.J.: 'Laser-trimmed four-port bandpass filter fabricated in single-mode photosensitive Ge-doped planar waveguide', *IEEE Photonics Technol. Lett.*, 1993, **5**, (2), pp. 191–194

6 SAIFI, M.A., SIBERBERG, Y., WEINER, A.M., FOLCKHARDT, H., and ANDREJCO, M.J.: 'Sensitivity of two core fiber coupling to light-induced defects', *IEEE Photonics Technol. Lett.*, 1989, **1**, (11), pp. 386–388

Design of ultrawideband photonic crystals for broadband antenna applications

K. Agi, E.R. Brown, O.B. McMahon, C. Dill III and K.J. Malloy

Indexing terms: Photonic bandgaps, Crystals, Optics

Face-centred-cubic photonic crystals with overlapping stop bands are stacked in tandem to obtain an ultrawideband photonic crystal. This crystal has a stop band that extends from 16 to at least 25GHz and has a minimum rejection of ~7dB at normal incidence. Different stacking configurations have been studied, and cavity modes between nonadjacent crystals with overlapping stop bands have been observed.

Photonic crystals are three-dimensionally periodic dielectric structures that exhibit a forbidden gap in frequency. One application of photonic crystals is to increase the radiation efficiency of antennas printed on dielectric substrates. For example, the energy from a simple dipole antenna, printed on a dielectric, is predominantly radiated into the dielectric (97% for $\varepsilon = 10$) [1]. Recently, it has been shown that by printing antennas on photonic crystal structures, the energy can be rejected from the substrate and radiated preferentially into the air [2]. This occurs when the frequency of radiation from the antenna lies within the stop band of the crystal, so that the substrate reflects the radiation into the air.

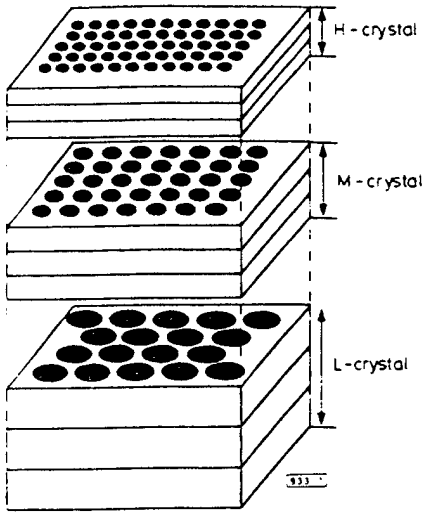

Fig. 1 *Ultrawideband (UWB) photonic crystal made by stacking in tandem high-, medium-, and low-frequency (H, M, and L), single-period photonic crystals with overlapping stop bands*

The operational bandwidth for efficient broadband antennas is governed by the width of the stop band in the photonic crystal. The stop-band width is dictated by the dielectric contrast (index step) and the size and shape of the 'atoms' in the photonic crystal [3], and is thus limited in extent. For example, a face-centred cubic crystal having $\varepsilon = 12$ and air atoms constituting 86% of the total volume has a stop-band width of ~20% of the centre frequency [4]. For the component crystals used here ($\varepsilon = 10$), the air atoms constitute only 60% of the total volume and the stop-band width is on average ~15% of the centre frequency. One way to broaden the stop-band for certain directions is to place, in tandem, multiple photonic crystals whose stop bands cover different frequency ranges that do not overlap [5]. This results in a broader overall operational bandwidth, but one in which the frequencies between the stop bands can propagate into the dielectric. To overcome this problem, photonic crystals with overlapping stop bands have been developed in the present work. The result is called an ultrawideband (UWB) photonic crystal, and is schematically shown in Fig. 1 (UWB is defined as a signal whose bandwidth is at least 25% of its centre frequency [6]).

The description of the fabrication of the component photonic crystals can be found elsewhere [7]. To characterise the stop

bands, a network analyser is used in conjunction with a pair of K-band horn antennas to perform scattering parameter (S_{21}) measurements. The transmission through the crystal is deconvolved from the system transmission by using a measurement without the crystal as the reference.

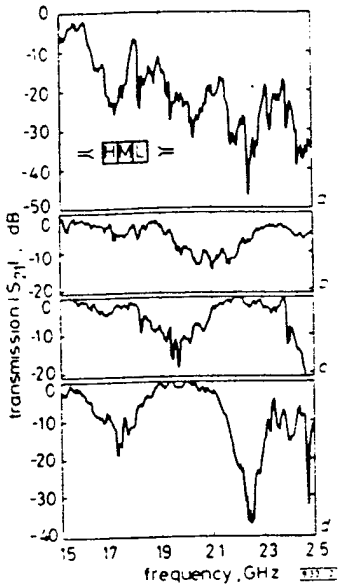

Fig. 2 *Transmission magnitude (S_{21}) for UWB photonic crystal H crystal response, M crystal response, S_{21} and for L crystal response*

a UWB photonic crystal ; Inset: stacking configurations
b *H* crystal
c *M* crystal
d *L* crystal

By placing the component crystals in tandem, the overall bandwidth might be expected to be the sum of the component bandwidths. However, in addition to the fundamental stop bands, there are higher order stop bands that contribute to the overall UWB stop band (see for example Fig. 2*c* and *d*). The exact source of these higher order bands is currently being investigated. In addition, there is a possibility of multiple pass interference between component crystals, particularly at frequencies within the overlap between the adjacent stop bands.

Fig. 2*a–d* show, respectively, the typical UWB crystal and the component high-, medium-, and low-frequency (*H*, *M*, and *L*) crystal transmissions at normal incidence for the stacking configuration depicted in the inset. The UWB crystal transmission (Fig. 2*a*) has a minimum rejection (maximum transmission) of ~7dB at 17.9GHz, a maximum rejection (minimum transmission) of ~48dB at 22.5GHz, and a stop band that extends from 16 to at least 25GHz.

The stacking sequence of the component crystals in the UWB crystal is important as cavity modes can exist between the component crystals. Insight into these cavity modes is found by rearranging and removing components of the UWB crystal. Fig. 2*b* and *c* show that the overlap in the *H* and *M* stop bands occurs between ~19.5 and 21GHz. Fig. 3 shows the UWB crystal with and without the *L* crystal, as depicted in the inset, at normal incidence (the markers indicate the region of overlap in Fig. 2). Here there exist cavity modes between the *H* and *M* crystals due to the overlapping stop bands. The cavity mode contribution will cause a shift in frequency when the *L* crystal is placed between the *H* and *M* crystals due to the change in free spectral range. This occurs between 19.5 and 20.5GHz. The shift at 20.5 to 21GHz is attributed to the removal of the stop band of the *L* crystal. Because the effective dielectric constant of the *L* crystal is not known, it is difficult to determine the exact frequency of the cavity modes. However, other measurements have been taken (not shown here) for various distances of air between the *H* and *M* crystals. These measurements were taken with the *L* crystal in between the *H* and *M* crystals, the *L* crystal removed (i.e. only air between the *H* and *M* crystals), and a material with a known dielectric constant placed between the *H* and *M* crystals. The measurements verify the existence of the cavity modes by the fact that the free spectral range of the cavity changes with changing dielectric constant between the *H* and *M* crystals.

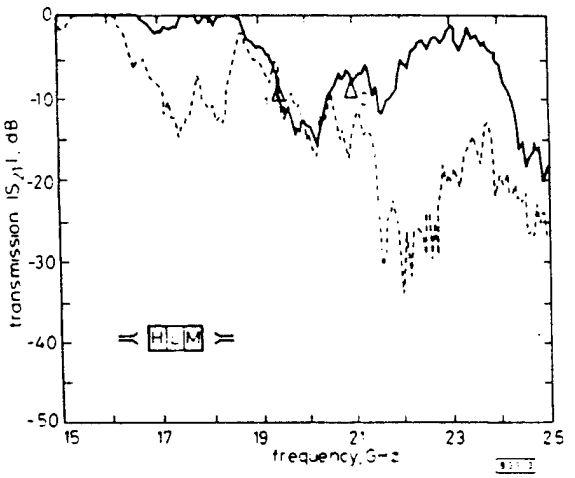

Fig. 3 *S_{21} for UWB crystal for H and M crystals separated by 2.7cm of air and H-L-M crystals stacked in tandem*

Inset: stacking configuration

Markers indicate overlap in stop bands between the *H* and *M* crystals

——— *H* and *M* crystals separated by 2.7cm of air
- - - - *H-L-M* crystals separated by 2.7cm of air

The overall stop band of a photonic crystal has been extended to cover the range from 16 to over 25GHz by stacking three photonic crystals with overlapping stop bands in tandem. The exact ordering of the component crystals is critical. It was found that crystals having overlapping stop bands have to be adjacent and in intimate contact with one another to avoid cavity modes. Finally, it was shown that an average rejection of ~20dB can be achieved over the 16–25GHz band by using three single-period photonic crystals.

Acknowledgment: This work was sponsored by the Air Force Office of Scientific Research in part through an AASERT Grant, and through the US Army Research Office.

12 October 1994
Electronics Letters Online No. 19941441

K. Agi and K. J. Malloy (*Center for High Technology Materials, University of New Mexico, Albuquerque, NM 87131, USA*)

E. R. Brown, O. B. McMahon and C. Dill III (*Lincoln Laboratory, Massachusetts Institute of Technology, Lexington, MA 02173-9108, USA*)

References

1 RUTLEDGE, D.B., NEIKIRK, D.P., and KASILINGAM, D.P.: 'Infrared and millimeter waves' (Academic, Orlando, FL, 1983), Vol. 10, Chap. 1

2 BROWN, E.R., PARKER, C.D., and YABLONOVITCH, E.: 'Radiation properties of a planar antenna on a photonic-crystal substrate', *J. Opt. Soc. Am. B*, 1993, **10**, (2), pp. 404–407

3 EVERITT, H.O.: 'Applications of photonic bandgap structures', *Opt. Photonics News*, Nov. 1992, pp. 20–23

4 YABLONOVITCH, E., GMITTER, T.J., and LEUNG, K.M.: 'Photonic band structure: The face-centered-cubic case employing nonspherical atoms', *Phys. Rev. Lett.*, 1991, **67**, (17), pp. 2295–2298

5 AGI, K., BROWN, E.R., DILL, C., III MCMAHON, O.B., and MALLOY, K.J.: 'An ultra-wideband photonic crystal', *in* BERTONI, H.L., CARIN, L., FELSEN, L.B., and PILLAI, S.U. (Eds.) 'Ultra-wideband, short-pulse electromagnetics 2' (Plenum, New York)

6 TAYLOR, J.D.: 'Ultra-wideband radar-potentials and limitations', IEEE Microwave Theory and Tech. Symp. Dig., 1991, pp. 367–370

7 BROWN, E.R., AGI, K., DILL, C., PARKER, C.D., and MALLOY, K.J.: 'A new face-centered-cubic photonic crystal for microwave and millimeter-wave applications', *Microw. Opt. Technol. Lett.*, Dec. 1994

Applications and Characterization of a New Face-Centered-Cubic Photonic Crystal

K. Agi,[1] E.R. Brown,[2] C.D. Dill,[2] K.A. McIntosh,[2] O.B. McMahon,[2] K.M. Molvar,[2] and K.J. Malloy[1]

[1]Center for High Technology Materials
University of New Mexico
Albuquerque, NM 87131

[2]Lincoln Laboratory, Massachusetts Institute of Technology
Lexington, MA 02173-9108

ABSTRACT

Recently, a new photonic crystal consisting of a face-centered-cubic (fcc) arrangement of cylindrical air atoms has been developed. In the present work, frequency-domain measurements are performed on this crystal in transmission using a network analyzer. In addition, time-domain measurements in transmission are performed by optoelectronically generating picosecond bursts of free-space electromagnetic radiation by photoconductively switching planar antennas. A direct comparison between the time-domain and frequency-domain measurement is performed. One application of the new fcc crystal involves stacking several sections with different lattice constants in tandem, thereby creating an ultra-wideband (UWB) photonic crystal.

Guided-Wave Optoelectronics
Edited by T. Tamir *et al.*, Plenum Press, New York, 1995

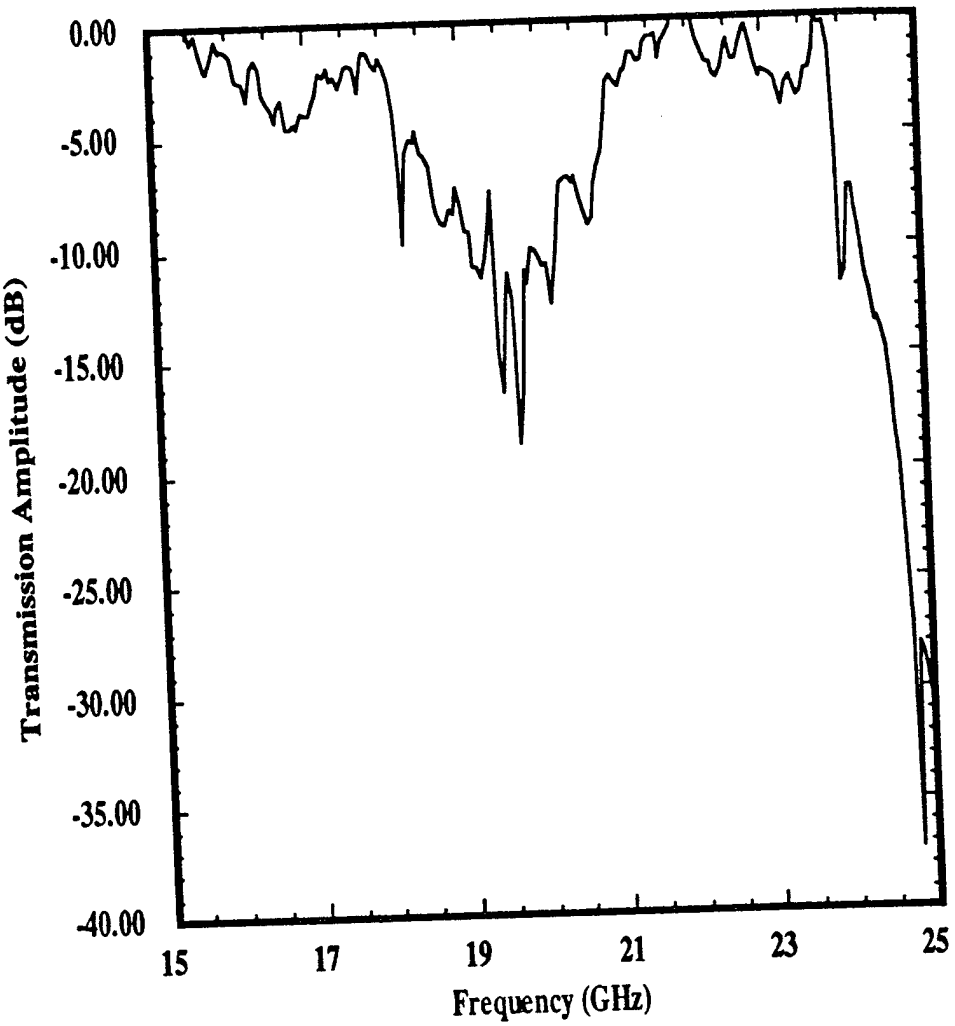

Figure 1. Continuous-wave (CW) frequency-domain measurement using network analyzer. Transmission ($|S_{21}|$) measurement of photonic crystal at normal incidence from 15 to 25 GHz.

A three-dimensionally periodic structure that exhibits an electromagnetic stop band in all 4π steradians is called a photonic bandgap (PBG) structure.[1] The original PBG structure, developed by Yablonovitch et al., was a face-centered-cubic (fcc) arrangement of quasi-spherical air atoms in a dielectric host. The fabrication of this crystal consisted of precisely drilling holes in a dielectric block of Stycast-12 (three holes drilled 35° off normal and rotated azimuthally by 120° at each lattice site).[2] Recently, a simpler method of fabricating an fcc photonic crystal has been developed. Briefly, the fabrication of the new crystal consists of drilling a triangular lattice of vertical holes in lossless dielectric plates (measurements on the dielectric host (Stycast, ε=10,13) indicate negligible loss). Three plates are then shifted and stacked one on top of the other to obtain a single period of an fcc lattice along the [111] direction of the cubic unit cell (a detailed description of the fabrication process can be found elsewhere[3]). The number of lattice periods can subsequently be increased by stacking more plates in the ordered sequence. The simple and robust nature of the new crystal is manifested by the ease of fabrication and mechanical stability associated with drilling cylindrical (vertical) holes.

The characterization of the crystals was done in two ways. First, K-band feedhorns were used to transmit and receive continuous-wave (CW) radiation through the sample. A network analyzer was used to measure the microwave transmission coefficient, S_{21}, from 15 to 25 GHz. The network analyzer was calibrated by first taking a direct measurement (e.g. no crystal) and using it as the baseline. The crystal is then placed in between the antennas and another measurement is taken. This calibration technique de-embeds the system response from the crystal response giving the frequency-domain transfer function of the crystal. The results of the transmission measurement at normal incidence are shown in Fig. 1 with the experimental set up shown in the inset. A shortcoming of this type of measurement is the upper frequency limit of the network analyzer.

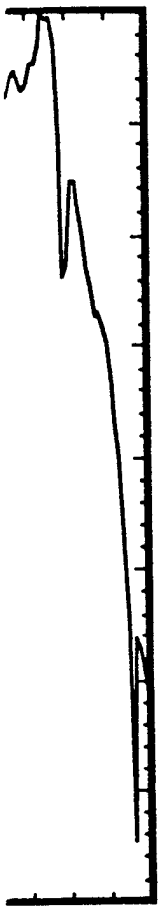

25

r. Transmission

In order to study the crystal over wider bandwidths, the second means of characterization was the transmission of short pulses in the time-domain. The experimental set up is shown in Fig. 2. A mode-locked titanium-sapphire laser is used to generate a train of a 250-fs-wide optical pulses at a repetition rate of 76 MHz and a wavelength of 750 nm. The 50 mW (average power) laser output beam is split into two approximately equal power beams. These optical beams are used to switch photoconductive gaps coupled to planar antennas. One beam is chopped at 1 kHz and is focused onto a transmitting antenna, which is dc biased at 40 V. The other is passed through an optical delay line and focused onto an unbiased receive antenna (the electric field of the received signal acts as the bias), which is

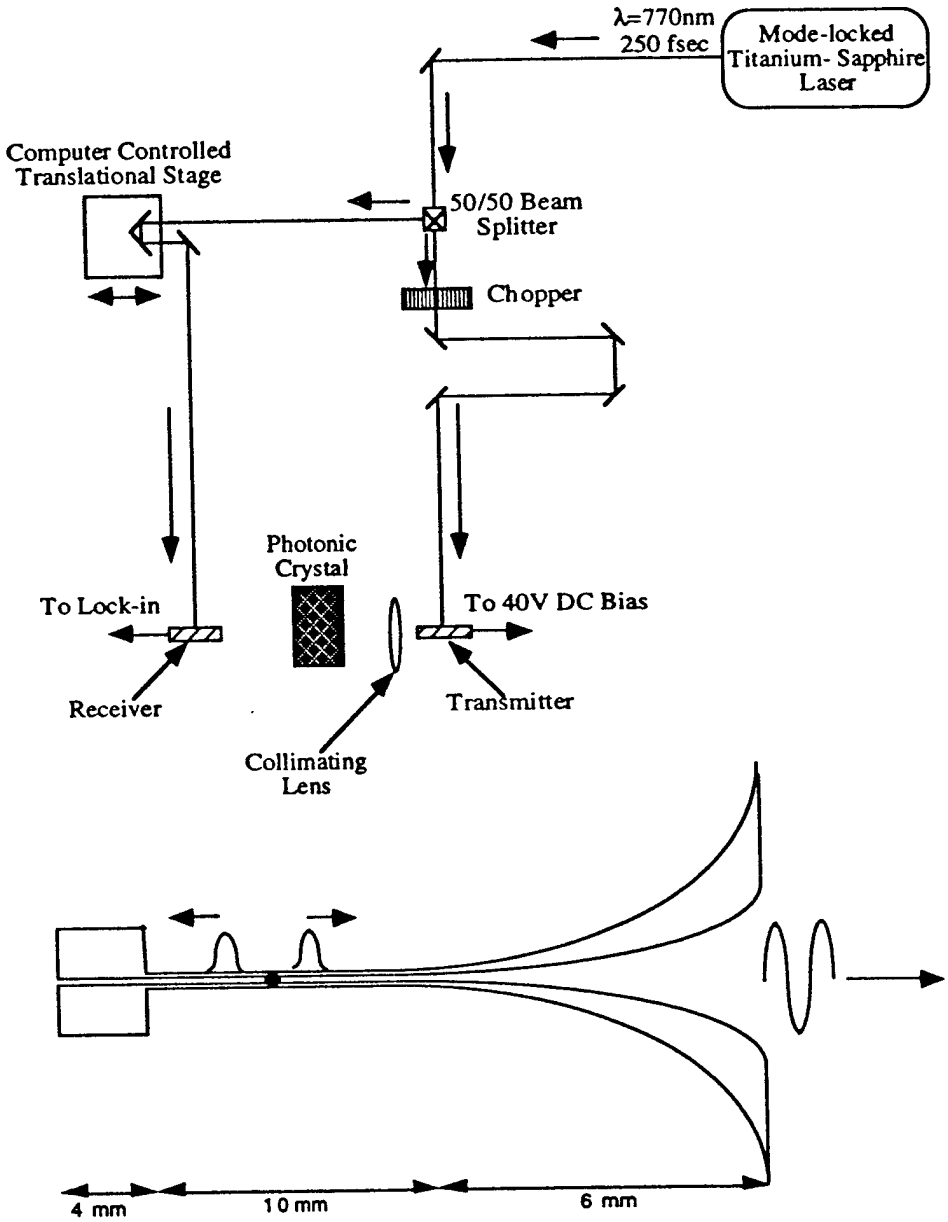

Figure 2(a). Experimental set up for the time-domain measurements. **(b)** Exponentially tapered coupled-strip antennas with a 1 cm coplanar transmission line feed. Two current pulses are generated at the point of switching that determine the frequency resolution of the system

-locked
ı- Sapphire
ıser

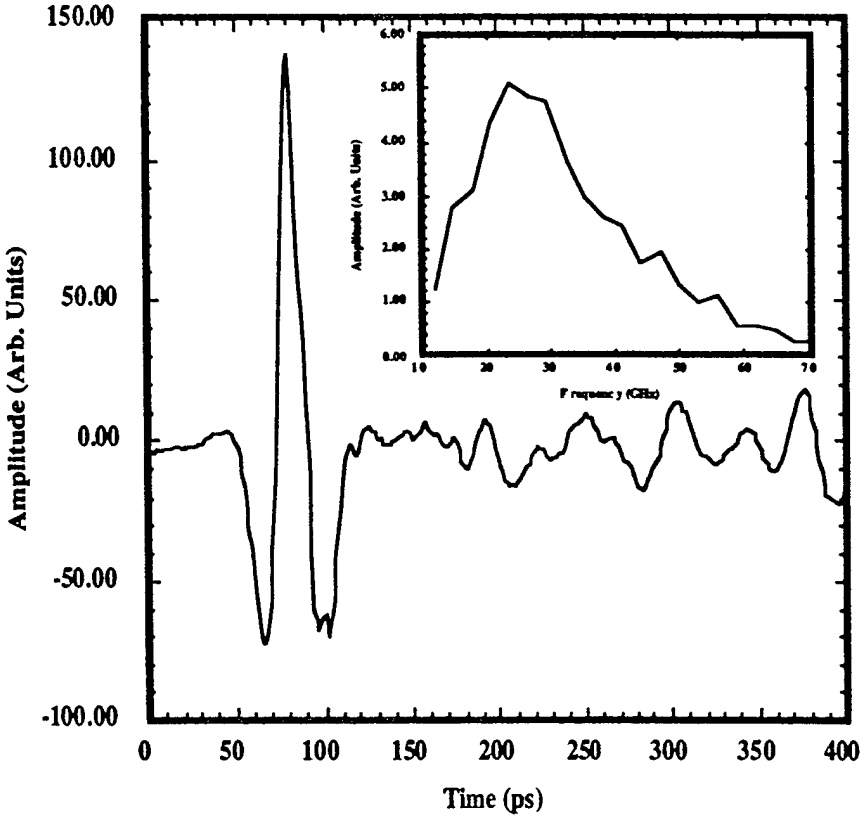

Figure 3. Typical time-domain reference pulse with the Fourier transform shown in the inset. The usable time window is approximately 400 ps which corresponds to a frequency resolution of 2.5 GHz. The pulse has a peak at 24 GHz and has usable frequency components out to 60 GHz.

apered coupled-
d at the point of

connected to a lock-in amplifier. As the delay between the optical pulses is increased, the received waveform can be mapped out.[4]

The transmitting and receiving antennas, shown in Fig. 2b, are exponentially tapered coplanar horns similar to those used by other groups in the past.[4-6] They are printed on low-temperature-grown GaAs (LTG-GaAs) using standard microfabrication techniques. The LTG-GaAs provides a short carrier lifetime (~0.8 ps)[7] such that the duration of the photoconductively generated current pulse is of the same order as the optical pulse. At the point of switching, two current pulses are generated in the transmitting antenna (see Fig. 2b). The first travels toward the end of the taper and is radiated into free space: the other travels down the coupled strips, reflects from the bonding pads, and is subsequently radiated from the taper. The time delay between radiated pulses dictates the resolution in the frequency domain of the system.

Due to the limited aperture of the antenna, the radiation emanating from the transmitter diverges. To overcome this, a two inch diameter collimating lens is placed in front of the transmitting antenna as shown in Fig. 2. The lens is a standard microwave lens whose loss in negligible in the frequency range of interest. The entire experiment is controlled by a Macintosh running LabVIEW® software. A typical reference pulse (e.g. without the photonic crystal between antennas) is shown in Fig. 3 with its Fourier transform shown in the inset. The power spectrum of the received waveform is centered about 24 GHz and has usable magnitude out to 60 GHz as dictated by the antenna dimensions.[8] The resolution of the measurement is approximately 2.5 GHz according to the 400 ps time window shown in the time-domain plot in Fig. 3. Although broadband measurements of three-dimensional PBG structures have been recently reported by Özbay et. al.,[9] their generation method utilized nonlinear transmission line technology as opposed to the photoconductive switching applied here.

The broadband response of the photonic crystal is shown in Fig. 4(a) with the corresponding time-domain plot shown in the inset. The frequency-domain has a dip in the response at approximately 23 GHz. This is the stop band that is seen in the CW frequency-domain response in Fig. 1. Since the resolution of the time-domain system is 2.5 GHz, the stop band isn't as pronounced as in the frequency domain. In addition, higher order stop bands, located between 34 and 47 GHz, appear in the measurement which aren't observed in the frequency domain response because of the 26 GHz limitation of the network analyzer. The nature of these stop bands is currently being investigated. A direct comparison of the time-domain and CW frequency-domain responses is performed. However, in order for a direct comparison, the time-domain system response needs to be deconvolved from the crystal response. The deconvolution technique used is similar to the

reased, the

ponentially
They are
fabrication
ich that the
the optical
ransmitting
ed into free
ads, and is
dictates the

g from the
is placed in
rowave lens
periment is
e pulse (e.g.
its Fourier
is centered
the antenna
according to
h broadband
ed by Özbay
y as opposed

4(a) with the
is a dip in the
W frequency-
2.5 GHz, the
er order stop
en't observed
the network
d. A direct
s performed.
e needs to be
similar to the

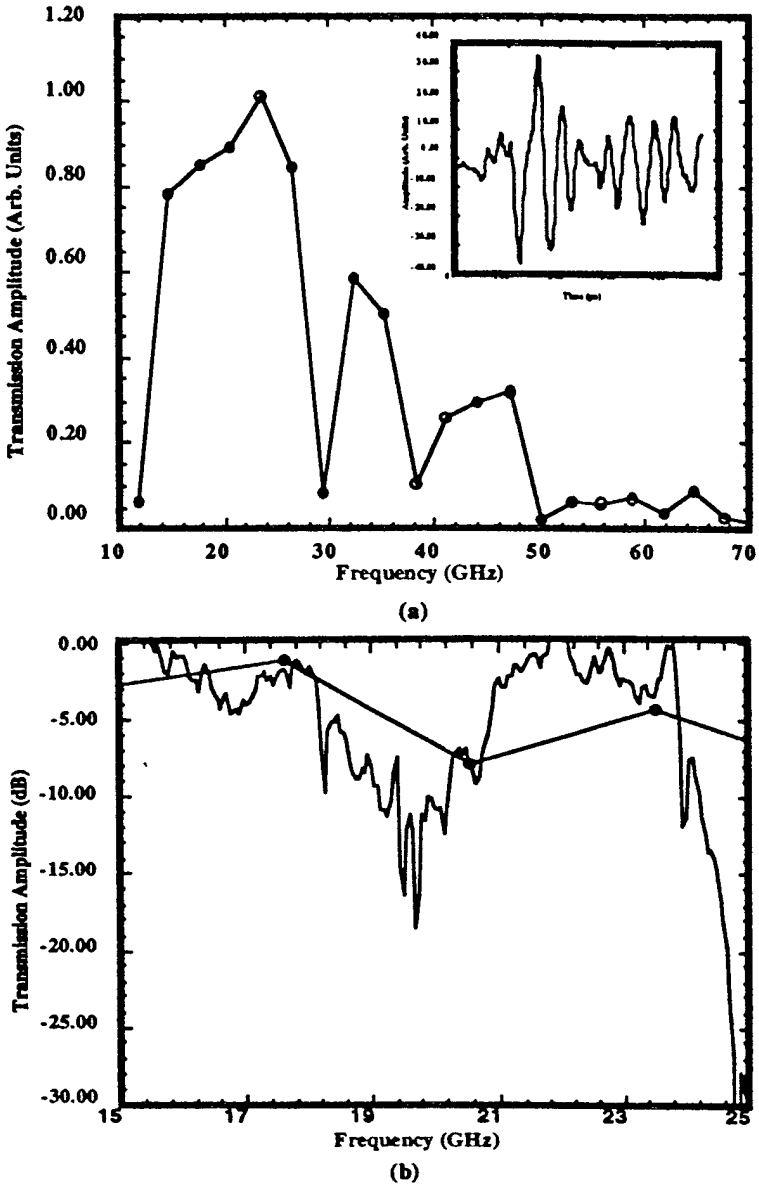

Figure 4. Transmission measurement of the photonic crystal at normal incidence. (a) Fourier transform of the time-domain data (shown in inset). The dip in frequency at 20 GHz corresponds to the stop band in Fig. 1. In addition the dip at 30 GHz corresponds to a higher order gap. (b) Direct comparison of the time-domain and the frequency-domain data. The points are the time-domain and the solid line is the frequency-domain. Good agreement is obtained within the resolution limit of the time-domain system.

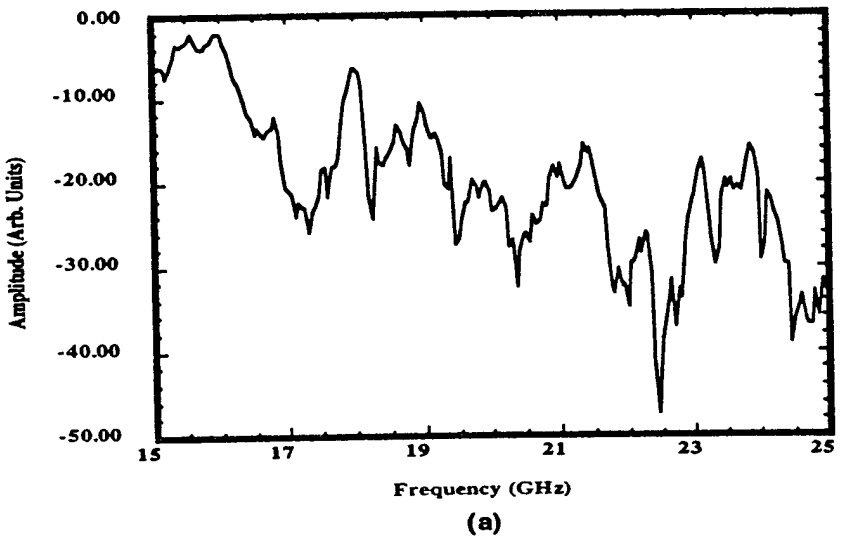

(a)

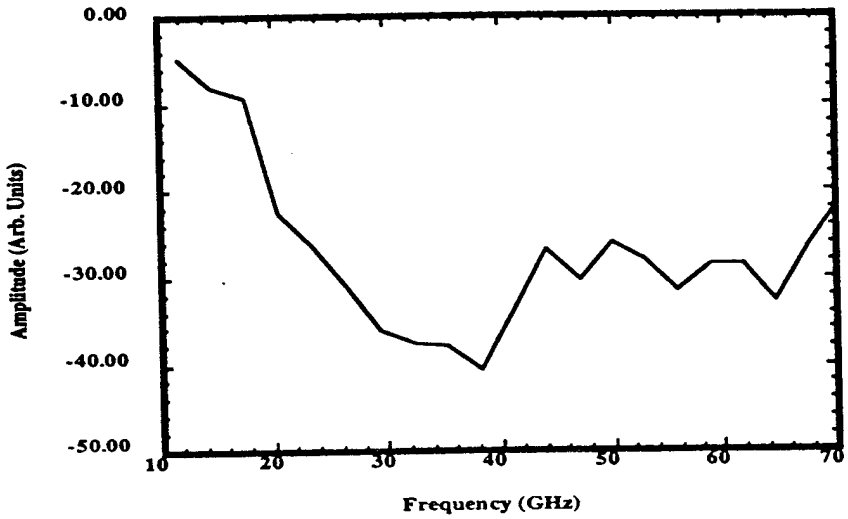

(b)

Figure 5. Transmission measurement of the ultra-wideband (UWB) photonic crystal at normal incidence. (a) Continuous wave frequency-domain response of UWB crystal. (b). The transfer function obtained from the time-domain response of the UWB crystal. The transformed time-domain measurement gives the broadband response whereas the CW measurement gives the narrowband detailed frequency response.

one used in the past whereby the Fourier transform of the crystal measurement is divided by the Fourier transform of the reference pulse.[6] This gives the frequency domain transfer function of the crystal and hence a direct comparison can be performed. The results are shown in Fig. 4(b). With the limited resolution of the time-domain measurements, the agreement between the frequency-domain and the time-domain is encouraging. However, in order to get better agreement, the resolution in the time-domain needs to be enhanced. Methods of resolution enhancement are currently being investigated

One application of the new fcc photonic crystal is to stack in tandem multiple, single-period photonic crystals to broaden the stop band, thereby creating an ultra-wideband (UWB) photonic crystal[10]. Figure 5(a) shows the CW frequency-domain response of a UWB photonic crystal containing one period each of three different fcc crystals. Figure 5(b) shows the time-domain waveform (shown in the inset) and its Fourier transform for the same UWB photonic crystal containing one period each of three different fcc crystals. While the limited frequency-domain results in Fig. 5(a) shows that the UWB stop band extends from 16 to 25 GHz, the time-domain data of Fig. 5(b) indicate that the stop-band extends well beyond 25 GHz. However, due to the limited resolution, it is unable to definitively resolve the stop bands of the component crystals.

In summary, measuring in the time domain allows a much broader band characterization of the photonic crystal compared to the CW frequency-domain measurement. By photoconductively switching planar antennas, short pulses of electromagnetic radiation were generated, detected, and used to perform time-domain measurements on photonic crystals. However, due to the finite time window, the resolution of the measurements was limited to 2.5 GHz. Therefore, the time-domain measurements are currently complementary to the high-resolution, but limited-bandwidth CW measurements taken with a network analyzer. The agreement between the direct comparison of the time-domain and frequency-domain show encouraging results within the resolution limit of the system. The resolution of the time-domain measurements can be enhanced by improvements in the antenna design (eliminating the back reflection from the contact pad) and by extending the scanned time delay of the system.

® LabVIEW is a registered trademark of National Instruments, Inc.

ACKNOWLEDGMENTS

This work was sponsored by the Department of the Air Force, in part through an AASERT grant from the Air Force Office of Scientific Research.

REFERENCES

1. E. Yablonovitch and T.J. Gmitter, "Photonic Band Structure: The Face-Centered-Cubic Case," Phys. Rev. Lett., vol. 63, no. 18, Oct. 30, 1989.

2. E. Yablonovitch, T.J. Gmitter and K.M. Leung, "Photonic Band Structure: The Face-Centered-Cubic Case Employing Nonspherical Atoms," Phys. Rev. Lett., vol. 67, no. 17, Oct. 21, 1991.

3. E.R. Brown, K. Agi, C.D. Dill, C.D. Parker and K.J. Malloy," A New Face-Centered-Cubic Crystal for Microwave and Millimeter Wave Applications," to appear in Opt. Microwave Tech. Lett., Dec. 15, 1994.

4. G. Arjavalingam, Y. Pastol, J.-M. Halbout and G.V. Kopcsay, "Broadband Microwave Measurements with Transient Radiation from Optoelectronically Pulsed Antennas," IEEE Trans. Microwave Theory Tech., vol. 38, no. 5, May 1990.

5. A.P. DeFonzo and C.R. Lutz, "Optoelectronic Transmission and Reception of Ultrashort Electrical Pulses," Appl. Phys. Lett., vol. 51, July 1987.

6. L. Carin and K. Agi, "Ultra-Wideband Transient Microwave Scattering Measurements using Optoelectronically Switched Antennas," IEEE Trans. Microwave Theory Tech., vol. 41, no. 2, Feb. 1993.

7. Measured FWHM value using reflectivity (pump/probe) experiment.

8. Y. Pastol, G. Arjavalingam, J.-M. Halbout and G.V. Kopcsay, "Characterization of an Optoelectronically Pulsed Broadband Microwave Antenna," Electron. Lett., vol. 24, no. 21, Oct. 13, 1988.

9. E. Özbay, E. Michel, G. Tuttle, R. Bismas, K.M. Ho, J. Bostak and D.M. Bloom, "Terahertz Spectroscopy of Three-Dimensional Photonic Crystals," Opt. Lett., vol. 19, no. 15, Aug. 1, 1994.

10. K. Agi, E.R. Brown, O.B. McMahon, C. Dill III and K.J. Malloy, "Design of Ultra-Wideband Photonic Crystals for Broadband Antenna Applications," submitted to Electron. Lett.

To appear in: IEEE Transactions on Plasma Science, Sixth Special Issue on High Power Microwave Generation, June 1996

Photonic Crystals: A New Quasi-optical Component for High-Power Microwaves

K. Agi[1], L. D. Moreland[2], E. Schamiloglu[2], M. Mojahedie[1], K. J. Malloy[1] and E. R. Brown[3]

[1]*Center for High Technology Materials*
Department of Electrical and Computer Engineering
University of New Mexico
Albuquerque, NM 87131

[2]*Pulsed Power and Plasma Science Laboratory*
Department of Electrical and Computer Engineering
University of New Mexico
Albuquerque, NM 87131

[3]*Lincoln Laboratory, Massachusetts Institute of Technology*
244 Wood Street
Lexington, MA 02173-9108

Abstract

The interaction of a high-power microwave beam with a face-centered-cubic photonic crystal is studied. A Sinus-6 high-power relativistic repetitively pulsed electron beam accelerator was used to drive a slow wave structure in vacuum to generate 450 MW at 9.65 GHz. It is shown that the photonic crystal, comprising of a periodic arrangement of air holes in a dielectric host, is capable of performing as a quasi-optical reflector similar to a metal. The crystals can be designed to operate as efficient frequency-selective reflectors over narrow frequency ranges. We propose that photonic crystals can have many applications in high-power microwave research.

I. INTRODUCTION

Photonic crystals (PCs) are three- or lower-dimensional periodic dielectric structures that exhibit ranges of frequencies (stop bands) where electromagnetic radiation is forbidden. If the stop bands are omnidirectional, the PC dispersion relation exhibits a forbidden region or bandgap. These structures are therefore known as photonic bandgap structures [1-2]. The width, depth and location of the stop band are determined by the shape, size and location of the macroscopic "atoms" (scattering centers), as well as the longitudinal (along the direction of propagation) periodicity of the structure. Figure 1 presents a schematic of the photonic crystal used in this work.

There are many low-power applications for PCs that are under investigation. For example, antennas printed on dielectric substrates suffer severe losses due to energy leakage into the substrate [3]. Printing the antenna on a PC substrate with the driving frequency in the stop band of the crystal enhances the radiation into free-space owing to the reflective properties of the crystal [4]. However, the operational frequency of the PC antenna is limited to the width of the stop band. For ultrawideband (UWB) excitation, PCs of different periodicities can be stacked in tandem to obtain a photonic crystal capable of providing UWB reflectivity [5]. All these applications utilize the frequency selective, reflective characteristics of the PC.

In this paper, we present results from experiments where a PC is used, for the first time, as a quasi-optical component for high-power microwaves (HPMs). Traditionally, reflectors used in HPM research have been made from conductors. For these applications, one can model these structures as reradiating surface current sources, as is prescribed by the Equivalence Principle [6]. These current sources, coupled with the finite conductivity of metals, provides for ohmic losses which can exceed dielectric losses in the frequency range of interest. The PCs used in these experiments have been fabricated exclusively from a low-loss, high-dielectric-constant material which can potentially address the ohmic loss issue. Furthermore, since the PC is a distributed reflector, the amount of energy reflected by each layer is significantly lower than a metal, which can alleviate surface breakdown problems as well. Although frequency-dependent reflective characteristics can be achieved using frequency selective surfaces such as gratings or inductive meshes, these structures are typically metallic or metal composites [7]. Suggested HPM applications emerging from this work utilize the PC as a quasi-optical reflector, filter, and beam forming component for both space- and ground-based systems. To the authors' knowledge, this is the first report of HPM measurements performed on photonic crystals. It is anticipated that PCs can be

further exploited as an important new component for HPM source research and applications.

The remainder of this paper is organized as follows. Section II describes the experimental set up, including the source and the fabrication of the PC. Section III discusses the results of the experiments, and Section IV provides conclusions and other potential applications of PCs in HPM systems.

II. EXPERIMENTAL SET-UP

The source of the HPMs used in this work is the Sinus-6 electron-beam accelerator-driven backward wave oscillator (BWO) [8]. Two different beam parameters were used and are summarized in Table I. A mode converter was placed between the BWO and the conical horn antenna to convert the output TM_{01} mode from the BWO into a TE_{11} mode. This mode converter was constructed based on the design of Denisov and colleagues at the Institute of Applied Physics (Nizhny Novgorod, Russia) [9]. The measured RF frequency and the peak power densities 1.16 m downstream from the horn antenna are also shown in Table I. All the results reported here are obtained by averaging over many shots from the Sinus-6.

The PC used in the experiments is a three-dimensional, face-centered-cubic (fcc) structure with cylindrical air atoms as the basis. The fabrication of these structures entails drilling vertical holes in a host dielectric (in contrast with the original PC [1] where three holes were drilled at 35° at each lattice site), as shown in Fig. 1. The host material used is Stycast, a TiO_2-based compound with a dielectric constant of 10. The three-dimensional periodicity is obtained by offsetting 3 plates in an A-B-C configuration leading to the fcc structure [10]. Each A-B-C (3 plates) configuration constitutes one period of a fcc structure in the longitudinal direction. Low-power network analyzer measurements indicate that with one period (3 plates), the attenuation in the stop band for these PCs is approximately 7 dB down from the reference [5].

Since the Sinus-6 BWO is a narrow-band source, two PCs having different periodicities were used in this study. The first crystal (termed the in-gap crystal) was designed to have a stop band centered about 9.5 GHz and a stop-band width of approximately 1.5 GHz (measured from the start of rejection to the beginning of transmission). The thickness of each plate was 1.27 cm (0.5 in.), corresponding to 3.81 cm (1.5 in.) per period. The other crystal (out-of-gap crystal) had a stop band centered about 19.5 GHz and a stop-band width of approximately 4 GHz. The thickness of these plates were 0.508 cm (0.2 in.) such that each period was 1.52 cm (0.6 in.).

The experimental setup is shown in Fig. 2. The initial experiments were to assess the performance of the photonic crystal when compared to a planar metallic reflector. The HPM source was operated at full power (see Table I) to obtain an air breakdown standing-wave pattern. The second set of experiments measured the angular dependence of the transmitted radiation through the photonic crystal. Here, the Sinus-6 BWO was operated at reduced power levels (Table I) to eliminate any air breakdown that may corrupt the measured radiation pattern. The physical dimensions of the PC and the metal plate were chosen to be 15.24 cm × 15.24 cm (6×6 in.), which corresponds to a half angle of 5° in the angular dependence measurements.

III. EXPERIMENTAL RESULTS

Figure 3(a) shows a metal plate placed 87 cm away from the edge of the horn antenna. The photograph shows ionization near the antenna indicating the existence of a standing wave between the antenna and the metal plate. Figure 3(b) is the same setup with the metal plate replaced by the two-period, in-gap crystal. Although both the metal plate and the in-gap crystal effectively generate an air breakdown standing wave pattern, it is evident by the visible number of peaks in the standing-wave that the metal reflects slightly more energy than the crystal. (Note that as expected, the separation of peaks in the two standing-wave patterns remains unchanged, indicating that the PC response was still linear under high field excitation). This can be compensated by increasing the number of periods in the crystal to enhance the amount of energy reflected [10]. However, to concurrently address practical issues such as size and weight, only two periods were used.

Figure 4 shows the transmission characteristics of the metal plate and the two-period, in-gap crystal along with the patterns in direct transmissions (i.e. no crystal or metal plate). For the PC, from -5° to +5° (corresponding to the physical dimensions of the crystal), the radiation is attenuated. On the other hand, the response of the metal from -5° to +5° varies from 20 kW cm^{-2} at approximately 1° to 100 kW cm^{-2} at +5°. This fluctuation in power density is caused by the re-radiation of the surface currents at the edge of the metal (edge diffraction). Beyond +5°, both the PC and the metal plate response approach the direct transmission response.

Figure 5 shows a comparison between the one-period in-gap crystal and the one-period out-of-gap crystal angular responses. As in Fig. 4, the direct transmission, which can be considered as a reference, is also shown. (Note once again that the physical dimensions of the PC ranged from -5° to +5°.) For the out-of-gap crystal, there is a 3 dB enhancement in the power density at 0°. For the in-gap crystal there is a redistribution of

the energy, but since there is significant reflection due to the stop band of the crystal, no enhancement is observed. The out-of-gap crystal enhancement suggests a simple method of obtaining higher power densities.

The receiving antenna used in these experiments consisted of an open-ended section of WR-90 waveguide with a geometrical cross sectional area of 2.32 cm^2, which can be approximated as a point detector. The discrete mapping revealed the enhancement in the out-of-band crystal. Previous low power transmission measurements used standard gain horn antennas which integrated the incident radiation over the relatively large surface of the horn, thereby masking the enhancement [11]. As in the previous case, both crystal responses approached the direct transmission response beyond 5°.

Integration of the responses in Figs. 4 and 5 yields total transmitted power. Upon integrating the direct transmission from -15° to +15°, a power level of approximately 400 MW is obtained. For the higher power levels, accurate measurement of the power was unattainable because of air breakdown; however it was estimated to be at least 450 MW. In order to obtain the PC power levels, the integration was performed from -5° to +5° (see Table II for a summary of the results). The power scattered from the metal plate is 6 dB below the reference while the power transmitted through the in-gap crystal is approximately 8 dB below the reference. This indicates that the in-gap crystal diffracts less than the comparable size metallic plate. The power transmitted through the out-of-gap crystal is 4.6 dB below the reference. This is not surprising since this crystal was designed with a stop band at 19.5 GHz, well above the operating frequency of the Sinus-6 BWO. In the long-wavelength limit for behavior of periodic structures, attenuation is dominated by effective bulk material properties.

IV. DISCUSSIONS AND CONCLUSIONS

The interaction of a HPM beam with a PC was studied. The reflection measurements indicated that similar standing-wave patterns exist for the metal plate and the two-period, in-gap PC. It is evident that the PC performance as a microwave reflector is comparable to that of a metal plate.

In the angular transmission studies, the PC response was more uniform than the metal plate because of edge diffraction for conductors. This implies that, for applications where finite reflector size is a consideration, the PC will provide less diffraction away from the crystal and more diffraction toward the center as indicated in Fig. 5. Figure 5 also showed a 3 dB enhancement in power density by using the out-of-gap photonic crystal.

This enhancement can be used to easily achieve higher power densities for HPM applications at the expense of some total power loss, but is not yet fully understood.

Integration of the radiation patterns indicated that more power is diffracted behind the metal plate as compared to the PC. This implies that by adding more periods to the PC, there will be an enhanced reflectivity without any losses due to edge diffraction. Hence a finite size PC may be a more efficient reflector than a comparable size conductor.

The PC was demonstrated to be an effective, frequency-selective, quasi-optical reflector of HPM radiation. The PC can be utilized as a simple frequency diagnostic, analogous to cutoff filters. Furthermore, the out-of-band PC was demonstrated to enhance radiated power density by 3 dB. For the out-of-gap crystal we are approaching the long-wavelength limit for a periodic structure so that it should behave as an effective dielectric medium. Although nulls appear in the enhanced radiation pattern, it is uncertain whether the observations can be attributed solely to bulk properties or the periodicity. This observed enhancement is currently being studied. Additional applications of this material to HPMs will certainly be emerging.

ACKNOWLEDGMENTS

This work was supported by the Air Force Office of Scientific Research in part through an AASERT grant and through a High Energy Microwave Devices Consortium funded by an AFOSR/DOD MURI grant. The authors would like to thank Ollie B. McMahon at Lincoln Laboratory for fabricating the PCs.

REFERENCES

[1]. E. Yablonovitch, T.J. Gmitter and K.M. Leung, "Photonic Band Structure: The Face-Centered-Cubic Case Employing Nonspherical Atoms," *Phys. Rev. Lett.*, vol. 67, pp. 2295-2298, 1991.

[2]. See Special Issue on "Development and Applications of Materials Exhibiting Photonic Bandgaps," *J. Opt. Soc. Am. B*, vol. 10, no. 2, 1993.

[3] D.B. Rutledge, D.P. Neikirk, and D.P. Kasilingam, in *Infrared and Millimeter Waves* (Academic, Orlando, FL, 1983), vol. 10, ch. 1.

[4]. E.R. Brown, C.D. Parker, and E. Yablonovitch, "Radiation Properties of a Planar Antenna on a Photonic-Crystal Substrate," *J. Opt. Soc. Am. B*, vol. 10, 1993, pp. 404-407, 1993.

[5] K. Agi, E.R. Brown, O.B. McMahon, C. Dill III, and K.J. Malloy, "Design of Ultrawideband Photonic Crystals for Broadband Antenna Applications," *Electron. Lett.*, vol. 30, pp. 2166-2167, 1994.

[6] R.F. Harrington, *Time-Harmonic Electromagnetic Fields* (McGraw-Hill, New York), pp. 106-110, 1961.

[7]. T.K. Wu, *Frequency Selective Surfaces and Grid Array* in Wiley Series in Microwave and Optical Engineering (Wiley, New York), 1995.

[8]. L.D. Moreland, E. Schamiloglu, R.W. Lemke, S.D. Korovin, V.V. Rostov, A.M. Roitman, K.J. Hendricks, and T.A. Spencer, "Efficiency Enhancement of High Power Vacuum BWO's Using Nonuniform Slow Wave Structures," *IEEE Trans. Plasma Sci.*, vol. 22, pp. 554-565, 1994.

[9] D.V. Vinogradov and G.G. Denisov, *Radiofizika* 33, p. 726, 1990; G.G Denisov (private communication, 1992).

[10]. E.R. Brown, K. Agi, C. Dill III, C.D. Parker, and K.J. Malloy, "A New Face-Centered-Cubic Photonic Crystal for Microwave and Millimeter-wave Applications," *Microwave Opt. Technol. Lett.*, vol. 7, pp. 777-779, 1994.

[11]. E.R. Brown, O.B. McMahon, C.D. Parker, C. Dill III, K. Agi, and K.J. Malloy, "Microwave Applications of Photonic Crystals," to appear in *Nato ASI Series Volume on Photonic Band-Gap Materials*, ed. C. Soukoulis (Kluwer, Dordrecht, 1995).

Table I

Summary of Beam Parameters

Cathode Voltage (kV)	Beam Current (kA)	Power Density ($kW\text{-}cm^{-2}$)	RF Frequency (GHz)
595	5.1	325	9.7
490	4.0	270	9.6

Table II

Summary of Diffracted and Transmitted Power from -5° to 5°

Direct Transmission	Metal Plate	In-Gap (2 periods) PC	Out-of-Gap (1 period) PC
173 MW	42 MW	28 MW	60 MW

Figure Captions

Figure 1. (a). Top view of the photonic crystal. (b). Extended view of the photonic crystal. Vertical holes are drilled in a dielectric host and then configured in an A-B-C configuration. Three plates constitute one period of a fcc lattice.

Figure 2. Schematic of the experimental setup. The receiver is scanned behind the photonic crystal in the angular dependence measurements. The polarization of the electric field is indicated.

Figure 3. (a). Breakdown pattern for the HPM beam being reflected from a planar metal plate. (b). Breakdown pattern for the HPM beam reflected from a two-period in-gap photonic crystal.

Figure 4. Measured radiation pattern of the reference direct transmission (circles), the two-period in-gap photonic crystal (triangles), and the metal plate (squares).

Figure 5. Comparison between the reference (circles), the one-period out-of-gap photonic crystal (squares), and the one-period in-gap photonic crystal (triangles). Note the enhancement in the out-of-gap response.

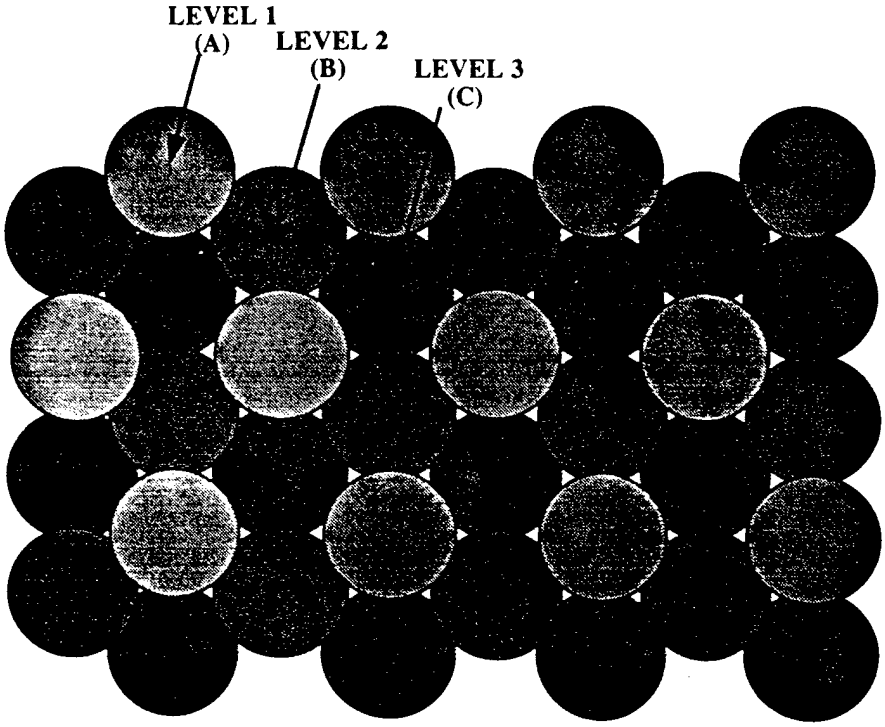

(a).

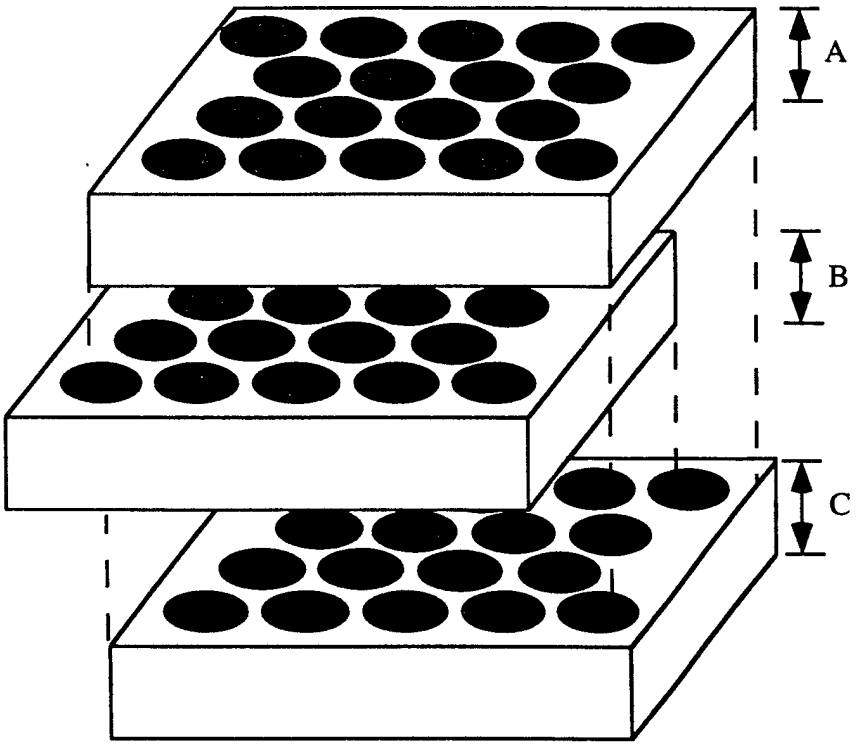

(b).

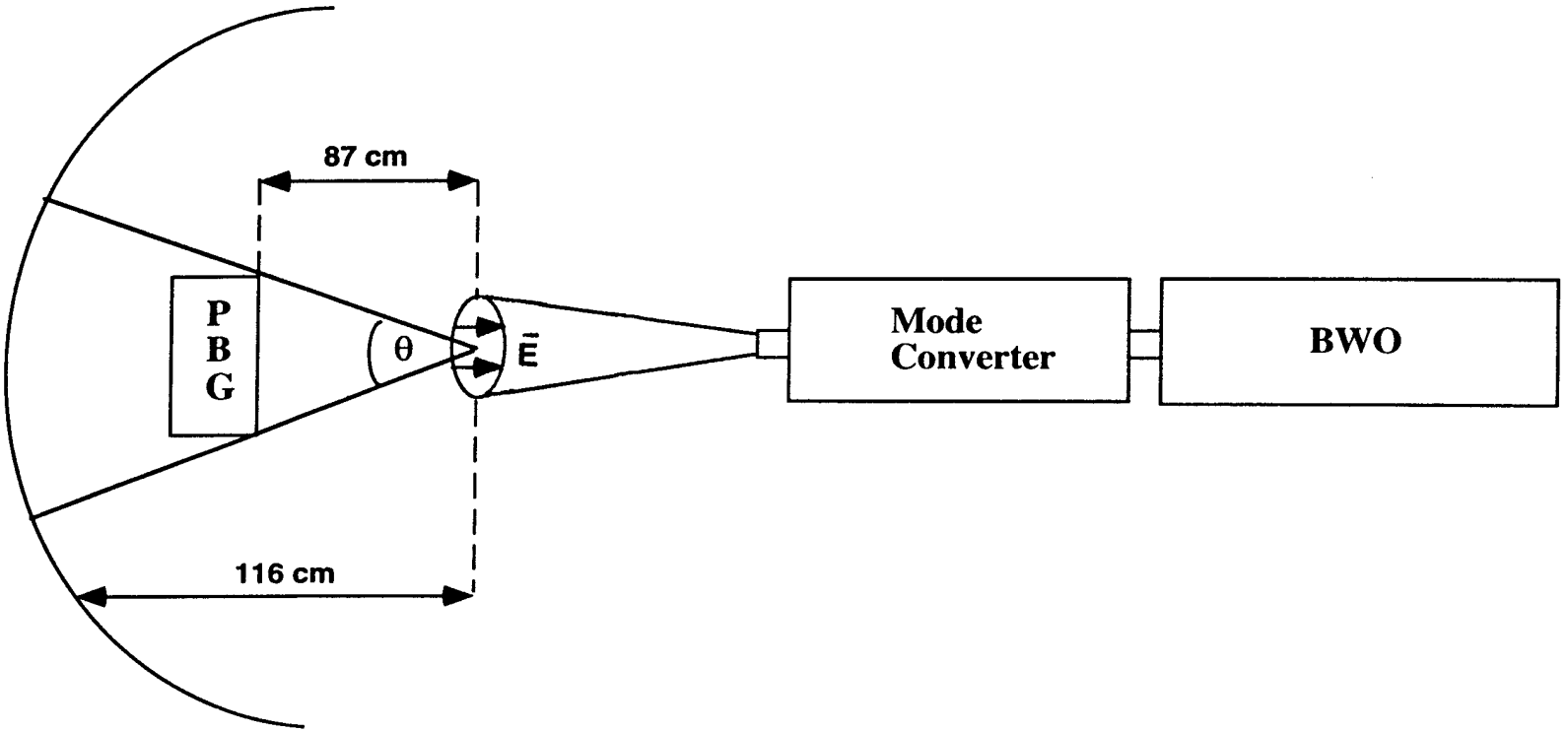
87 cm
P
B
G
θ
E
Mode
Converter
BWO
116 cm

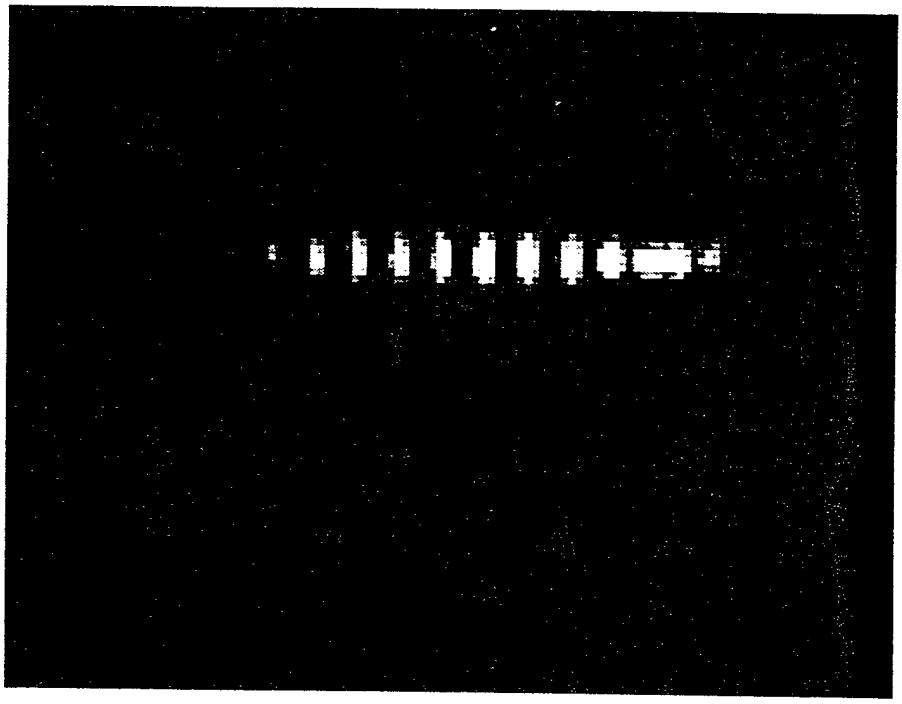

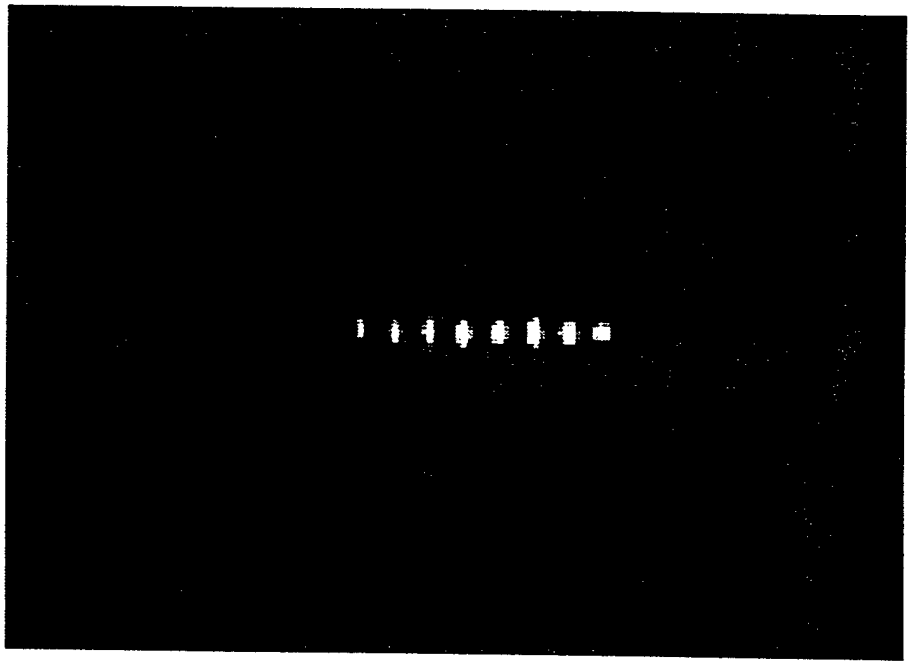

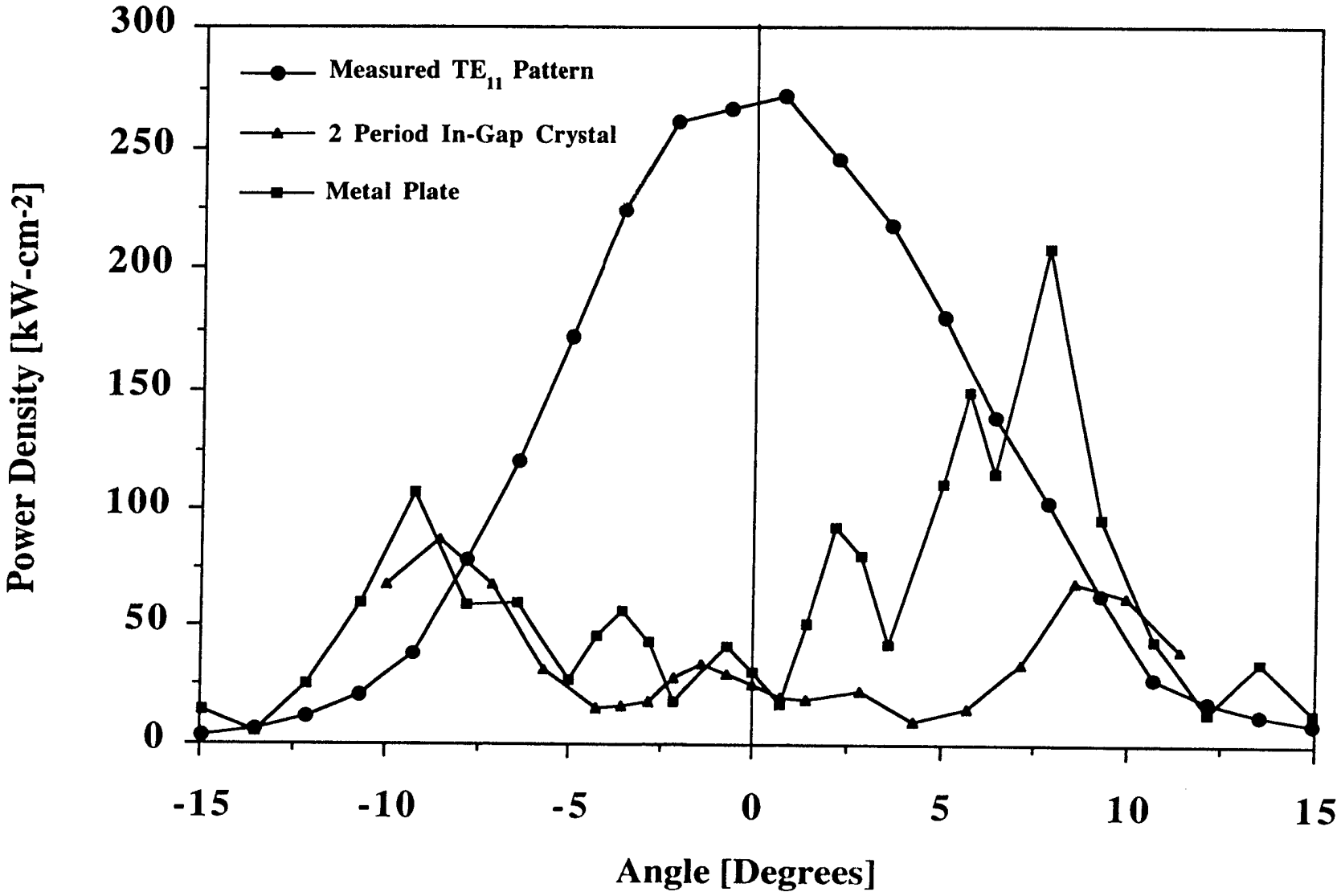
Measured TE_{11} Pattern
2 Period In-Gap Crystal
Metal Plate
Power Density [kW-cm-2]
300
250
200
150
100
50
0
-15
-10
-5
0
5
10
15
Angle [Degrees]

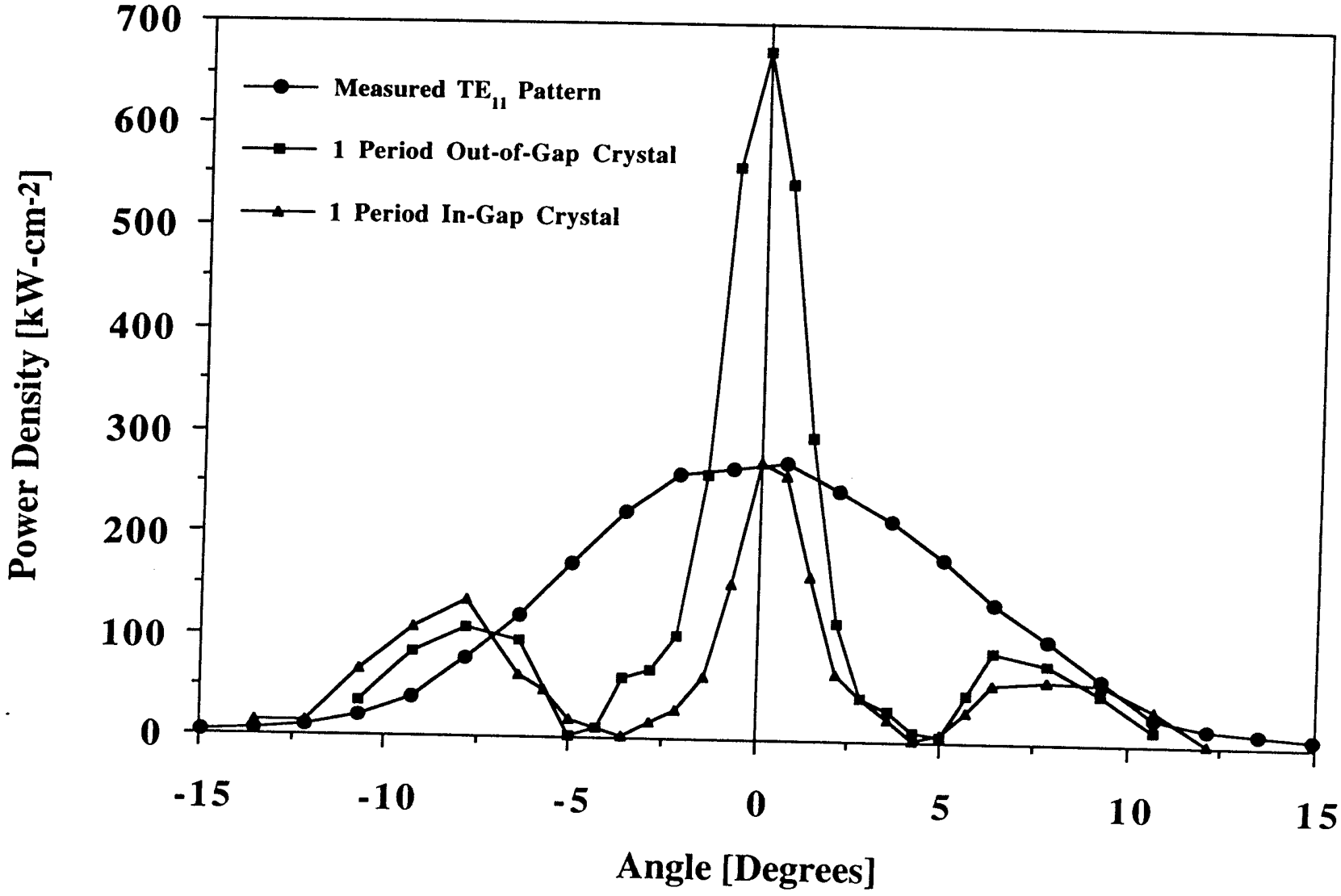
Measured TE_{11} Pattern
1 Period Out-of-Gap Crystal
1 Period In-Gap Crystal
Power Density [kW-cm-2]
700
600
500
400
300
200
100
0
-15
-10
-5
0
5
10
15
Angle [Degrees]

To appear in Ultrawideband
Short-pulse III, Ed.
A.P. Stone, C. Baum,
L. Carin, Plenum Publisher

THE TIME EVOLUTION OF PHOTONIC CRYSTAL BANDGAPS

K. Agi, M. Mojahedi and K.J. Malloy

Center for High Technology Materials
University of New Mexico
Albuquerque, NM 87131

ABSTRACT

The concept of a scaled group delay time is applied to a finite one-dimensional periodic array of dielectrics as a means of obtaining a group velocity. The scaling factor is shown to be the physical distance and this derived group velocity is compared to the group velocity of an infinitely periodic structure. Joint time-frequency analysis is performed on the response of a one-dimensional structure and the time-to-formation of the pass bands is shown to be determined by the peak group velocity in a given band. These concepts are then extended to three-dimensional photonic crystals and shown to give good agreement.

INTRODUCTION

Photonic crystals (PCs) are three- or lower-dimensional periodic dielectric structures that exhibit pass- and stop-bands. The one-dimensional PC has a wide range of applications in the optical domain as reflectors, filters and anti-reflection coatings[1]. However, for lower frequency microwave/RF applications, conventional technology has limited the use of the one-dimensional PCs. On the other hand, the two- and three-dimensional PCs, such as frequency selective surfaces (two-dimensional) or photonic bandgap crystals (three-dimensional), have found some applications in the microwave domain such as substrates for narrowband antennas[2], filters[3], and frequency selective reflectors for high power microwave systems[4]. For ultra-wideband (UWB) systems, usage of PCs requires a better understanding of the time evolution of the pass- and stop-bands in the crystal. Fortunately, the ability to generate short electromagnetic pulses has made it possible to investigate the interaction of UWB signals with highly dispersive structures[5]. This paper addresses the issue of the band formation in PCs. Initially, one-dimensional structures are used to gain insight to the problem, and subsequently the ideas are extended into the experimental properties of a three-dimensional structure.

ONE-DIMENSIONAL PHOTONIC CRYSTALS

The analysis of one-dimensional PCs begins with the study of an infinitely periodic array of dielectric slabs. In order to study the evolution of the pass- and stop-bands, the group velocity of the system needs to be calculated. The group velocity is the inverse of the first derivative in the Taylor series expansion of the Bloch propagation constant (K) about a given frequency[6]. For this simple case, the required dispersion relation (ω vs. K) can be obtained analytically by applying periodic boundary conditions to the electric field[1].

To determine the evolution times in a finite periodic structure, a group velocity needs to be defined which should approach the group velocity of an infinitely periodic crystal in the limiting case. In order to discuss group velocity, the concept of group delay, which is simply the derivative of the phase of the transfer function with respect to frequency[7], is utilized. If the group delay is scaled by a length, the result is the desired group velocity.

In order to obtain the phase of the transfer function, a transmission line model is used. In this model, one period of the dielectric multi-layer is represented by two transmission lines with characteristic impedance Z_i, length d_i, and propagation constant k_i, for i=1,2, such that the overall ABCD matrix can be obtained[6]. The one period matrix is raised to the power of N, where N is the number of periods in the structure, and hence the transmission coefficient can be determined from the resultant matrix[8]. Figure 1 shows the transmission magnitude and unwrapped phase through the structure with the corresponding dispersion curve for the infinitely periodic structure shown as an inset.

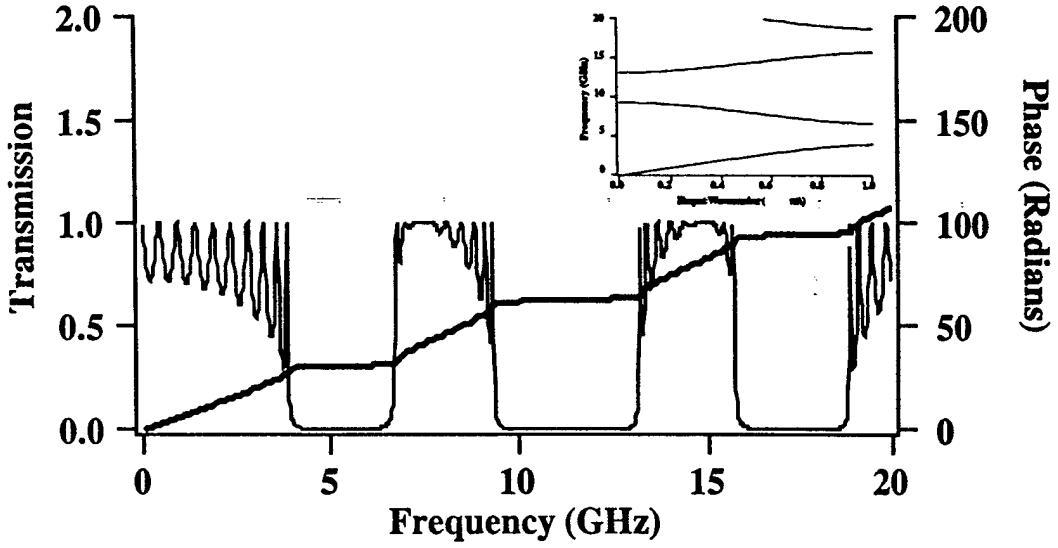

Figure 1. Magnitude (thin line) and unwrapped phase (thick line) of the transmission response of a 10 period multi-layer dielectric structure. $d_1=d_2=0.635$ cm, $n_1=3.162$, $n_2=1$. The inset is the corresponding dispersion curve obtained from the eigenvalue equation for the infinite structure.

To determine the scaling factor, consider an infinitely periodic structure. The relation between any field point and a field point NΛ away is given by Bloch's transformation theorem:

$$E(x+N\Lambda,K)=E(x,K)e^{iKN\Lambda}$$

where N is the number of periods and Λ is the physical length ($\Lambda=d_1+d_2$) of one period. The ratio of the two fields leads to a transfer function whose magnitude is 1 and whose phase, Φ,

is KNΛ. The derivative of the phase with respect to frequency, which is the group delay, is given by

$$\frac{\partial \Phi}{\partial \omega} = \frac{N\Lambda}{v_g}$$

From the above it is clear that the scaling factor is the physical distance of the structure as opposed to the optical path length ($\Lambda=d_1+d_2$ vs. $n_1d_1+n_2d_2$, where n_i is the index of refraction). Figure 2 shows the comparison of the group velocity of the infinite structure (markers), calculated from the derivative of the dispersion curve, with a 10 period multi-layer (solid line), calculated from the scaled group delay. Away from the transition regions between the stop bands and the pass bands (i.e. band edges), the infinitely periodic result is approximately the average value of the finite structure. Near the band edges there is an insufficient number of periods to approximate the group velocity to any reasonable accuracy. However, the work here will be relying on the peak group velocity which occurs well away from the band edges.

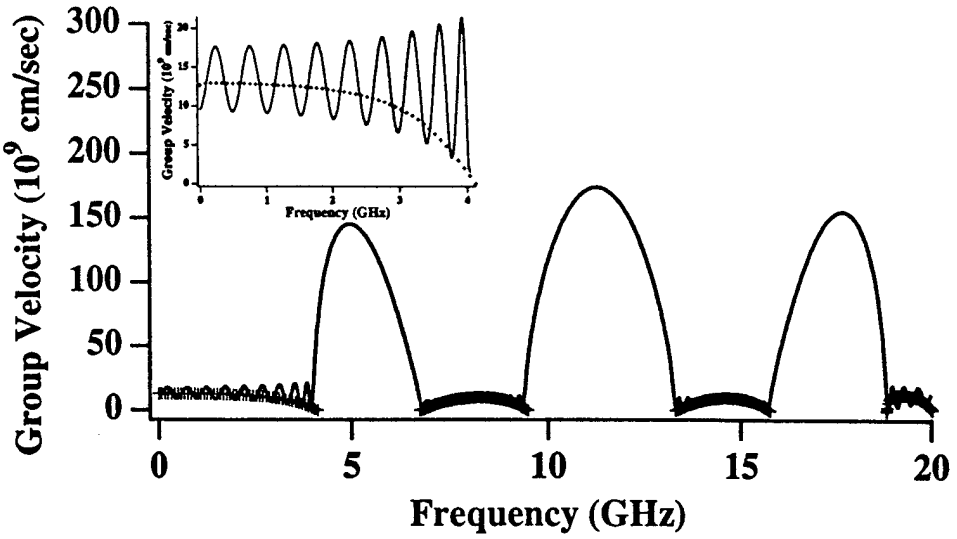

Figure 2. Group velocity calculated for the infinitely periodic array of dielectrics (markers) and a 10 period finite periodic structure (solid line). The inset is an expanded view of the first band.

The joint time-frequency analysis (JTFA) response can be obtained from the transmission response in Figure 1. Figure 3 shows the spectrogram using an adaptive, short-time fourier transform and Gabor algorithms[9], where in all cases, the vertical axis is time, the horizontal axis is frequency and the relative intensities are shown as the spectrogram. Independent of algorithm, the time-to-formation of the pass-bands, which is the start of the pulse to where the first wave appears, is governed by the peak group velocity. In other words, the first wave to appear is the undiffracted wave that is traveling at the peak group velocity for a given pass band. For all bands, there is good agreement between the delay time obtained from the JTFA spectrogram, the scaled group delay obtained from the phase of the transfer function and the derivative of the dispersion curve for the infinitely periodic structure. A summary of the results is given in Table 1.

Table 1. Summary of the group velocities obtained by scaling the JTFA delay time, scaling the group delay and the derivative of the dispersion curve for the infinitely periodic structure.

Band Number	JTFA (cm/s)	Group Delay (cm/s)	Infinite (cm/s)
1	1.41×10^{10}	1.29×10^{10}	1.308×10^{10}
2	1.12×10^{10}	0.97×10^{10}	0.99×10^{10}
3	1.01×10^{10}	0.94×10^{10}	0.97×10^{10}

On the other hand, the completion of the band, which is defined as the time from the start of the pass band to the end of the pass band, is difficult to deduce from the JTFA due to the algorithm dependence of the spectrograms. Hence it is difficult to differentiate between the real features and the extraneous ones. In other words, the decomposition of the time signal, to obtain the JTFA spectrogram, is dependent on the basis of the decomposition. This basis dependence creates cross-terms in the spectrogram which may be mistaken for real features. Hence, to avoid this dependence, the focus will be the formation time.

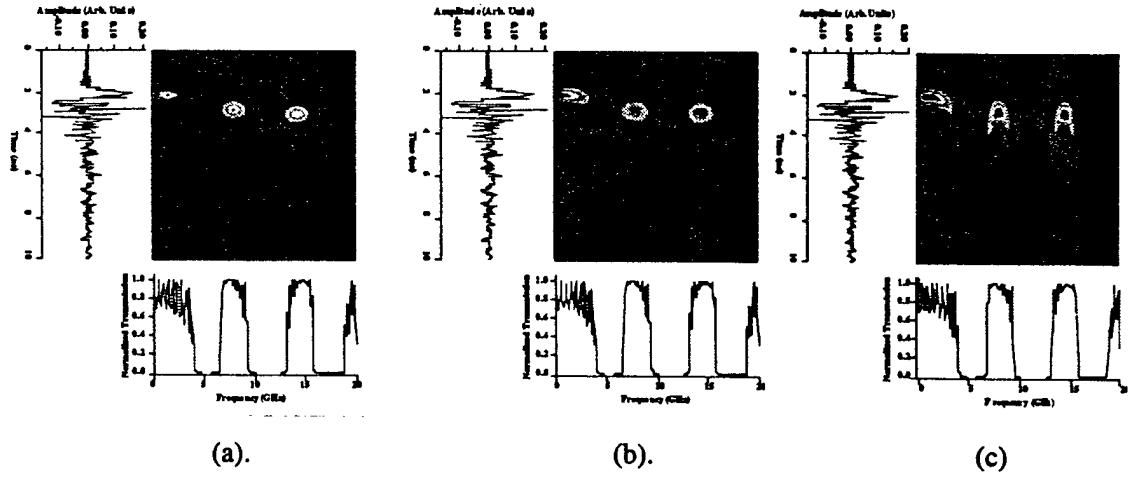

(a). (b). (c)

Figure 3. Joint time-frequency analysis using (a). adaptive algorithm, (b). short-time fourier transform and (c). Gabor transform. The time-to-formation of each pass band is determined by the undiffracted wave that is traveling at the peak group velocity for the particular band.

THREE-DIMENSIONAL PHOTONIC CRYSTALS

The concepts developed in the one-dimensional case are extended here. For the three-dimensional PC, a four-period face-centered-cubic structure is used. A detailed description of the structure can be found in the paper by Brown, et al[10]. The transmission response (S_{21}) of the PC is experimentally obtained using a vector network analyzer (HP 8510) from 15 to 25 GHz. Here the phase information is preserved, hence the group delay can be calculated. Figure 4 shows the magnitude and unwrapped phase for the frequency response of the crystal at normal incidence (L-point), obtained in the experiment. The points shown in Figure 4 are a linear curve fit to the data. This facilitates the determination of the slope and hence the group delay for the structure. In order to obtain the group delay, the slope of the phase curve is divided by 2π to scale the frequency into radian frequency correctly. Since there are only two pass bands that exist in the frequency range of the network analyzer, the calculations of the group delays will be limited to these two bands.

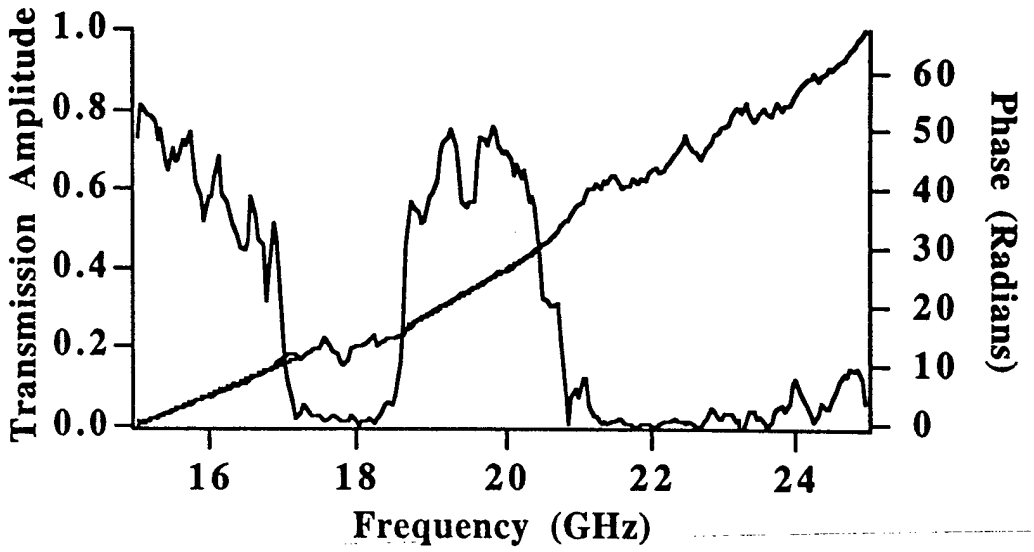

Figure 4. Magnitude and unwrapped phase of the experimental transmission response of a four-period, three-dimensional, face-centered-cubic photonic crystal. The points are a linear fit to the phase data which facilitate in the determination of the slope to obtain the group delay.

As in the one-dimensional case, the transmission response is inverse fourier transformed and the JTFA spectrogram is obtained. The adaptive algorithm is used to determine the spectrogram and is shown in Figure 5. Once again, the time-to-formation is determined from the delay in the spectrogram and calculated from the derivative of the phase. Here, the group delays can be compared directly using the two methods since there is no scaling factor in calculating delay times. For the three-dimensional PC, the transmission response for various high-symmetry directions (incident angles) are measured and the corresponding delays are calculated. The results are shown in Table 2. Good agreement is obtained with the two methods in determining the time-to-formation of the pass bands.

Table 2. Comparison of group delay and JTFA delay for various angles of incidence for the three-dimensional PC.

Crystal Direction	Band Number	Group Delay (ns)	JTFA Delay (ns)
L-point (0°)	1	0.844	0.9
	2	1.250	1.3
K-point (35.26°)	1	0.994	1.0
	2	2.020	1.9
W-point (39.2°)	1	0.943	1.0
	2	1.910	1.8

In summary, a group delay (velocity) is derived for a finite periodic structure. For the one-dimensional PCs, the group velocity is compared to the group velocity obtained by taking the derivative of the dispersion curve for an infinitely periodic structure. It is determined that the first wave to appear in all cases is the one travelling at the peak group velocity for each band. For the three-dimensional structure, the complex transmission is experimentally obtained and the phase is used, as in the one-dimensional case, to determine the group delay in the bands. The group delay is then compared to the results obtained using JTFA, where, the JTFA algorithm provides a method of pictorially obtaining a delay. Good agreement is

obtained using the group delay and the JTFA algorithm for both the one-dimensional and three-dimensional structures.

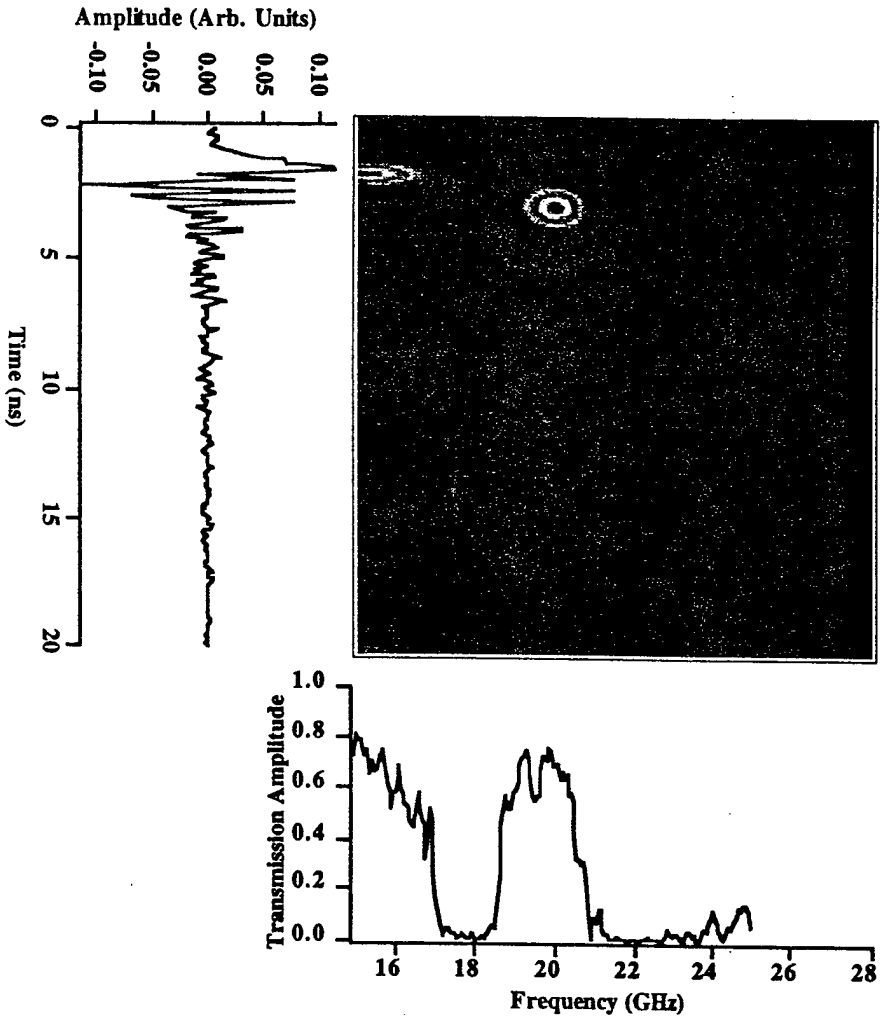

Figure 5. Joint time-frequency response, using the adaptive algorithm, of a four-period, three-dimensional face-centered-cubic photonic crystal at normal incidence. The delay shown is in good agreement with the group delay calculated by taking the derivative of the phase.

ACKNOWLEDGEMENTS

This work was supported by the Air Force Office of Scientific Research in part through an AASERT grant.

REFERENCES

1. A. Yariv, P. Yeh, *Optical Waves in Crystals*, John Wiley and Sons, New York (1984).
2. E.R. Brown, C.D. Parker and E. Yablonovitch, Radiation properties of a planar antenna on a photonic-crystal substrate, JOSA B, 10:2 (1993).
3. T.K. Wu, *Frequcncy Selective Surfaces and Grid Arrays*, John Wiley and Sons, New York (1995).

4. K. Agi, L.D. Moreland, E. Schamiloglu, M. Mojahedie, K.J. Malloy and E.R. Brown, Photonic crystals: a new quasi-optical component for high-power microwaves, to appear in IEEE Trans. Plasma Sci.. June, 1996.
5. D. Kralj, L. Mei, T.T. Hsu and L. Carin, Short-pulse propagation in a hollow waveguide: analysis, optoelectronic measurement and signal processing.
6. D. Pozar, *Microwave Engineering*, Addison Wesley, Massachusetts (1990).
7. G.L. Matthaei, L. Young and E.M.T. Jones, *Microwave Filters, Impedance-Matching Networks, and Coupling Structures*, McGraw-Hill, New York (1964).
8. M. Born and E. Wolf, *Principles of Optics*, Pergamon Press, Oxford (1989).
9. L. Cohen, *Time Frequency Analysis*, Prentice Hall, New Jersey (1995).
10. E.R. Brown, K. Agi, C. Dill III. C.D. Parker and K.J. Malloy, A new face-centered-cubic photonic crystal for microwave and millimeter-wave applications, Microwave and Opt. Tech. Letters, 7:17 (1994).